SYNTHESIS, MICROSTRUCTURE AND MECHANICAL PROPERTIES OF BULK ULTRAFINE GRAINED Ti-47Al-2Cr (at %) ALLOY

A thesis submitted in partial fulfilment
of the requirements for the degree of
Doctor of Philosophy
in Materials and Process Engineering
at
The University of Waikato
by

VIJAY N NADAKUDURU

THE UNIVERSITY OF
WAIKATO
Te Whare Wānanga o Waikato

Hamilton, New Zealand
2009

Abstract

Hot isostatic pressing (HIP) and powder compact forging of Ti/Al/Cr composite powders of composition Ti-47Al-2Cr (at%) have been carried out to synthesize bulk ultrafine grained Ti-47Al-2Cr alloy. The Ti/Al/Cr composite powders were produced using high energy mechanical milling of elemental Ti, Al, Cr powders in a retsch planetary mill. The microstructure and mechanical properties of the bulk consolidated alloy produced using different processing techniques has been investigated. The mechanical properties of the alloy were studied in tension and compression both at room and elevated temperatures especially to know the formability of the material.

The bulk alloy samples produced by HIP for 2 hours at 1000^{o}C had porosity of approximately ~ 5%, indicating that the HIP time was not sufficient to close the pores. The microstructure mainly consisted of TiAl as the major phase and Ti(Al) and Ti_3Al as minors, the unreacted Ti(Al) phase in the microstructure was mainly due to the initial powder condition, in which a small fraction of powder particles were rich in Ti. Tensile testing of the alloy samples was carried out at different temperatures. At room temperature the alloy was fairly brittle, without any plastic deformation, and had a fracture strength of ~ 100 MPa. At elevated temperatures the samples became ductile, as reflected by considerable amounts of tensile elongations at 800^{o}C and above. The maximum amount of elongation was found to be between 70 – 80% at 900^{o}C. The tensile yield strength at 800^{o}C was in the range of 84-90 MPa and decreased to 55-58 MPa with the testing temperature of the samples to 900^{o}C. In compression the alloy showed plastic yielding and yield strength of ~ 1.4 GPa at room temperature. Compression testing at 900 ^{o}C revealed that compressive deformations equivalent to a height reduction of 50% could be easily achieved without cracking.

Direct powder compact forging using canned powder compacts of the Ti/Al/Cr composite powder was successfully used to produce bulk consolidated Ti-47Al-2Cr alloy samples. It has been observed that the density of the bulk consolidated

alloy sample after forging varied from the centre to the periphery. XRD analysis showed that the forged samples, consisted of TiAl (as major phase) along with Ti(Al) and $Ti_{3.3}Al$ phases. Mechanical testing of the samples showed that the samples exhibited brittle type of fracture both in tension and compression at room temperature and the fracture strength of the samples was in the range of 115 – 130 MPa in tension and 1.38-1.4 GPa in compression without any yielding. When being tested at 900^{o}C, the samples became very ductile showing yield strength in the range of 70-90 MPa and elongation to fracture between 80-165% in tension, and a yield strength of ~ 65 MPa and 50% deformation in compression was easily achievable.

Nearly fully dense Ti-47-2Cr alloy samples with density of ~98% were produced by using HIP at 1000^{o}C for a duration of 3 hours. TEM observations revealed equiaxed grains with grain sizes in the range of 200-500 nm. The tensile testing of the alloy samples at different temperatures revealed that the brittle to ductile transition temperature of the alloy was in the range of 700 and 750^{o}C, similar to that reported from literatures. The alloy showed significantly higher strengths both at room and at elevated temperatures, due to the low level of porosity in the sample. Elongation of 95 – 117% at 750^{o}C and 70-100% at 800^{o}C was observed.

The ultrafine grained Ti-47Al-2Cr alloy produced using a combination of mechanical milling and HIP/powder compact forging has demonstrated good formability at elevated temperatures leaving a large space for secondary processing to improve the quality of the material.

Publications

Journal

1. Thermomechanical Consolidation of Ti/Al/Cr Composite (Composition: Ti-47Al-2Cr (at%)) Powders
   Author/s: V. Nadakuduru, D. Zhang, P. Cao, B. Gabbitas
   Material Science Forum, 618-619 (2009) pp. 501.

2. Microstructures and Mechanical Properties of Ultrafine Grained Ti-47Al-2Cr (at%) Alloy Produced Using Powder Compact Forging
   Author/s: V. Nadakuduru, D. Zhang, P. Cao, B. Gabbitas
   International Journal of Modern Physics, 23 (2009) pp. 1739.

3. Ultrafine Grained Ti-47Al-2Cr (at%) alloy prepared by High Energy Mechanical Milling and Hot Isostatic Pressing
   Author/s: V. Nadakuduru, P. Cao, D. Zhang, B. Gabbitas
   Advanced Materials Research, 29-30 (2007) pp. 139.

Conference Proceedings

1. High Temperature Mechanical Properties of Ti-47Al-2Cr (at%) Alloy Produced Using Powder Compact Forging of a Mechanically Milled Powder
   Author/s: V. Nadakuduru, D. Zhang, P. Cao, B. Gabbitas
   Processing, Microstructure and Performance of Materials
   8–9 April 2009, Auckland, New Zealand

2. Microstructures and Mechanical Properties of Ultrafine Grained Ti-47Al-2Cr (at%) Alloy Produced Using Hot Isostatic Pressing of powders
   Author/s: V. Nadakuduru,P. Cao, D. Zhang, B. Gabbitas
   Proceedings of the 11th World Conference on Titanium on (JIMIC5), 3-7 June 2007, Kyoto, Japan

3. Ultrafine Grained Ti-47Al-2Cr (at%) alloy prepared by High Energy Mechanical Milling and Hot Isostatic Pressing
   Author/s: V. Nadakuduru, P. Cao, D. Zhang, B. Gabbitas
   Proceedings of the 4th International Conference on Advanced Materials and Processing, 10-13 December 2006, Hamilton, New Zealand.

4. Mechanical Behaviour of Ti-47Al-2Cr (at %) alloy produced using Hot Isostatic Pressing of Mechanically Milled Powders.
   Author/s: V. Nadakuduru, D. Zhang, P. Cao, B. Gabbitas
   Proceedings of the SMNZI Materials Conference, 10-11 December, 2009, Hamilton, New Zealand.

Acknowledgements

Firstly, I would like to express my profound gratitude and deep appreciation to my honourable academic chief supervisor Professor Deliang Zhang for his guidance support, enthusiastic encouragement throughout the entire period of this research work that enabled me to complete this important milestone in my life. I am also thankful to my co-supervisor Dr. Brian Gabbitas for providing insightful comments and suggestions that helped in defining the research goals.

I am also thankful to Dr. Peng Cao, for his kind help and support during the project. I would like to thank the Foundation for Research, Science and Technology, New Zealand for the financial support to the project

I am thankful to the Department of Engineering technicians who provided the technical support for this research, especially Paul Ewart, Yuanji Zhang, Helen Turner, Brett Nichol, Indar Singh, Steve Hardy, Stuart Finlay. I would like to thank Mary Dalbeth and Cheryl Ward for their official support.

I would also like to thank the members of the metallic group (Tasnim, Aamir, Masleeyati, Asma, Stella, Amro, and Tarik) for their constant encouragement and valuable suggestions through the progress of my experimental work and writing up this thesis.

I am also thankful to Barry Robinson (South Auckland Forgings limited) for the kind help during experiments. I am also grateful to Dr.Yu Lung Chiu (University of Birmingham) for his kind help.

Finally, I would like to thank my parents for all they have given me throughout my lifetime. I am grateful to my brother and sisters for their constant support.

Last but not the least. I would like to thank all people who directly or indirectly helped during the project work.

Table of Contents

List of Figures

pg

List of Tables

Abbrevations

UFG	ultrafine grained
HEMM	high energy mechanical milling
PM	powder metallurgy
EPM	elemental powder metallurgy
IM	ingot metallurgy
TMP	thermomechanical processing
HIP	hot isostatic pressing
CIP	cold isostatic pressing
TIP	thermally induced porosity
ECAP	equal channel angular pressing
MIM	metal injection moulding
GBS	grain boundary sliding
BDTT	brittle to ductile transition temperature
SPB	superplastic behaviour
PCA	process control agent
XRD	X-ray diffraction
DTA	differential thermal analysis
SEM	scanning electron microscopy
TEM	transmission electron microscopy
EDM	electro discharge machining
RT	room temperature
DSA	dynamic strain aging

Chapter 1
Introduction and Literature Review

1.1 Introduction

Interest in ultrafine grained (UFG) and nanostructured bulk materials with grain sizes in the ranges of 100 to 1000 nm and < 100 nm respectively have received much attention in the past two decades, since these materials have shown considerable property advantages over their coarse grained counterparts [1-3]. The UFG and nanostructures can also significantly improve the ductility and formability of the generally brittle gamma-TiAl based intermetallic compounds, stiffness, high strength retention at elevated temperatures and high creep resistance [4-11]. These materials are very important due to their high specific strength, high corrosion resistance. The challenge of realizing the promising potential of UFG and nanostructured titanium based alloys is developing processes and establishing optimised processing conditions for producing high quality bulk materials containing a very low level (0-2vol%) of structural defects such as residual pores and non-atomically bonded interfaces. This can open new opportunities of using gamma TiAl based materials for making parts in a variety of automobile and aerospace applications by replacing nickel based superalloys, titanium alloys and other high temperature alloys.

The factors that limit gamma TiAl based alloys from being widely used include their low room temperature ductility and elevated temperature formability. The room temperature ductility of TiAl based alloys can be enhanced by improving the microstructures of the alloys in terms of the volume fraction of the α_2-Ti_3Al phase, and the structure and size of the lamellar colonies through heat treatment and composition modification [7, 9, 11, 12]. Using powder metallurgy processes to synthesize TiAl based alloys and form components made from such alloys has the advantages of ensuring high microstructural and compositional homogeneity

and allowing near-net shape forming of parts. Powder metallurgy also offers opportunities to produce ultrafine grained and even nanostructured alloys which are expected to have much improved formability and possibly even better room temperature ductility. When pre-alloyed powders are not available or are too expensive, high energy mechanical milling (HEMM) of mixtures of pure Ti, Al and other elemental or master alloy powders is an effective and affordable way of producing the powders needed for synthesizing ultrafine grained and nanostructured TiAl based alloys. HEMM is expected to be an important technique to refine the microstructure, since this process involves severe plastic deformation, which can cause recrystallization of the particles as well as fracturing and cold welding which can also result in refining of the microstructures [13-15]. HEMM is capable of producing both mechanically alloyed TiAl based alloy powders and Ti/Al based composite powders with uniform powder particle microstructure. Producing Ti/Al based composite powders has a better practicality than producing mechanically alloyed powders because the latter may require very long milling time which leads to high powder production costs and lower production rate. The present study uses elemental powders of Ti, Al, Cr as starting materials to produce composite powders using HEMM technique. Processing techniques such as powder compact forging and hot isostatic pressing are used for the production of bulk ultrafine grained Ti-47Al-2Cr (at%) alloy. The relationship between processing condition, microstructure and mechanical properties of this particular alloy has been studied, by conducting tensile and compressive testing at room and elevated temperatures and microstructural characterization using various techniques.

The objectives of this work are:

- To understand the effects of various powder consolidation techniques on microstructure, mechanical properties and formability of bulk ultrafine structured gamma Ti-47Al-2Cr (at %) alloy.
- To understand the microstructure/mechanical property relationship of the ultrafine structured Ti-47Al-2Cr (at %) alloy.
- To find out an optimized processing method to synthesize bulk ultrafine structured Ti-47Al-2Cr (at%) alloy.

The thesis consists of six chapters. The first chapter consists of this introduction and literature review on the TiAl based alloys, their general background, processing techniques used for their production and the microstructures and mechanical properties of these alloys. Chapter two describes the experimental methods used in this project. Chapters three to chapter five are devoted to presenting and discussing the results. Chapter three presents and discusses the microstructures and mechanical properties of Ti-47Al-2Cr (at%) alloy samples, produced using mechanical milling and hot isostatic pressing. Chapter four presents and discusses the microstructures and mechanical properties of Ti-47Al-2Cr (at%) alloy samples produced using powder compact forging of mechanically milled powders. Chapter five presents and discusses the brittle to ductile transition of Ti-47Al-2Cr (at%) alloy produced using hot isostatic pressing. Chapter six summarises the conclusions and recommendations for the future work.

1.2 Literature Review

During the past three decades, a lot of effort has been made around the world to develop applications of intermetallic based alloys in gas turbine engines. The objective was to replace steels or Ni based alloys having a density of (8-8.5 g/cm^3) by materials with a much lower density of 4-5 g/cm^3. In the 1970s, research was mainly concentrated on Ti_3Al based alloy systems leading to the development of α_2 and super α_2 alloys. Although encouraging results were obtained, no applications were successful, because of enormous experimental difficulties. In the 1980s the main interest was switched to gamma TiAl based alloys, which had far better creep and oxidation properties than α_2. The interest in gamma TiAl based alloys was further enhanced by the fact that a number of potential applications of these alloys were found in automotive and nuclear industries.

1.2.1 General background of TiAl based alloys

TiAl based alloys, which have a low density (much lower than that of superalloys), high specific strength, and high strength retention ability at elevated temperatures, high dimensional and good environmental stabilities, are found to be promising

materials especially for high temperature applications. Although classical titanium alloys have already allowed improvements in the high temperature applications such as gas turbine engines by replacing nickel and iron base superalloys, they were not able to meet these new requirements. This paved the way for developing more reliable materials to be used at elevated temperatures above 600^{o}C. At temperatures above 600°C, the mechanical strength and creep resistance of titanium alloys become inadequate [16]. Moreover, oxidation problems arise at such high temperatures because of the formation of a brittle layer with high oxygen content which can lead to premature fracture under cyclic loading conditions. Finally, titanium alloys are subject to "titanium fire" activating (a great problem for engine applications), which is a phenomenon that results from both the low thermal conductivity of the metal and the very high heat of formation of TiO_2. So the intermetallic alloys based upon titanium, in particular, Ti_3Al and TiAl based alloys, have been examined and developed for high temperature applications (Figure 1.1). Compared with titanium, they present several advantages, such as higher elasticity modulus, lower density, better mechanical behaviour at elevated temperatures (Table. 1.1) and higher oxidation resistance by formation of a surface passive alumina layer.

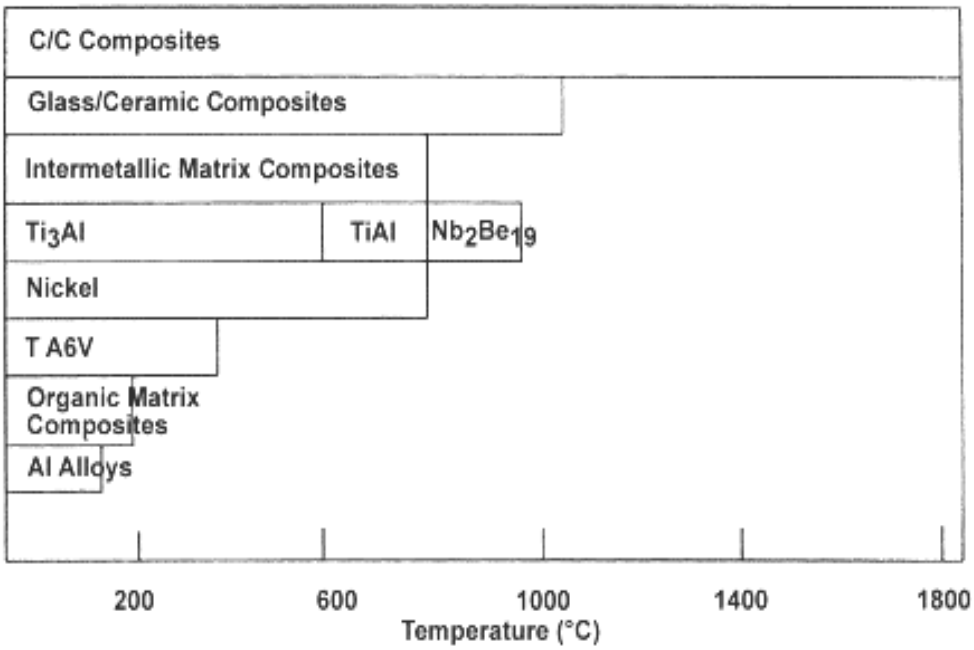

Figure 1.1: Service temperature ranges of different selected alloys, intermetallics and composites [17].

Table 1.1: Comparison of properties of TiAl, Ti_3Al, NiAl, Ni_3Al, Ti alloy and Ni based super alloys [16].

Intermetallic Alloys						
Intermetallic Alloys	**TiAl**	**Ti_3Al**	**NiAl**	**Ni_3Al**	**Ti alloy**	**Ni super-alloys**
Density (g/cm^3)	3.8	4.2	5.9	7.5	4.5	8-9
E (GPa)	160-180	100-150	~190	~180-190	95-115	190-220
YS (MPa)	~400-650	~700-1000	~200-500	~100-800	300-1300	250-1300
Elongation (%)	< 5	< 5	< 2	1-50 (with B)	10-40	5-50
T limit due to creep (°C)	800-900	750		>1000	600	1100
T limit due to oxidation (°C)	800-900	650	>1000	>1000	600	1100
Fracture toughness ($MPa\ m^{1/2}$)	10-20	10-20	~5		40-80	~25-50

TiAl based alloys which are also known as titanium aluminides are ordered intermetallic compounds which are formed in a particular composition range in the Ti-Al system (Figure.1.2). In an ordered intermetallic compound, a specific type of element occupies specific lattice site and the same arrangement is repeated in the crystal structure, as shown in Figure 1.3 [18]. For an alloy where elements form a solid – solution, these lattice sites are occupied randomly by atoms of different elements. The titanium aluminide family is composed of three main compounds: (a) Ti_3Al which is designated as α_2-phase and ordered according to $D0_{19}$ structure with a hexagonal symmetry and of lattice parameters a_{ord} = $2a_{disor}$=0.58 nm; c_{ord} = 0.48 nm; (b) TiAl (noted γ) which is ordered up to the melting point has an $L1_0$ type face-centred tetragonal structure consisting of atomic layers perpendicular to the c-axis; and (c) $TiAl_3$ which is ordered according to the $D0_{22}$ structure. The $D0_{22}$ structure is related to two $L1_2$ type unit cells stacked along the c-axis with an antiphase boundary of 1/2[1 1 0] (0 0 1) type at every other (0 0 1) plane [17, 19, 20].

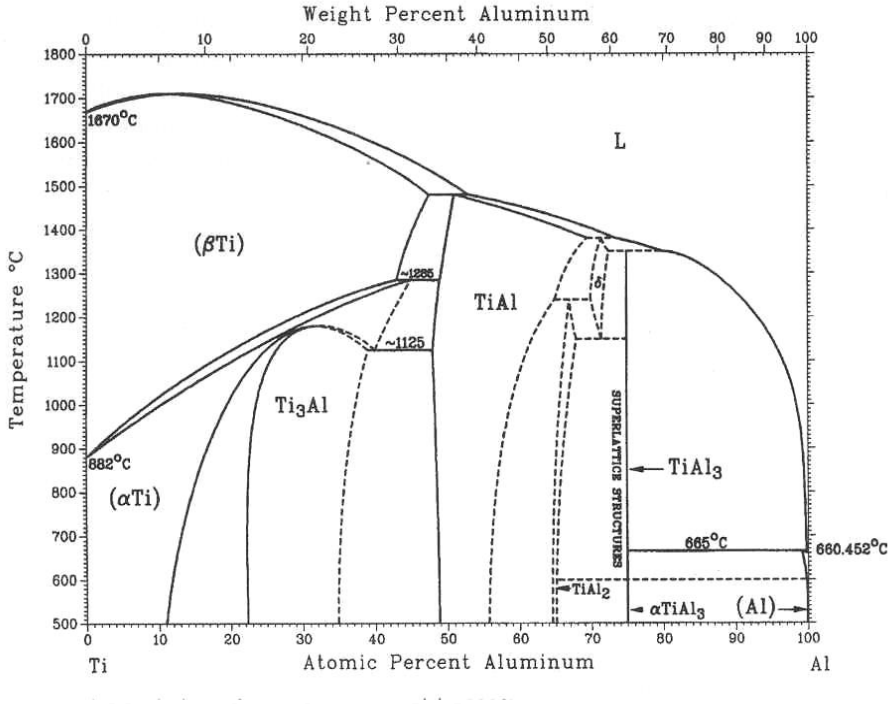

Figure.1.2: Ti-Al binary phase diagram [17].

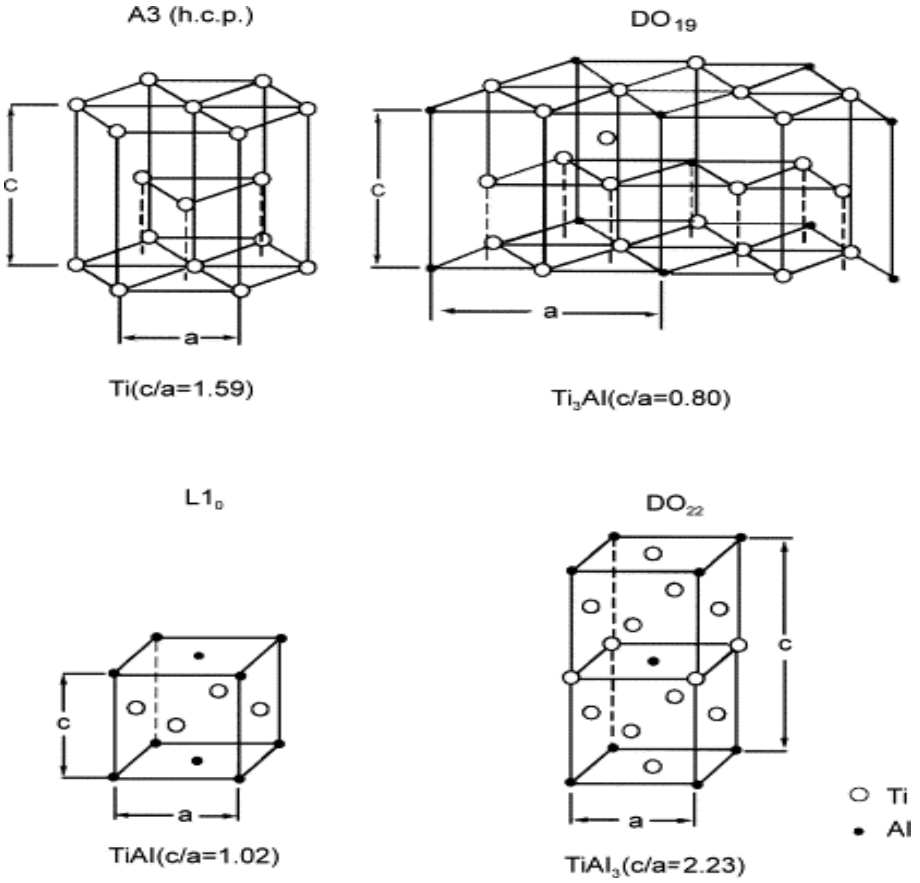

Figure 1.3: The lattice structures in titanium and titanium aluminides [18]

The first two alloys have a rather large homogeneity range and can accept, in solid solution, certain additional elements in substitution. These additions are important to develop a favourable microstructure and a material which is stable at processing temperatures. Also compounds such as $TiAl_2$ and Ti_xAl_y [21] were found to be unfit for industrial applications, because of their poor mechanical properties. The lattice structures associated with titanium aluminides of interest for space applications are, Ti_3Al (alpha – 2) & TiAl (Gamma). The lattice structure of gamma-TiAl is shown in Figure 1.3. The ordered arrangement of the atoms in the lattice provides these materials with inherent strength and stiffness retention to high temperatures. These intermetallics have limited low temperature ductility and toughness. Microstructures in β stabilised α_2 (Ti_3Al) titanium aluminides are analogous to those developed in conventional α + β alloys. To solve the problem of low ductility, alloying additions are made to stabilize β phase. The material based on Ti_3Al can be used up to a temperature of 700^{o}C [17].

Among the TiAl based intermetallic alloys, γ alloys based on TiAl exhibit high strength to density ratio, and good oxidation and creep resistance at elevated temperatures. They are considered to be one of the most promising intermetallic alloy classes for high temperature applications up to 900^{o}C in the aerospace industry [17, 22]. Many publications have listed gamma titanium aluminides in the promising high temperature aerospace materials being developed globally [8, 9, 23-26]. There are at least three major pay off areas for γ TiAl based alloys in advanced jet turbine engines: (a) high specific stiffness, being 50% greater than structural materials commonly used in aircraft engines; (b) good creep resistance in the temperature regime of 600^{o}C to 750^{o}C, which enables γ TiAl based alloys to substitute Ni based alloys which have twice the density of the γ TiAl alloys for certain applications; and (c) high fire resistance (nearly as high as that of Ni based alloys) which enables the γ TiAl based alloys to replace heavier and more expensive fire resistant designated Ti based alloys [23, 26]. Generally stiffness is valuable whenever clearances are concerned, such as frames, seal supports, cases and linings (e.g. consisting of honeycomb structures). The higher specific stiffness (E/ρ) also shifts acoustically exited vibrations towards higher frequencies, which is usual beneficial for structural components, e.g. turbine blades and parts within

the nozzle area. There have been few applications in the commercial sector, for example in Japan Mitsubishi Motors Corporation is marketing Lancer Evolution series cars since 1999. These cars use TiAl turbo chargers in place of Inconel 713C turbo chargers [27]. For aerospace applications TiAl rotors have offered better transient response & burst test performance than Inconel 723 & ceramic rotors [28].

However, the major obstacle to the practical use of TiAl and Ti_3Al alloys is the lack of ductility at room temperature. The absence of plasticity at classical fabrication temperatures is also a source of difficulties, in particular, in rolling TiAl into thin sheets or foils. Furthermore, the low toughness generates a high sensitivity to microcracks or surface defects, leading to fracture under a stress equal to yield stress. Gamma alloys derived from TiAl are also disadvantaged by a high amplitude primary creep. This is the reason why it has been envisaged to incorporate in these alloys additional elements in order to improve their specific mechanical properties.

1.2.2 Processing Routes

The manufacturing processes microstructure controlling and mechanical properties of TiAl based alloys have been of great importance for the last two decades. Since γ TiAl based alloys are difficult to process, the biggest problem which is holding back the manufacturing of these alloys is their processing and therefore extensive investigation has been undertaken on the processing methods. They include traditional ingot metallurgy (IM) and powder metallurgical (PM) for the alloys with composition range of 45-48 at% Al. Alloying elements such as manganese, chromium, niobium etc have been added for improving certain desired properties e.g. ductility and oxidation resistance. Both IM [29-35] and PM [11, 35-41] routes were successful in producing these alloys. The later method was found to be more promising because the problem due to elemental loss, segregation and fracturing were not observed. Also the thermomechanical processing of the ingots by plastic deformation at high temperatures is no longer necessary with PM methods, as there is no cast structure that has to be destroyed. A few thermomechanical processing techniques are found to be promising to

produce bulk fine, UFG, nanostructured TiAl based alloys in the case of PM alloys and for the modification of microstructure and density in the case of IM alloys. In some cases combinations of the above techniques have been used in order to obtain a refined microstructure as per the requirement.

1.2.2.1 Powder Metallurgy and Thermomechanical processing

Powder metallurgy is a processing technique, in which elemental powders or prealloyed powders are used as staring materials. In using PM route, it is essential to refine the microstructure of the powder particles before consolidating the powder, in order to obtain UFG or nanostructured bulk materials. It is not an easy task to obtain a high density bulk material by the powder metallurgical approach. However it is worthwhile to take the challenge, since the production of UFG gamma TiAl alloys results in an substantial decrease in the hot working temperature through grain refinement [42-45], which is said to be favourable for secondary processing, leaving a wide space to improve the quality of the material.

From literature, several thermomechanical processing (TMP) techniques have been used as primary or secondary processing techniques for producing bulk TiAl based materials and also to refine the microstructures. The processing techniques include hot isostatic pressing (HIP), extrusion and forging, hot pressing and reactive sintering/ spark plasma sintering, equal channel angular pressing (ECAP), rolling and spray forming. The PM process utilises either the pre-alloyed powders [46-50] or elemental powders [51-57]. The PM process utilising elemental powders was found to be much cheaper. While using elemental powders, the large difference in the diffusivity between Ti and Al results in pores in the consolidated material which is mainly due to the kirkendal effect [54-57]. HEMM can be used to overcome this problem, by refining the microstructure [13, 14, 58-64]. The microstructure can also be improved by HEMM, since the powders can be consolidated at temperatures much lower than that used for consolidating rapidly solidified powders [65].

The extent of thermal exposure also plays important role in the PM routes, since the desirable feature of the microstructure which is far from being in equilibrium is removed if the exposure time is too long. So it is essential to control the thermal

exposure in order to maintain novel characteristics and enhanced behaviour in the compacted material. The oxygen content of the powder processed material depends on the starting material, cleanliness of processing, and the particle size of the powder particles, since the smaller particles have a higher specific surface area, and thus often a higher oxygen content [66]. A proper degassing procedure before consolidation is also essential to control the oxygen content in the processed materials. So there are a lot of parameters to be controlled to obtain a high quality bulk material while using PM route. The TiAl based alloys produced by using a combination of PM and TMP are described below.

Hot Isostatic Pressing (HIP)

Both mechanically alloyed and composite powders can be consolidated by HIP, which is generally conducted in $\alpha+\gamma$, $\alpha+\beta+\gamma$, $\alpha_2+\gamma$ phase fields. Many studies have demonstrated that TiAl alloys with microstructures ranging from coarse grained structures to UFG and to nanostructure can be produced using HIP as the primary or secondary processing technique [50, 67-76]. Studies on the HIP consolidation by Ulrike et. al [72] has demonstrated that the temperature of HIP plays an important role in the microstructure of the alloy. HIP at temperatures up to 1200^oC was found to produce near gamma microstructure consisting of mainly α_2 and γ phases, and the HIP at higher temperatures of 1300 - 1400^oC led to a near lamellar microstructure with coarse lamellar spacing. The yield strength of the material was found to be dependent on the fraction of the equiaxed γ grains in the as HIPed microstructure. Also in the HIP and heat treated conditions, the yield strength was found to decrease somewhat, with increasing HIP temperature, which was likely attributed to the finer grain size associated with the lower HIP temperature.

Studies using prealloyed powders have shown that heat treatment of the as-HIPed material is essential to improve the mechanical properties of the TiAl alloy, by achieving desired microstructure [69, 70, 73]. Wegmann et al. [50], have demonstrated that homogeneous microstructures with fine grain sizes can be achieved using low HIP temperatures, which can be forged crack free at relatively low temperatures than that used for HIP. A combination of HIP and forging resulted in an alloy with superplastic properties. HIP consolidation using

elemental powders were also successful [76]. It has been found that refining the microstructure of the powder particles was crucial. Subzero temperature milling was found to be effective, as compared to RT milling in refining the microstructure.

Irrespective of the type of powders used, porosity was found in the HIP consolidated materials, the reason of porosity was found to be thermally induced porosity (TIP) while using atomized prealloyed powders [69]. In the case of mechanically milled powders, the HIP temperature and time were found to have an effect on the density of the material. Nevertheless, by controlling the temperature and time, HIP process was found to be successful in producing highly dense bulk TiAl based alloys.

***Extrusion* and Forging**

The microstructural development and hot working behaviour of PM γ TiAl based alloys using extrusion and forging as primary or secondary processing techniques has been of interest during last two decades, but the literature on this topic is not very rich. Lee et. al [77] showed that direct extrusion of elemental powder mixture of near gamma TiAl composition, resulted in a high density TiAl alloy. Although as extruded alloys were found to possess good mechanical properties, extrusion followed by heat treatment resulted in an improvement of the mechanical properties. Also Wu et. al [78] have demonstrated that extrusion of a mixture of Ti and Al powders resulted in TiAl based alloys with good mechanical properties, as compared to that of IM based materials. The grain size and lamellar interface spacing were found to be finer in the PM TiAl alloys produced via extrusion [79] than those in conventionally IM processed fully lamellar TiAl alloys.

Innovative techniques such as direct powder forging were also found to be promising to produce TiAl based alloys [80]. However a lot of work has yet to be done on this processing technique to achieve a very good understanding of the process, and to know the ideal processing parameters. In using extrusion or forging of canned powder compacts, it is very important to follow the proper degassing procedure, and control the extrusion ratio (for extrusion), strain rates

(for powder forging), to obtain a high density material with good mechanical properties.

Reactive Sintering and Spark Plasma sintering

A few studies also demonstrated the reaction synthesis process as a successful technique for synthesizing TiAl based alloys, where the exothermic heat of reaction between elemental powders was utilized to obtain intermetallic compounds. The process requires the use of low pressure during synthesis to obtain fully dense consolidated materials and near net shaped product. This leads to ease of fabrication for this class of difficult to process materials. If a Ti/Al powder mixture is used in the reaction sintering, the possibility of the formation of pores due to kirkendal effect is high, as discussed earlier. Literature shows that solid state hot pressing, reaction synthesis and spark plasma sintering (SPS) are successfully used to produce bulk UFG and nano TiAl based alloys [59, 81-87] with good mechanical properties [59, 82, 84, 85, 87, 88]. The above techniques were found to be promising in producing high dense bulk materials. In some cases the oxygen content was found to be much less than the bulk alloys produced through HIP [70]. Among sintering techniques, SPS process appears to be a promising route to produce TiAl alloys, because this process uses relatively low sintering temperatures and high sintering rates, leading to synthesis of a dense and fine-grained material in a relatively short period of time. Couret et al [87] have demonstrated that the particle size plays an important role during spark plasma sintering. Sintering is more efficient for larger powder particles due to a higher current density at the particles contacts and a small fraction of oxide on the surface of the particles.

Calderon et al. [82] have produced TiAl-X alloys with two phase microstructures and average grain sizes varying in the range of 100 nm and 150 nm. The level of strength obtained in the TiAl–X alloys is higher than that obtained in typical TiAl materials. Also Hwang et al. [83] have reported that consolidated alloys with recrystallized grains smaller than 1 μm can be produced using spark plasma technique in which considerable strength levels were reported. From the literature review, it can be concluded that UFG and nanostructured TiAl based alloys can be easily achievable using SPS technique. However the mechanical properties of the

alloys produced in the reported works have only demonstrated high strengths, but limited ductilities.

Equal Channel Angular Pressing (ECAP)

It has been well established that materials subjected to plastic deformation of a large strain through ECAP generally exhibit improved properties. In ECAP microstructural homogenization is achieved by applying simple shear in multi-passes through the use of the die containing a channel bent into a L – shaped configuration. There are many reports showing that UFG materials can be produced through ECAP, which include metals with FCC crystal structures such as Al, Cu, Ni, metals with BCC crystal structures such as low carbon steel, and metals with HCP crystal structures such as titanium and magnesium alloys.

A few reports have demonstrated that ECAP can be used to produce UFG TiAl based alloys from powders [89, 90]. A study by Morris et al. [90], on Al-TiAl composite reported that the material strength obtained by ECAP is very high after two passes but hardly changes after two additional passes. This strength increase is smaller for composite with larger particle content and also for smaller size (milled) particles. The changes also lead to a loss of ductility. Increase in milling time of the reinforcement particles was reported to affect the ductility of the composite adversely. It was demonstrated that in the extruded materials both the strength and ductility are lower when the reinforcement particles have been milled for longer times. After two ECAP passes the material containing 25% atomized particles has 3% ductility as compared to 0.5% for the material with 37% atomized particles and 0.9% ductility in the case of 25% particles milled for 5 h. The loss of ductility appears due to the incompatibility of deformation behaviour between the matrix and the particles, which leads to weakening of the Al–TiAl interface during ECAP.

According to Morsi et al. [89] using elemental powders in ECAP is beneficial in reducing the extrusion/consolidation pressure requirements compared to using prealloyed powders containing intermetallic phase. The former allows room temperature pressing. The numbers of passes also play an important role in ensuring the microstructural homegenity of the alloy. The literature on the

synthesis of bulk TiAl alloys using powder consolidation by ECAP is not very rich. Although ECAP of TiAl based materials looks promising, a lot of work is yet to be done in this area, especially to establish the optimum processing conditions.

Rolling

Rolling is used as a secondary processing technique to produce thin sheets for aerospace applications**.** The production of sheets and foils of γ TiAl based alloys using PM route, has been studied by a few investigators. Clemens et. al [9, 91] have investigated two sheet processing routes, in which isothermal forging or HIP was used to produce the consolidated material for rolling. The PM processing route used in their study generally involved HIP of prealloyed powders produced by atomisation and multistep rolling under near isothermal conditions in the ($\gamma+\alpha_2$) field. Anisotropy in the mechanical properties of the sheets has been observed, due to sheet texture resulting from rolling [92, 93]. The compositions of the sheets produced and studied include Ti-46.5Al-4(Cr, Nb, Ta,B), (γ TAB) Ti-47Al-4(Cr, Mn, Nb, Si, B) and Ti-47Al-2Cr-0.2Si (at%) alloys. The fine grained near gamma microstructures of these sheets led to good mechanical properties [9, 93-95]. This process was reported to be the best process developed so far when compared to other thermomechanical processes in producing large sized TiAl based alloy sheets [9, 10].

Spray Forming

Spray forming combines alloy powder production and compaction, and is more advantageous than conventional powder metallurgy techniques, as the number of processing steps are comparatively less, resulting in a product with a low level of contamination. The production of bulk TiAl alloys using spray forming technique has been demonstrated by a few investigations, which focussed on different aspects such as microstructure and mechanical properties of spray formed materials [96-102]. The as-spray formed materials produced were further processed using HIP or forging to improve their properties [102, 103]. The as-spray formed and forged material with an average grain size of 2.9μm was reported to posses better mechanical properties compared to as-HIPed γ TAB alloy, with an average grain size of 4 μm [102]. It was reported that 2.2 μm was the smallest grain size achieved using a combination of spray forming and forging

at 1100^{o}C [103]. Although a few studies demonstrated spray forming of the TiAl alloys, until now only a limited knowledge on the mechanical properties of spray formed TiAl alloys has been gained, indicating that further research is necessary to get a better understanding of the process.

Metal Injection Moulding Plus Sintering

Metal injection moulding (MIM) plus sintering is used for manufacturing of small components with complex shapes economically. The process involves combining fine metal powders with plastic binders which allow the metal to be injected into a mold using equipment similar to standard plastic injection molding machines. After the part is molded and before the binders are removed, the part is referred to as a 'green part'. The next step is to remove the binders with solvents and thermal processes. The resultant metal part is sintered at sufficiently high temperatures. The products produced by MIM plus sintering are used in a broad range of applications including medical, dental, firearms, aerospace, and automotive.

The MIM process of Ti and Ti based alloys is challenging, since fine powders with low impurity levels are required, and also the impurity pick up during the process makes the process more difficult. Some investigations showed that very good mechanical properties can be achieved using MIM plus sintering for producing Ti parts. However, in the production of TiAl based alloys using MIM plus sintering, the difficulties exceed those for conventional Ti alloys since the tolerance of oxygen, nitrogen, and carbon in TiAl based alloys is much lower than that for Ti alloys. Open literature showed only a few investigations used MIM for the production of TiAl based alloy products [104-106]. The room temperature tensile properties of the TiAl alloys produced using MIM plus sintering were not very good with both plasticity and the strength level being low when compared to those of the TiAl alloys produced using other PM processing techniques.

Investigations by Gerling et. al [104] on Ti-47Al-4(Nb,Mn,Cr,Si,B) alloy, has demonstrated a combination of a high strength of 433 MPa and strain to fracture (1.7%). The impurity concentration of the alloy was reported to be low, when compared to the Ti-48Al-2Mo alloy studied by K. Katoh et. al [106]. However the strength levels were found to be approximately the same in both the cases. In all

these studies, the residual binder present in the samples after the debinding step was reported to be the main source of oxygen, carbon and nitrogen pickup, resulting in slightly high impurity levels.

Table 1.2 shows that fine, UFG and nanostructured TiAl based alloys can be easily synthesised using a combination of PM route and thermomechanical processing. It is observed that the processing temperature and the TMP technique used have a considerable effect on the final grain size.

Table 1.2: Thermomechanical processing techniques used and the grain sizes achieved for gamma TiAl alloys using the PM route.

Composition Studied (at %)	Processing Technique	Grain size	Ref	Composition Studied (at %)	Processing Technique	Grain size	Ref
Ti-47Al-4(Nb,Cr, Mn,Si,B) PM (prealloyed powder)	HIPed at 1075 ^{o}C + Forged 850^{o}C	0.9µm	[50, 103]	Ti-47.1Al-1.1Cr-2.4V EPM	Canned Extrusion 1150 ^{o}C + Annealing 1350 /950/1250 ^{o}C	~ 30 µm	**[77]**
Ti-47Al-4(Nb,Cr, Mn,Si,B) PM (prealloyed powder)	PIM1410 ^{o}C + HIPed 1300 ^{o}C	8 µm	[103]	Ti-47.5Al-3Cr PM (prealloyed)/ Mechanically alloyed	HIP 1250^{o}C+ Heat treated 1300 ^{o}C	13µm	**[107]**
Ti-47Al-4(Nb,Cr, Mn,Si,B) PM (prealloyed powder)	Sprayed + HIPed at 1220 ^{o}C	0.9µm	[103]	Ti-47Al-3Cr PM(prealloyed /Mechanial Alloyed powder)	HIPed 975 ^{o}C	180nm (d_{γ})	[**108]**
Ti-47Al-4(Nb,Cr, Mn,Si,B) PM (prealloyed powder)	Sprayed + Forged 1100^{o}C	0.9µm	[103]	Ti-47Al-2Cr-1Nb-1Ta PM (prealloyed)	Extruded 1150 ^{o}C	Inhomo geneous 0.5-5 µm	**[109]**
Ti-47Al-2Cr-1Nb-1Ta PM (prealloyed powder) Canned Extrusion 1150 ^{o}C	Canned Extrusion 1150 ^{o}C	0.5 - 1 µm (d_{γ})	[35]	Ti-47Al-4(Cr,Nb,Mn,Si,B) PM (prealloyed)	HIPed + Rolled(α+γ)-phase field+ Annealed 1000^{o}C	10 - 15 µm	**[92]**

1.2.2.2 Ingot Metallurgy Plus Thermomechanical Processing

Ingot metallurgy plus thermomechanical processing involves producing the materials via melting/casting and then processing the as-cast material using HIP, isothermal forging or extrusion to break down the cast structure, and finish processing (e.g. rolling, superplastic forming, closed-die forging).

The thermomechanical processing (TMP) methods are used to improve the quality of the as-cast material. HIP is generally used to eliminate any residual casting shrinkage pores present in the as-cast alloys. Further TMP is often required to refine the microstructure after HIP. Xu et al. [110] have demonstrated that canned forging of the as-cast + HIPed TiAl alloy improved the microstructure. The microstructure of the as-cast and HIPed ingot consisted of regions with different compositions, and was homogenized during forging. Secondary TMP also induces dynamic and static recrystalization to refine the microstructure, and associated improvement of the mechanical properties. According to Xu et al. [111] the jacketed forging of as-cast TiAl alloy, in the + γ field, improves the as cast microstructure resulting in crack free pancakes with up to 75% thickness reduction.

Forging is an important TMP technique to improve the quality of the as-cast TiAl based alloys [112, 113]. On the other hand extrusion of the TiAl ingots has been studied by a few researchers, the extrusion of an appropriate ingot of TiAl was proposed for long products such as flat-bar and rod stock. The process has been adapted by GKSS in Germany in 2001, for the extrusion of 80 kg ingots of Ti-45Al-10Nb into a uniform rectangular cross section with good tensile mechanical properties [114, 115]. Extrusion and isothermal forging are the processes used for the manufacture of semifinished products and components based on γ TiAl. These processes are continuously optimized and adapted for novel alloys, and have been used to produce compressor blades for engine testing, but the processing costs were reported to be very high. The blades have been produced by GKSS in Germany for Rolls Royce using an alloy composition of Ti-45Al-8Nb with small amounts of C and B which resulted in excellent high temperature strength. The blades were a few centimeters long and even for these small parts, the production

was complicated by the heterogeneous microstructures found in the blades. Despite the enormous efforts made over the last two decades or so, no cast components have been produced which meet aerospace requirements of reliability and cost. A combination of extrusion and isothermal forging was also investigated by BMW in Germany and Rolls Royce for the production of compressor blades and vanes [115].

The high dimensional reduction ratio in extrusion and forging is essential in refining the grain sizes in the ingots processed materials. Rolling of ingots to produce thin sheets for aerospace applications was investigated by a few researchers**.** Clemens et al. [9, 91] have demonstrated the application of two sheet processing routes; isothermal forging plus rolling and HIP plus rolling for the production of Ti-47Al-2Cr-0.2Si (at%) sheets with improved mechanical properties. Table 1.3 shows the various IM plus TMP techniques used and the final grain size obtained. The results suggest that it is difficult to obtain UFG and nanostructured materials, using a combination of IM and thermomechanical processing.

Other advanced TMP techniques such as equal channel angular pressing (ECAP)/Extrusion have been used for the secondary processing of TiAl based alloy ingots, produced by the ingot metallurgy route. Generally the application of ECAP to HCP metals such as Ti and its alloys is challenging, because of the limited deformability of these materials associated with the fact that since slip mainly occurs in basal or prism planes in HCP metals [116, 117]. A few reports have demonstrated that ECAP can be used as secondary processing technique to produce fine grained TiAl based alloys [117-119].

From the above discussion it is clear that processing of TiAl-based alloys requires further development before components with quality acceptable to aerospace applications can be produced at an acceptable cost. The thermo-mechanically processed samples are extremely expensive and at present the microstructural heterogeneity of the ingot imposes a size limit on components. Casting technology needs to be improved and the microstructural control, aiming at refining the microstructure requires further work.

Table 1.3: IM plus TMP techniques used and the grain size obtained for near gamma TiAl alloys

Composition Studied (at %)	Processing	Grain size	Ref
Ti-47Al-2Cr-0.2Si IM	Forged-rolled-annealed 1000^{o}C	9.5 µm	[120]
Ti-47Al-2Nb-1Mn-0.5(W,Mo,Si) IM	HIPed – annealed 1010 ^{o}C	70 - 180 µm	[121]
Ti-47Al-2Cr IM	HIP 1250 ^{o}C + Forged 1200 ^{o}C + Two step heat treatments	10-12 µm	[122]
Ti-48Al-2Cr (at %) IM	HIP 1250^{o}C + Heat treatment 1100^{o}C (24-48hrs)	10 µm	[123]
Ti-47Al-2Cr-1.8Nb-0.2W-0.15B IM	Extruded (> T_{α}) + Heat treated 1320 ^{o}C/900 ^{o}C annealing	~ 30 -33 µm	[39]
Ti-46Al-2Cr-2Nb-0.2W-0.15B IM	Extruded (> T_{α}) + Heat treated 1350 ^{o}C/900 ^{o}C annealing	~ 258 µm	[39]
Ti-48Al-2Cr-2Nb-0.15B IM	Extruded (> T_{α}) + Heat treated 1320 ^{o}C/900 ^{o}C annealing	~ 30 -33 µm	[39]

1.2.3 Microstructures of TiAl Based Alloys

The microstructure of TiAl based alloys play an important role in controlling their mechanical mechanical properties and the workability. The TiAl based alloys, produced using IM routes often have macrosegregations [124, 125], which can be avoided by using PM routes [126]. It is essential to obtain a fine and homogeneous microstructures suitable for further processing. The different types of microstructures obtained in these alloys are: (a) near gamma, which consists of globular γ- TiAl grains with a small fraction of α_2 grains (b) duplex, which consist of lamellar regions in the γ matrix; (c) partially lamellar; which consists of γ /α_2 lamellae situated at the interfaces of γ and α_2 phase regions; and (d) fully lamellar, which consists of alternate γ /α_2 lamellae. The microstructural evolution of both

IM and PM TiAl based alloys is strongly dependent on the TMP and the heat treatment conditions.

1.2.3.1 Effect of Alloying Elements

Advanced γ-TiAl alloys contain a number of alloying additions, including major alloying elements such as Cr, Mn, V, Nb, Ta and W, and minor elements such as C, Si or B. Since phase equilibrium data for such multi-element systems are generally not available, it is difficult to maintain the optimal volume fraction of the α_2 phase while exploiting the beneficial effects of the alloying additions. The microstructure is affected by the alloying elements and their behaviour is much dependent on the amount and types of the alloying elements present in the alloy. The beneficial effects of an alloying element may be affected by several factors, such as the overall composition of the alloy, processing temperature, processing condition, and heat treatment condition.

According to Lamirand et. al [12], the microstructure of the binary TiAl based alloy is near lamellar, with few γ grains at grains boundaries, where as the ternary and quaternary ones are duplex. While the quaternary alloy exhibits fewer γ grains compared to ternary one, leading to smaller grain sizes. It was reported in their study that chromium destabilizes the lamellar microstructure with respect to γ grains whilst niobium tends to stabilize it. For the alloys containing 0.1 wt% oxygen, the microstructures were still modified by chromium and niobium additions but their effects were minimized because of the stabilization effect of oxygen on the lamellar microstructure. These effects were no longer visible for alloys containing 0.2 wt% oxygen and more. Also there was no evolution of the α_2 volume fraction and interlamellar spacing when chromium and niobium were added. The grain sizes of the ternary and quaternary alloys were similar, with values typically around 400 μm except for pure alloys whose microstructure is duplex. On the other hand, grain sizes of the binary alloys were relatively larger, of about 1.2 mm, whatever the oxygen content is. Also it was demonstrated by Song et. al [127] that the effect of occupying Al site was expected to be relatively high when alloying with Cr and relatively low with Mn and V, which was improve to benefit the deformability of TiAl.

It was reported that addition of Nb, Zr and Ta was effective in stabilising the β phase, since these elements had similar effects on the β phase at high temperatures and resulting in identical α/β transus temperatures, and suggesting that Ta is a stronger solution strengthener than Nb [128, 129]. The fact that Nb and Ta both slow down the formation of feathery and lamellar microstructures implies that it may be related to their low diffusivity. There are not many studies on diffusion in TiAl alloys, but it has been shown that Nb is a slow diffuser in both TiAl and Ti_3Al with a diffusion coefficient about an order of magnitude lower than that of Ti. The effect of carbon on the microstructure was studied by Tian et al. [130] and it was shown that carbon was an efficient solid solution strengthener in TiAl, and also acted as a precipitation strengthener by fine dispersion of carbide.

Elements like boron and yttrium are added to refine the microstructure. The addition of 1 at% boron refines the microstructure irrespective of the composition [128]. Also Li et al. [131] has demonstrated that the grain size decreases gradually from 200 to 60 μm with Y addition from 0.3% to 1 .0%. The α_2 /γ lamellar spacing ranged from 1.3 μm in Ti-47A1 alloy to 0. 18 μm in Ti-47A1-0.1Y alloy. Therefore, Y addition significantly refines the microstructures of Ti-47A1 alloys, including the refinement of both grain size and lamellar spacing.

1.2.3.2 Effect of Heat Treatment

Heat treatments of TiAl based alloys can refine the microstructure [39]. However, heat treatments at high temperatures are generally not preferred if UFG and nanostructures are required. Instead, a number of TMP techniques or a combination of multi step heat treatments are conducted in succession to homogenize the microstructures and reduce grain sizes. A variety of microstructures as discussed above can be achieved using heat treatment at different temperatures. The microstructural response of the TiAl based materials to heat treatment has been studied by many researchers [73, 77, 80, 123, 132, 133]. Wang et al. [132] have studied the effect of heat treatment on Ti-49Al (at%) PM alloy, and found that both the lamellar volume fraction and grain size were influenced by heat treatment. Partial lamellar structure was observed in their study with heat treatments at 1300^{o}C for 2hours and 1350^{o}C for 2-5hours respectively,

and with increasing the holding time α_2 phase disappeared. Heat treatments at 1350^{o}C for 18-42hours and 1450^{o}C for 18-42hours resulted in duplex and fully lamellar microstructures. Also the lamellar fraction and grain size increased with increasing temperature. The same trend was observed by Lee et al. [77] and Zhan et al. [73] after heat treatment of PM TiAl alloys.

Also Wang et al. [133] has demonstrated that multistep heat treatments on Ti-47Al-2Nb-2Cr (at %) IM alloy resulted in grain refinement of coarse lamellar microstructure (500 μm) to 30 μm, without involving faster cooling techniques such as oil/water quenching. From their study it has been demonstrated that lower Nb alloys needed faster cooling rates to produce fine microstructures, since the Nb addition shifted the $(\alpha + \gamma)/\gamma$ phase boundary to the Al side, resulting in overall composition being close to γ phase, which inturn promoted the massive transformation process. According to the study conducted by Wang et al. [123], the rapid heat treatment studies of Ti-48Al-2Cr (at.%) IM alloy significantly reduced the grain size. After eight cycles of rapid heating, rapid cooling and short holding, the grain size dirtribution was found to be uniform, and the average grain size was reduced to ~ 10 μm.

1.2.4 Mechanical Properties of γ TiAl Based alloys

1.2.4.1 Room Temperature Mechanical Properties

Strength

The strength of the TiAl based alloys was found to be mainly dependent on the microstructure. The Hall-Petch relation was obeyed in most of the studies. According to Liu et al. [39], the inter lamellar spacing plays an important role on the yield strength. It was reported from their study that a smaller inter lamellar spacing led to a higher yield strength. According to Kim et al [10], differences exist in yield strengths between duplex and lamellar material. In general the yield strength of TiAl based alloy with duplex microstructure is higher than the TiAl based alloy with lamellar microstructure. However lamellar spacing plays an important role in increasing the strength of TiAl based alloys. The strength levels for finer lamellar microstructures exceeded that of duplex structures. The fine

grained equiaxed near gamma and duplex microstructures with small amount of lamellar colonies show moderate strength at room temperatures, while in the case of fully lamellar structure strength is high for fine grained microstructures with narrow lamellae thickness. The yield strength of TiAl based alloys from different studies was reported to be in the range of 450 – 750 MPa (Figure 1.4) depending on the grain size and microstructure.

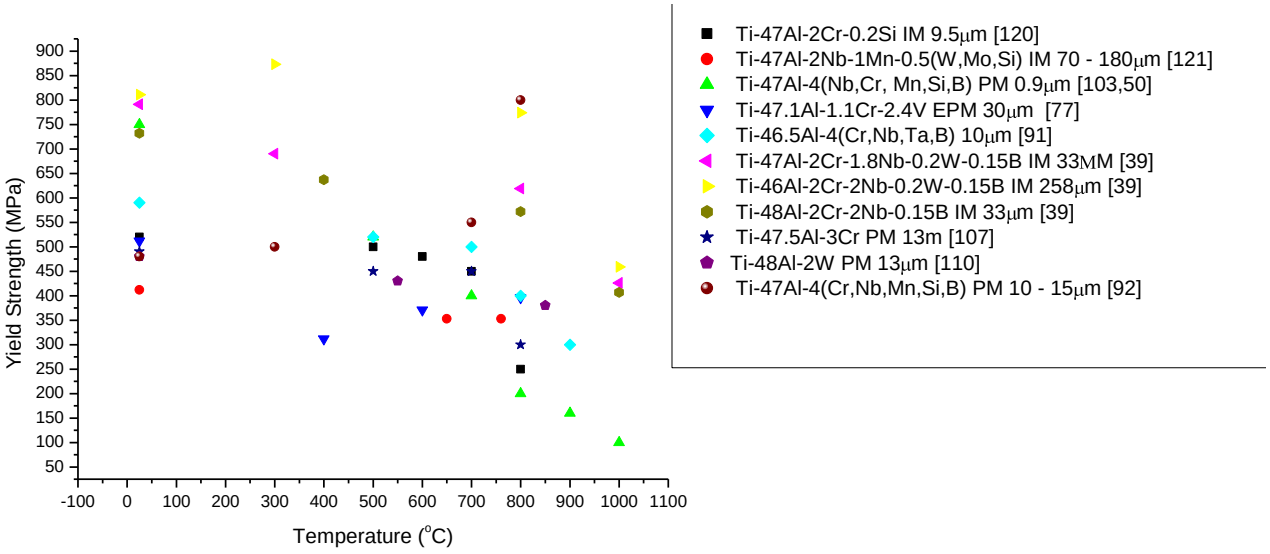

Figure 1.4: The temperature dependence of tensile yield strength for near gamma alloys of different grain sizes.

In compression the TiAl based alloys showed high yield strengths as compared to that in tension (Figure 1.5). At ambient temperatures, UFG γ TiAl based alloys are characterized by high values of hardness and compressive yield strength. From open literature, the maximum strength of UFG γ TiAl based alloys is 2500 MPa [134], which is almost double of that of coarse grained counterparts [135, 136]. According to the Hall-Petch equation, the yield strength should decrease with increase in grain size, which explains the reason why TiAl based alloys with coarse grain sizes show low yield stresses.

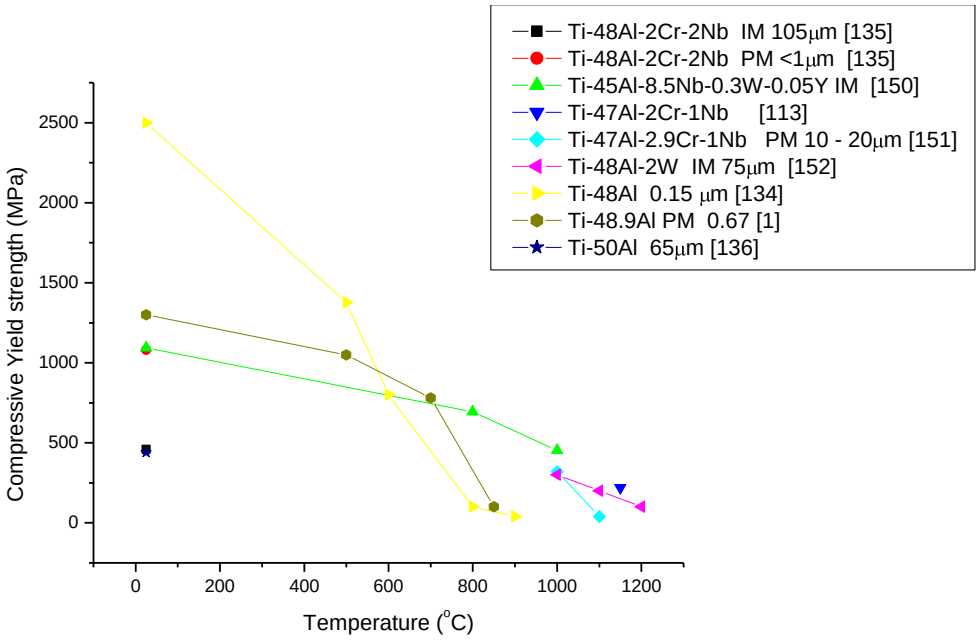

Figure 1.5: Yield strength in compression as a function of temperature for the TiAl based alloys of near gamma composition with different grain sizes.

Ductility

The ambient temperature tensile ductility of γ TiAl based alloys of a near gamma composition range with respect to grain size is shown in Figure 1.6. The near gamma alloys [39], are generally found to be brittle at ambient temperatures. The ductility of the TiAl based alloys in most of the cases was found to be in the range of 0 – 2%, indicating low elongations. According to Kim et.al [10] ductility is primarily controlled by the amount of general yielding which will be greater for small grain sizes. As grain size decreases, however, microstructure nonuniformity and the lowered crack initiation toughness limit the ductility enhancement. So the low room temperature ductility of UFG and fine grained TiAl based alloys was expected to be high due to the microstructural homogeneity in these materials. Achieving a homogeneous microstructure in addition to UFG is important. Until now, it has been found to be a challenge to improve the room temperature ductility of these alloys. Although PM route is more promising in producing UFG structures, which was expected to improve the ductility. The problems of high oxygen and carbon content especially while using elemental powders was found to be a problem. However a few studies on Ti-47Al-2Cr (IM) alloy with grain size 10μm [122] and Ti-47Al-1.1Cr-2.4V (PM) alloy with grain size 30μm [77], have

reported good ductilities of 6.7% and 3.3% respectively, mainly due to homogeneous microstructure. Xu et. al, [110] has shown that near lamellar microstructure exhibited inferior ambient temperature properties due to its poor ductility, higher brittle to ductile transition temperature and anisotripic tensile properties. Anisotropic behaviour in properties was observed in the lamellar microstructures, and attributed to the lamellar orientation with respect to the loading axis. The deformability was good when principal slip occured in a direction parallel to the lamellae. The fine grained equiaxed duplex microstructures with small amount of lamellar colonies showed moderate tensile ductility at room temperatures, while in the case of fully lamellar microstructure considerable room temperature ductility can be achieved for relatively fine grained microstructures with narrow lamellae thickness. In general the finer the lamellar spacing was, the better the room temperature ductility was, but this has not been quantified [10, 137].

On the other hand the alloying elements were found to have considerable effect on the room temperature ductility. Elements such as Cr, and V increased the ductility at room temperature, since they lower the stacking fault energy which increases the separation between the partial dislocations, stabilizing the twin partial dislocations. Addition of Mn, S may degrade ductility and strength, because they have the tendency to segregate at the grain boundaries during thermomechanical processing and heat treatment, promoting intergranular fracture [138]. This means that Cr and V are preferred alloying elements to improve the room temperature ductility. It was reported that addition of Zr up to 2 at% concentration, improved the mechanical properties (both strength and ductility) at room and elevated temperatures [139]. Interstitial elements such as O (oxygen), N (Nitrogen), and C reduce the ductility when their concentration is too high. It was reported that oxygen content of 0.03% or below was expected to increase the room temperature ductility of the TiAl based alloys [140, 141]. Especially, while using elemental powder metallurgy, the high oxygen content and the inhomogeneous microstructures obtained in these alloys leads to very low ductilities [142]. Since oxygen is a α stabilizer, a high amount of oxygen is expected to stabilize the α_2 phase which in turn effects ductility of the TiAl based alloys. Although the α_2 phase absorbs the interstitial elements such as carbon, oxygen improving the

ductility of the TiAl based alloys, a high amount of it is detrimental because of its inherent brittle nature, it has been suggested that 10-15% of α_2 phase is optimum for ductility [143, 144].

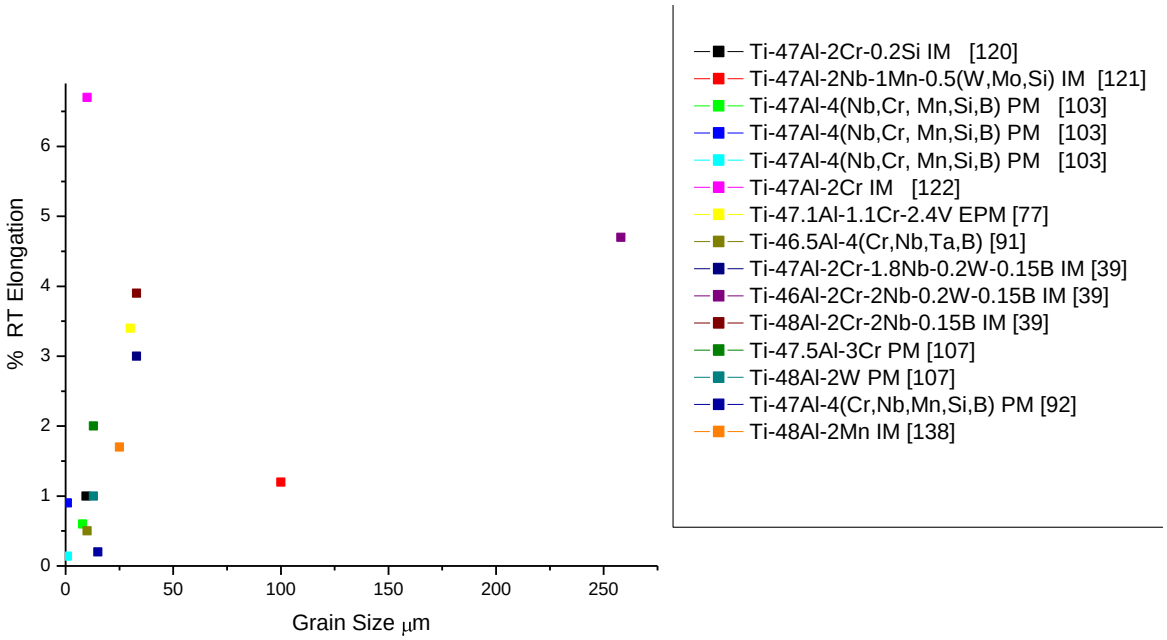

Figure 1.6: The ambient temperature tensile ductility of γ TiAl based alloys of a near gamma composition range with respect to grain size.

The ductility was found to increase in compression due to the more active slip systems present in these alloys as compared to that in tension. Some studies have demonstrated that the deformability in compression is ten times more than that in tension [136]. The compressive ductility was higher for coarse grained materials as compared to UFG TiAl alloys, since the material with a very high yield strength may fracture due to the very small flaws in the specimen [134]. So compressive ductility in the UFG TiAl based alloys was reported to be more dependent on the crack nucleation and propagation during compression.

Fracture Behaviour

The fracture behaviour at ambient temperature was reported to be mainly dependent on microstructure. In most of the cases cleavage fracture was found to be dominant at room temperatures, the fracture remained brittle at temperatures in the range from RT up to 800°C, depending on the grain size and microstructure of the alloy. At room temperature the dominant fracture mode in duplex structure

was reported to be transgranular in the equiaxed gamma grains and interlamellar in the lamellar grains. In the near lamellar structure the fracture mode is transgranular in the equiaxed gamma grains and interlamellar with some degrees of translamellar fracture in the lamellar grains. The fully lamellar structure was found to exhibit three characteristic fracture features: translamellar, interlamellar and stepwise fracture, and the duplex structure was found to be ductile at room temperature [110, 145]. The fracture of near gamma alloys is predominantly transgranular cleavage [39].

The fracture behaviour of TiAl based alloys in compression was studied by a few researchers. According to Nonaka et. al [136] the crack nucleation and propagation play an important role. It was demonstrated that most of the cracks initiated at the centre where the hoop stress and bulge strain are largest, and propagate in direction parallel to the compressive axis. Works on compressive fracture behaviour on TiAl alloys by Cao et. al [146] have also demonstrated that crack may be driven by the tensile stresses perpendicularly to the compressive axis (cleavage crack parallel to the compressive axis) or driven by the shear stress (tearing crack inclined to the compressive with an angle close to 45^{o}). In both cases, the driving stress is much lower comparing to the case of the tensile test at same load, which in turn needs a larger load to propagate the crack, resulting in higher fracture stress. The superior strength and plasticity measured in compression tests relative to those measured in the tensile tests are attributed to the less deteriorate effects of the micro-cracking damage and the higher resistance to the shear cracking than the resistance to the tensile cracking of TiAl alloys.

1.2.4.2 Elevated Temperature Properties

Strength

The temperature dependence of tensile yield strength of near gamma alloys of different grain sizes is shown in Figure 1.4. Generally the yield strength of most of the alloys decreases with increasing temperature. The rate of decrease of the yield strength was found to be dependent on the grain size. The smaller the grain size is, the faster the decrease of yield strength with temperature. However fully lamellar structures have demonstrated better high temperature properties as

compared to duplex structures. PM processed TiAl based alloys with fully lamellar microstructure having α_2 and γ lamellae thickness 10-50 nm and 100-350 nm were found to be superior in creep resistance to that of TiAl alloys produced using conventional processing techniques [35]. So it can be concluded that, achieving the desirable microstructure is essential to obtain remarkable mechanical properties. It is essential to obtain UFG grain size, initially in these alloys, to reduce processing temperatures, especially to improve the hot formability of these materials. On the other hand coarse grain size is preferred, if creep resistance is of main concern [134]. Depending on the requirement a few alloying elements are added to improve high temperature properties. Elements such as Nb, W and Ta improve the oxidation and creep resistance, since these elements result in a more effective substitutional solid solution strengthening [23, 91, 128, 147-149].

The effect of temperature on the compressive yield strength of TiAl alloys produced using different processing techniques is shown in Figure 1.5. Both the drop in yield strength and reduced brittle to ductile transition temperatures make UFG TiAl based alloys as promising materials for hot working in compression. The ultrafine grained microstructures with randomly high angle boundaries promote deformation at elevated temperatures and lead to highly workable materials [134]. The yield stresses of the UFG TiAl based alloys at temperatures greater than 800^{o}C were reported to be quite low ~ 40 MPa as compared to their coarse grained counterparts (Figure 1.5). The dominant deformation mechanisms at elevated temperature was found to be dislocation climb, while in some cases grain boundary sliding (GBS) accommodated by diffusional processes within the gamma TiAl phase, indicating superplastic behaviour [1]. Grain boundary sliding was only observed in the grain size range of 0.3-5μm [1, 134]. The diffusional deformation mechanisms at elevated temperatures (> 800^{o}C) for coarse grained TiAl alloys [113, 150-152] were found to be the same as that for UFG TiAl alloys.

Ductility

Elevated temperature ductility γ TiAl alloys is reflected by the brittle to ductile transition temperature (BDTT), which shows the lowest temperature at which these alloys can be hot worked. Figure 1.7 illustrates the temperature dependence

of elongation of near gamma TiAl based alloys with different grain sizes, in which the elongations have drastically increased above 600^{o}C. The BDTT of these alloys was also found to be between 650 and 800 ^{o}C, depending on the alloy composition, grain size and microstructure [107], with fine grained microstructures causing lower BDTT.

Above BDTT the ductility increases considerably due to a significant increase in mechanical twinning as well as dislocation activity [23]. However Wu et al. [78] have reported a BDTT of ~ 500^{o}C, which was mainly due to the homogeneous microstructure consisting of a higher volume percent of equiaxed gamma TiAl phase. It was reported that high temperature tensile deformation induced cavitation by the formation of voids at a distance from the neck, near the fracture end [1]. Some studies have demonstrated the increase in caviation as the distance from fracture end increased [1, 50], but reducing the grain size was a counter measure to reduce caviation. The PM TiAl based alloys were found to be more prone to cavitation due to the thermally induces porosity and in some cases the residual porosity. Also tensile tests at elevated temperature showed superplastic behaviour of the alloys in some cases, since testing at high temperatures and low strain rates accentuates superplastic behaviour. The large amount of elongation is achieved by the suppression of necking in these materials which have a strain rate sensitivity (m). The super plastic behaviour (SPB) occurs at $T > 0.5T_m$, where T_m is the melting point of the TiAl based alloys in Kelvin scale.

Since the flow stress of these materials is considerably low at low strain rates, complex shapes can be readily formed under superplastic conditions. The requirements of superplasticity are fine grain sizes (< 10 μm) and a dispersion of second phase particles, which inhibits grain growth at elevated temperatures. However SPB of intermetallic materials can noticeably differ from the SPB of ordinary metals and alloys due to the existence of a sharply directional covalent component of interatomic bonding in them. An ordered atomic structure, limited number of slip systems, low dislocation mobility, high activation energy for diffusion and a complex grain boundary structure. All these factors have proven that SPB for intermetallics occurs at temperatures above $0.7T_{m,}$ which is hardly applicable for manufacturing articles under SP conditions. At this juncture UFG

and nanostructured materials which are expected to decrease the homologeous temperatures of superplasticity of TiAl based alloys comparable to that of ordinary metals and alloys makes them ideal materials for near net shaped technology. So the development of superplastic TiAl to produce near net shaped structural components has become technologically feasible and attractive [153]. The main deformation mechanism for the superplastic TiAl based alloys was found to be grain boundary sliding (GBS) [1]. Cavitation also occurs in superplastic condition, but a uniform elongation without necking is observed here.

In compression the TiAl based alloys are formable without cracking. In most cases, deformation of > 50% was easily achievable at ~ 800^{o}C. However the smaller the average grain size is, the lower the formability temperature of these alloys is. Oehring et al. [134] has demonstrated that deformation of > 50% can be easily obtained at 600^{o}C, which was mainly due to the UFG structure. According to Beddoes et al. [151], the formable temperature was > 1000^{o}C for a TiAl based alloy with coarse grained structure. The same type of behavior was reported for a coarse grained material studied by Kim et al. [152]. Cracking of the specimens, during high temperature compression was also reported by a few studies. According to Beddoes et al [151], the chance of cracking of the TiAl alloy containing Cr was high as compared to the alloy with W addition. This was mainly attributed to the large fraction of the β phase in the TiAl alloy containing W, which controlled the grain coarsening by dynamically recrystallization of the grains, during compression. Overall the compressive formability of the TiAl based alloys at elevated temperatures is good, but the formable temperatures of these alloys was mainly dependent on the microstructure and grain size.

Fracture Behaviour

The fracture surface of the TiAl based alloys fractured at elevated temperatures consisted of largely tearing and microvoid related dimpling. Change in the fracture mode from transgranular (cleavage) to predominantly intergranular was observed when the deformation temperature was increased from 800 to 1200^{o}C. The fraction of the intergranular component was found to increase with increasing temperature [39, 108, 154]. On the other hand the size and alignment of cavities

to the tensile direction was reported to be important, in the initiation of fracture of these alloys [155].

Since most of the studies have demonstratred good formability of the TiAl based alloys in compression, the literature on the elevated temperature compressive fracture behaviour was found to be scarce.

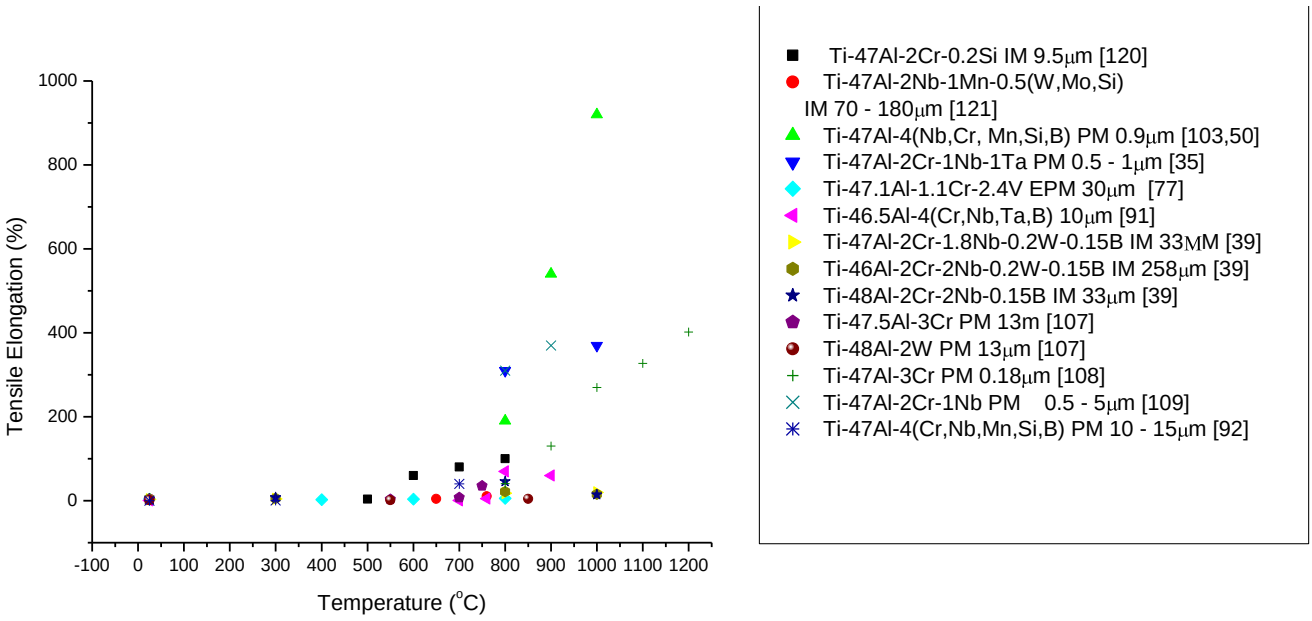

Figure 1.7: Temperature dependence on tensile elongation of near gamma TiAl based alloys with different grain sizes.

1.2.5 Discussion

Extensive research on TiAl based alloys has led to the optimisation of the alloy composition, the understanding of their behavior during processing and the establishment of the mechanical properties/microstructure relationships. The microstructures in these alloys were found to be strongly dependent on the processing technique used and conditions. Both IM and PM routes have been successfully used in producing these alloys. IM alloys are found to be good for high temperature mechanical strength due to their cast texture and large grains. However segregation and reproducibility are partly unsolved problems in gamma TiAl ingot manufacture. The PM approach has been found to be a serious

alternative to the IM route. By using PM route and prealloyed powders, the severity of the problem associated with element loss and segregation is drastically decreased, but this approach is highly expensive. In addition the problems of oxygen pickup and powder contamination are a major concern. On the other hand, using PM route and elemental powders proved to be economical and promising technique in producing UFG and nanostructured materials. Although a few studies have demonstrated the production of high quality materials, the problems associated with contamination and oxygen pickup are difficult to solve. In addition the inhomogenity of the microstructure of the consolidated material is found to be a common feature, for the alloys produced using this route. So a lot of research work by many investigators has been concentrated on improving the microstructures of these alloys using various thermomechanical processing techniques. The thermomechanical processing of TiAl based alloys produced by both IM and PM routes produce fine, UFG, nanostructured TiAl based alloys (in the case of PM alloys) and for the improvement of microstructure (in the case of IM alloys).

The TiAl based alloys in general are found to be brittle at room temperature, but the fine, UFG and homogeneous microstructures obtained, through thermomechanical processing and heat treatments have demonstrated better ductility (~ 5%) at room temperature. At elevated temperatures, the UFG TiAl based alloys become softer with low flow stresses, indicating favourable conditions for hot working of these alloys. Since grain refinement and grain growth in these alloys prevail, depending on whether a certain strain rate or stress level is exceeded or not, a balance between dynamic recrystallization and grain growth is reported to be crucial for elevated temperature deformation.

The main reason for the grain growth in the nanostructured and UFG TiAl alloys is due to the large amount of stored grain boundary enthalpy. On the other hand UFG and nanostructured TiAl alloys increase the uniformity of deformation at elevated temperatures facilitating grain boundary sliding and interaction of lattice dislocations with grain boundaries, inhibiting the deformation twinning. This results in high plasticity at low temperatures, indicating superplastic behaviour. The UFG TiAl based alloys provide fast stress relaxation compared to their coarse

gained counterparts during the deformation consisting of interaction of dislocations with grain boundaries and the grain boundary sliding. So most of the UFG TiAl alloys were reported to exhibit superplastic behaviour at lower temperatures when compared to their coarse grained counterparts. This reflected by the reduced brittle to ductile transition temperatures. The deformation mechanisms under superplastic conditions in these alloys were found to be grain boundary diffusion controlled either by grain boundary diffusion or bulk diffusion depending on the temperature at which superplasticity occurs. The low flow stresses and high deformations of the UFG TiAl based alloys indicated favourable conditions for near net shape casting. However a lot of work is yet to be done on the processing side such as developing the thermomechanical processing of ECAP and thermal treatments to modify the microstructure, and also on the microstructure texture property relationships of the rolled, powder forged, extruded TiAl based alloys produced using PM route.

On the other hand, the manufacture of structural components has shown a degree of maturity achieved in the fundamental understanding of TiAl based alloys and the engineering technologies. Gamma TiAl based alloys are used both for stationary gas turbines and jet engines. The high structural stiffness, reduced leakage, lower thermal mechanical stresses and improved resistance to self sustained combustion appear to be feasible by using TiAl blades and casings in high pressure compressors. Also due to high fatigue resistance and reduced rotor stresses, the use of TiAl based alloys to make low pressure turbine blades is also beneficial [156]. In automobile applications [4], TiAl rotors have offered better transient response and burst test performance than Inconel 723 and ceramic rotors [28]. Motor components such as piston bolts, valves and connecting rods etc, are currently being made using γ TiAl alloys, due to their combination of low density and good high temperature mechanical properties. TiAl turbo charger used in the Lancer Evolution series cars has also been successful, since they have perform better than the Inconel 713 alloy [27]. Exhaust valves produced by elemental powder metallurgy have been tested successfully by Liu et. al [157]. The γ TiAl based alloys are also considered as potential materials for the airframe structures, TiAl foils produced using superplastically forming of sheet material can be laser

welded to form honeycomb structures combining high stiffness, low weight and low thermal conductivities [156].

1.2.6 Summary

The production of Gamma TiAl based alloys using different processing techniques, and their microstructure and mechanical properties have been reviewed. The main conclusions of the literature review are as follows

- IM processing route hs been successful in producing TiAl based alloys, however the problems due to segregation, elemental loss and fracturing were frequently encountered. Also several processing steps are needed to refine the grain size, made the process complicated.

- PM route using prealloyed powders have resulted in high quality materials, with homogeneous microstructures and remarkable mechanical properties, but the prealloyed powder metallurgy is expensive and the problems of oxygen pickup and contamination has to be minimized.

- Elemental powder metallurgy route has been reported to be an economical and promising technique in producing UFG and nanostructured TiAl based alloys, but the problems of contamination and oxygen pickup are more severe as compared to prealloyed powder metallurgical route.

- Microstructures of the TiAl based alloys are mainly dependent on several factors including: composition, processing route, processing temperature, and the number of processing steps used.

- Achieving a high quality material with homogeneous microstructure is important in improving the mechanical properties, especially at room temperature.

- At elevated temperatures the UFG TiAl based alloys have good formability both in tensile and compressive directions.

- More research has yet to be done on the production of γ TiAl based alloys using EPM, especially using the processing techniques like canned/uncanned powder forging, rolling and a combination of these processing techniques can be promising, if successful EPM will be the best cost effective processing technique to produce near net shape materials.

References

1. R. Bohn, T. Klassen and R. Bormann, *Mechanical behaviour of submicro-grained γ-TiAl Based alloys at elevated temperatures,* Intermetallics, 2001. **9**: p. 559.
2. Gleiter, H, *Nanostructured materials: basic concept and microstructure,* Acta Materialia, 2000. **48**: p. 1-29.
3. K. S. Kumar, H.V. Swygenhoven., S. Suresh, *Mechanical behaviour of nanocrystalline metals and alloys,* Acta Materialia, 2003. **51**: p. 5743-5774.
4. T. Noda, *Application of cast gamma TiAl for automobiles,* Intermetallics 1998. **6**: p. 709-713.
5. D. Eylon, M. M. Keller, P. E. Jones, *Development of permanent-mold cast TiAl automotive valves* Intermetallics, 1998. **6**: p. 703-708.
6. F. Appel, R.Wagner, Materials Science and Engineering R, *Microstructure and Deformation of two phase γ Titanium Aluminides* 1998. **22**: p. 187–268.
7. D. M. Dimiduk, *Gamma titanium aluminide alloys-an assessment within the competition of aerospace structural materials,* Material Science and Engineering A, 1999. **263**: p. 281–288.
8. M. Yamaguchi, H. Inui, K. Ito, *High-temperature structural intermetallics* Acta Materialia, *Acta* Materialia, 2000. **48**: p. 307–322.
9. H. Clemens, H.Kestler, *Processing and Applications of Intermetallic γ-TiAl based alloys,* Advanced Engineering Materials, 2000. **2**: p. 551–570.
10. Y. W. Kim, *Strength and ductility in TiAl alloys,* Intermetallics, 1998. **6**: p. 623– 628.
11. R. Gerling, H.C, F.P. Schimansky, *Powder Metallurgical Processing of Intermetallic gamma titanium aluminides,* Advanced Engineering Materials, 2004. **6**: p. 23– 38.
12. M. Lamirand, J. L. Bonnentien, G. Ferriere, S. Guerin, J. P. Chevalier, *Relative effects of chromium and niobium on microstructure and mechanical properties as a function of oxygen content in TiAl alloys,* Scripta Materialia, 2007. **56**: p. 325-328.
13. C. Suryanarayana, Progress in Material Science, *Mechanical alloying and milling,* 2001. **46**: p. 1.
14. D. L. Zhang, *Processing of advanced materials using high energy mechanical Milling,* Progress in Material Science, 2004. **49**: p. 537.
15. F.H. Froes, C.Suryanarayana, K. C. Russel, C. M. Ward Close, *Proceedings of the International Conference on Novel Techniques in Synthetics and Processing of Advanced Materials,* TMS, 1995. Warrendale PA, *p. 1.*
16. Xia, K., ed. *Advanced Engineering Materials, Unit-1*. p: 430.
17. S. Djanarthany, J.C.Viala and J. Bouix, An *overview of monolithic titanium aluminides based on Ti3Al and TiAl,* Materials Chemistry and Physics, 2001. **72**: p. 301-319.
18. M.H. Yoo, C.L.Fu. J.K.Lee, *Deformation and twinning in metals and ordered Intermetallics-Ti and Ti- Aluminides,* Journal De Physique. III, 1991. **11**: p. 1065.

19. C. McCullougha, J.J.V., C.G Levia and R. Mehrabiana, *Phase equilibria and solidification in Ti-Al alloys,* Acta Metallurgica, 1989. **37**(5): p. 1321-1336.
20. Z.G. Liu, G. Frommeyer, M. Kreuss, *Field ion microscopy and atom probe investigations on two phase intermetallic TiAl/Ti_3Al alloy,* Scripta Metallurgica. et Materialia. , 1991. **25**: p. 1205.
21. A. Loiseau and A. Lasalmonie, New ordered superstructure in non stoichiometric TiAl, Acta Crystallographica, 1983. **39**: p. 580.
22. V. A. C. Haanappel, H. Clemens, M. F. Stroosnijder, *The high temperature oxidation behaviour of high and low alloyed TiAl-based alloys,* Intermetallics, 2002. **10**: p. 293-305.
23. Y.W. Kim, *Ordered Intermetallic Alloys, Part III: Gamma Titanium Aluminides***,** Journal *of Metals*, 1994. **46**: p. 30.
24. M. Yamaguchi, H.Inui, K. Ito, *Structural intermetallics*, *TMS*, 1993. Warrandale, PA, USA, P.127
25. C.M. Austin, T.J. Kelly, J.C. Chesnutt, *Structural intermetallics*, *TMS, 1993*. Warrandale, PA, USA, p.143
26. X. Wu, *Review of alloy and process development of TiAl alloys*, Intermetallics, 2006. **14**: p. 1114-1122.
27. T. Tetsui, *Development of TiAl turbo charger for passenger vehicles*, Material Science and Engineering A, 2002. **329-331**: p. 582-588.
28. Y. Nishiyama, T.M., T. Nakamura, H. Hino, S. Isobe and T. Noda, *International Gas Turbine congress*, 1987. Tokyo, p. 26
29. L. L.Rishel, N.E.B., R. Raban, V. Z. Gandelsman, T. M. Pollock and A. W. Cramb, *Cast structure and property variability in gamma titanium aluminide,* Intermetallics, 1998, **6**: p. 629-636.
30. M. Sujata, D. H. Sastry, C. Ramachandra, *Microstructural characterization and creep behaviour of as-cast titanium aluminide Ti–48Al–2V,* Intermetallics, 2004, **12**: p. 691-697.
31. Y.H. Wang, J.P. Lin, Y.H. He, Y.L. Wang, G.L. Chen, *Microstructures and Mechanical Properties of as cast Ti–45Al–8.5Nb–(W,B,Y) alloy with Industrial scale.* Materials Science and Engineering A, 2007. **471**: p. 82-87.
32. Y. Wang, J.N. Wang, J. Yang, B. Zhang, *Control of a fine-grained microstructure for cast high-Cr TiAl alloys,* Materials Science and Engineering A, 2005. **392**: p. 235-239.
33. D. Hu, J. F. Mei, M. Wickins, R. A. Harding, Microstructure *and tensile properties of investment cast Ti-46Al-8Nb-1B alloy* Scripta Materialia, 2002. **47**: p. 273-278
34. X.Y. Li, S. Taniguchi, *Correlation of high temperature oxidation with tensile properties for Ti–48Al–2Cr–2Nb and Ti–48Al–2Cr–2Fe alloys* Intermetallics, 2005. **13**: p. 683-693
35. L. M. Hsiung, T. G. Nieh, *Microstructures and properties of powder metallurgy TiAl alloys,* Materials Science and Engineering A, 2004. **364**: p. 1-10.
36. M. Thomas, J.L. Raviart, F. Popoff, *Cast and PM processing development in gamma aluminides,* Intermetallics, 2005. **13**: p. 944-951.
37. C. T. Liu, P. J. Maziasz, D. R. Clemens, J. H. Schneibel, V. K. Sikka, T. G. Nieh, J. Wright and L. R. Walker, *Gamma titanium aluminides*, *TMS*, 1995. Warrendale, p. 679

38. J. N. Wang, A. J. Schwartz, T. G. Nieh, C. T. Liu, V. K. Sikka and D. Clemens, *Gamma titanium aluminides,* TMS, 1995. Warrendale PA, p. 949.
39. C. T. Liu, J. H. Schneibel, P. J. Maziasz, J. L. Wright, D. S. Easton, *Tensile properties and fracture toughness of TiAl alloys with controlled microstructures*, Intermetallics, 1996. **4** p. 429-440.
40. P. J. Maziasz and C. T. Liu, *Development of ultrafine lamellar structures in two phase γ- TiAl* alloys**,** Metallurgical and Materials Transactions A, 1998. **29**: p. 105.
41. Y. Gao, J. Zhu, H. M. Shen, Y. N. Wang, *Stress induced phase transformation in two-phase TiAl intermetallic alloys*, Scripta Metallurgica et Materialia, 1993. **28**: p.651.
42. R. M. Imayev, V. M. Imayev and G. A. Salishchev, *Formation of submicrocrystalline structure in TiAl intermetallic compound, Journal* of Materials Science, 1992. **27**: p. 4465.
43. R.M. Imayev, G.A.Salishchev, V. M. Imayev, N. K. Gabdullin, M. R. Shageiv, *Structure and Superplasticity of Intermetallics*, Material Science Forum, 1994. **170-172**: p. 453.
44. G. A. Salishchev, O.N.Senkov, R. M. Imayev, V.M. Imayev, M.R. Shageiv, A. V. Kuznetsov, F. Appel, M. Oehring, O. A. Kaibyshev, F. H. Froes, *Processing and Deformation Behavior of Gamma TiAl Alloys with Fine-Grained Equiaxed Microstructures*, Advanced Performance. Materials, 1999. **6**: p. 107.
45. V. M. Imayev, G.A.. Salishchev, M.R. Shageiv, A.V. Kuznetsov, R. M. Imayev, O. N. Senkov, F. H. Froes, Low temperature superplasticity of submicro crystalline Ti-48Al-2Nb-2Cr alloy produced by multiple forging, Scripta Materialia, 1999. **40**: p. 183.
46. J. Beddoes, W. Wallace, M.C. de Malherbe, *Densification of γ-TiAl powder by hot isostatic pressing*, International Journal of powder Metallurgy, 1992. **28**: p. 313.
47. L. Zhao, J.B., D. Morphy, and W. Wallace, *Effect of HIP conditions on the Microstructure of a near γ-TiAl+W powder alloy, Materials and Manufacturing Processes*, 1994. **9**: p. 695-707.
48. J .H. Ahn and H. Chung, Mechanical alloying of $Ti_{50}Al_{50}$ powders and their consolidated properties, Materials and Manufacturing Processes, 1994. **9**: p. 637.
49. X. W. Du, J.N.Wang, J. Zhu, *The influence of Si alloying on the crept property of a TiAl alloy prepared by powder metallurgy*, Intermetallics, 2001. **9**: p. 745.
50. G. Wegmann, R.Gerling, F. P Schimansky, H. Clemens, A. Bartels, *High temperature mechanical properties of hot isostatically pressed and forged gamma titanium aluminide alloy powder,* Intermetallics, 2002. **10**: p. 511.
51. H. Huang, P. Virtanen, T. Tiainen and Y. Ji, *Synthesis of γ TiAl based alloy by mechanical alloying and reactive hot isostaic pressing*, Journal of Materials Engineering and Performance, 1998. **7**: p. 784.
52. J. C. Rawers, W. Wrzesinski, *Heat treatment of reaction-sintered hot pressed TiAl*, Scripta Metallurgica Materialia, 1990, **24**: p. 1985.
53. J. B. Yang, K.W.Teoh, and W. S. Hwang, *Preparation of (γ + α2) type TiAl intermetallics from elemental powders by solidstate hot pressing*, Materials Science and Technology, 1997. **13**: p. 695-701.

54. G. X. Wang, M. Dahms, *TiAl–based alloys prepared by elemental powder metallurgy*, Powder Metallurgy International, 1992. **24**: p. 219.
55. G. X. Wang, M. Dahms, *Synthesizing gamma-TiAl alloys by reactive powder processing*, Journal of Metals, 1993. **45**: p. 52.
56. Sullivan, P.L, *HIP processing of TiAl intermetallic using blended elemental powders*, Journal of Materials Processing Technology, 1993. **38**: p. 1.
57. G.-X. Wang, M. Dahms, An effective method for reducing porosity in the titanium aluminide alloy $Ti_{52}Al_{48}$ prepared by elemental powder metallurgy, Scripta Metallurgica Materialia, 1992, **26**: p. 1469
58. L.X. Hu, X.Q. Li, and, E. D. Wang, *Research on thermostability of Ti-Al composite powders prepared by mechanical alloying*, Chinese Journal of Mechanical Engineering, 2002. **15**: p. 35.
59. Qu, S., Li Xiaoqiang, Li Yuanyuan, Hu Lianxi and Wang Erde, *Manufacturing a TiAl alloy by high-energy ball milling and subsequent reactive sintering*, *Rare Metal.* 2006. **25**: p. 21.
60. M. Oehring, T. Klassen and R. Bormann, *The formation of metastable Ti–Al solid solutions by mechanical alloying and ball milling*, Journal of Materials Research, 1993, **8**: p. 2819.
61. F. Zhang, L. Lu, M. O. Lai, *Study of thermal stability of mechanically alloyed Ti–75% Al powders*, Journal of Alloys and Compounds, 2000, **297**: p. 211.
62. T. Klassen, M. Oehring and R. Bormann, *The early stages of phase formation during mechanical alloying of Ti–Al*, Journal of Materials Research, 1994. **9**: p. 47.
63. E. Szewczak, J.W. Wyrzykowski, *Influence of the mechanical alloying parameters on crystallite size of Ti-Al powders*, Nanostructured Materials, 1999. **12**: p. 171.
64. P. Bhattacharya, P.Bellon, R. S. Averback and S. J. Hales, *Nanocrystalline TiAl powders synthesized by high-energy ball milling: effects of milling parameters on yield and contamination*, Journal of Alloys and Compounds, 2004. **368**: p. 187-196.
65. B.W. Choi, Y.G. Deng, C. McCullough, B. Paden, R. Mehrabian, *Densification of rapidly solidified titanium aluminide powders-I. Comparison of experiments to hiping models*, Acta. Metallurgica et Materialia, 1990. **38**: p. 2225–2243.
66. G. X. Wang, M. Dahms, B. Dogan, *Microstructures and tensile properties of some γ-TiAl alloys made from elemental powders*, Scripta Metallurgica et Materialia, 1992. **27**: p. 1651-1656.
67. V. Imayev, R. Imayev, and A. Kuznetsov, *Mechanical properties of thermomechanically treated Ti-rich [gamma]+[alpha]2 titanium aluminide alloy*, Scripta Materialia, 2003. **49**(10): p. 1047-1052.
68. U. Habel, C.F. Yolton and J.H. Moll In: Y.-W. Kim, D.M Dimiduk and M.H. Loretto, Gamma *titanium aluminides, TMS*, 1999. Warrendale, PA, USA, p. 301.
69. G. Wegmann, R. Gerling and F. P Schimansky, *Temperature induced porosity in hot isostatically pressed gamma titanium aluminide alloy powders*, Acta Materialia, 2003. **51**: p. 741-752.

70. L. Zhao, J. Beddoes, D. Morphy, W. Wallace, *Microstructures and Mechanical properties of a PM TiAl-W alloy processed by hot isostatic pressing,* Material science and engineering A, 1995. **192-193**: p. 957-964.
71. J. H. Jeon, A. B. Godfrey, P. A. Blenkinsop, W. Voice, Y. D. Hahn, *Recrystallization in cast 45-2-2 XD titanium aluminide during hot isostatic pressing,* Materials Science and Engineering A, 1999. **A, 271**: p. 128-133.
72. U. Habel, B. J. McTiernan, *HIP temperature and properties of gas atomised γ titanium aluminide alloy*, Intermetallics, 2004. **12**: p. 63-68.
73. G. Zhang, P. A. Blenkinsop, M. L. H. Wise, *Phase transformations in HIPped Ti-48Al-2Mn-2Nb powder during heat-treatments,* Intermetallics, 1996. **4**(6): p. 447-455.
74. R. Gerling, A.Bartels, H. Clemens, H. Kestler and F. P Schimansky, *Structural characterization and tensile properties of high niobium containing gamma TiAl sheet obtained by powder metallurgical processing,* Intermetallics, 2004. **12**: p. 275-280.
75. J. Hebeisen, P.Tylus,D. Zick, D.K. Mukhopadhyay, K. Brand, C. Suryanarayana and F. H. Froes, *Hot Isostatic Pressing of Nanometer Sized γ TiAl powders*, *Proceedings of 4th International Conference on Powder Metallurgy in Aerospace Materials*. 1995. USA, p. 363
76. H.B. Yu, D.L. Zhang, Y.Y. Chen, P. Cao and B. Gabbitas, *Synthesis of an ultrafine grained TiAl based alloy by subzero temperature milling and HIP, its microstructure and mechanical properties,* Journal of Alloys and Compounds, 2009. **474**: p. 105-112.
77. I. S. Lee, S.K.Hwang, W.K. Prak, J.H. Lee, D. H. Park, H. M. Kim and Y. T. Lee, *Direct consolidation of TiAl-X alloy from elemental powder mixture,* Sripta Metallurgical et Materialia, 1994. **31**: p. 57.
78. Y. Wu, X.W.Li., S. X. Zhou and S.K. Hwang, *Indirect Extrusion of Tial-Based Intermetallics From Elemental Powders Metallurgy,* Journal of Iron and Steel Research, International, 2007. **14**: p. 104-109.
79. L. M. Hsiung, T.G. Nieh, and D.R. Clemens, *Effect of extrusion temperature on the microstructure of a powder metallurgy TiAl-based alloy,* Scripta Materialia, 1997. **36**: p. 233-238.
80. T. K. Lee, J.H.Kim, and S.K. Hwang, *Direct consolidation of γ TiAl-Mn-Mo elemental powder mixtures and control of porosity through a basic study of powder reactions,* Metallurgical and Materials Transactions A, 1997. **28**: p. 2723-2729.
81. J. Dutkiewicz, W.Maziarz, H. Heinrich and G. Kostorz, *Structure of Ti–Al–Nb intermetallics produced by mechanical alloying and hot-pressing techniques,* Materials Chemistry and Physics, 2003. **81**: p. 414-416.
82. H. A. Calderon, V. G. Febles, M. Umemoto, M. Yamaguchi, *Mechanical properties of nanocrystalline,Ti-Al-X alloys,* Materials Science and Engineering A, 2002. **329-331**: p. 196-205.
83. S. J. Hwang, M. S. Kim, S. Y. Jung, S. S. Kim and M.H. Oh, *Consolidation of the Mechanically Milled TiAl Alloys by Spark Plasma Sintering,* Journal of Metastable and Nanocrystalline Materials, 2003. **15-16**: p. 361.
84. Z.M. Sun, H. Hashimoto, *Fabrication of TiAl alloys by MA-PDS process and the mechanical properties,* Intermetallics 2003. **11**: p. 825.

85. Z. M. Sun, Q. Wang, H. Hashimoto, S. Tada and T. Abe, *Synthesis and consolidation of TiAl by MA–PDS process from sponge-Ti and chip-Al*, Intermetallics, 2003. **11**: p. 63.
86. G. Molenat, M.Thomas, J. Galy and A. Couret**,** *Application of Spark Plasma Sintering to Titanium Aluminide Alloys*, Advanced Engineering Materials, 2007. **9**: p. 667.
87. A. Couret, G.Molenat., J. Galy and M. Thomas, *Microstructures and mechanical properties of TiAl alloys consolidated by spark plasma sintering*, Intermetallics, 2008. **16**: p. 1134.
88. E. Paransky, E.Y.Gutmanas, I. Gotman and M. Koczak, *Pressure-assisted reactive synthesis of titanium aluminides from dense 50Al-50Ti elemental powder blends*, Metallugical and Materials Transactions A, 1996. **27**: p. 2130-2138.
89. K. Morsi, S. Goyal, *Equal channel angular pressing followed by combustion synthesis of titanium aluminides*, Journal of Alloys and Compounds, 2007. **429**(1-2): p. L1-L4.
90. M. A. M. Morris, I. G. Urrutia, D.G. Morris, *Effect of equal channel angular pressing on strength and ductility of Al–TiAl composites*, Material science and Engineering A, 2005. **396**: p. 3-10.
91. H. Clemens, A. Lorich, N. Eberhardt, W Glatz, W Knabl and H. Kestler, *Technology, Properties and Applications of Intermetallic γ- TiAl alloys*, Z. Metallkd, 1999. **90**: p. 569 – 580.
92. A. Bartels, H.Kestler, H. Clemens, *Deformation behavior of differently processed γ-titanium aluminides*, Materials Science and Engineering A, 2002. **329-331**: p. 153.
93. W. Schillinger, B. Lorenzen, A. Bartels, *Anisotropic mechanical behavior of textured γ-TiAl caused by the directionality of twinning*, Materials Science and Engineering A, 2002. **329-331**: p. 644.
94. G. Das, P. A. Bartolotta., H. Kestler, H. Clemens, *Structural metallics, TMS* Meeting, 2001. Warrandale PA, USA, p. 121
95. H. Kestler, H.Clemens, H. Baur, R. Joos, R. Gerling, G. Cam, A.Bartels, C. Scleinzer, W. Smarsly, *Gamma Tiatnium Aluminides, TMS Meeting*, 1999. Warrendale PA, USA, p. 423
96. K. W. Liu, R. Gerling, and F. P. Schimansky, *Microstructure and tensile properties of spray formed gamma Ti48.9at%Al*, Scripta Materialia, 1999. **40**: p. 601-608.
97. B. Li, E. J. Lavernia, *Spray forming and co-injection of particulate reinforced TiAl/TiB2 composites*, Acta Materialia, 1997. **45**(12): p. 5015-5030.
98. D. G. Morris, M. A. Morris, S. Gunter, M. Leboeuf, G. Hollrigl, *Spray deposition of intermetallics based on Al_3Ti and TiAl*, Scripta Metallurgica et Materialia, 1992. **27**: p. 1645.
99. F. P. Schimansky, K. W. Liu, and R. Gerling, *Spray forming of gamma titanium aluminides*, Intermetallics, 1999. **7**: p. 1275-1282.
100. B. Li, J. Wolfenstine, J. C. Earthman and E. J. Lavernia, *Compressive creep behavior of spray-formed gamma titanium aluminide*, Metallurgical and. Materials Transactions A, 1997. **28**: p. 1849.
101. R. Gerling, F. P. Schimansky, G. Wegmann, J. X. Zhang, *Spray forming of Ti 48.9Al (at.%) and subsequent hot isostatic pressing and forging*, Materials Science and Engineering A, 2002. **326**: p. 73-78.

102. G. Wegmann, R. Gerling, F. P. Schimansky, J. Xu Zhang, *Spray forming and subsequent forging of [gamma]-titanium aluminide alloys,* Materials Science and Engineering A, 2002. **329-331**: p. 99-105.
103. R. Gerling, F. P. Schimansky and H. Clemens, *Powder production techniques and PM processing routes for Gamma Titanium Alumininide, TMS , 2003*. USA, p. 249
104. Gerling, R. and F.P. Schimansky, *Prospects for metal injection moulding using a gamma titanium aluminide based alloy powder,* Materials Science and Engineering A, 2002. **329-331**: p. 45-49.
105. R. Gerling, E. Aust, W. Limberg, M. Pfuff, F.P. Schimansky, *Metal injection moulding of gamma titanium aluminide alloy powder,* Materials Science and Engineering: A, 2006. **423**: p. 262-268.
106. K. Katoh, A.Masumoto, *proceedings of 6th symposium on High performance material for severe environments*. 1995. Tokyo, p. 49.
107. J. Beddoes, L.Zhao, P.Au, W. Wallace, *The brittle – ductile transition in HIP consolidated near γ TiAl + W and TiAl + Cr powder alloys,* Material Science and Engineering A, 1995. **192/193**: p. 324-332.
108. M. R. Shagiev, O.N.Senkov, G. A. Salishchev and F. H. Froes, *High temperature Mechanical properties of a submicrocrystalline Ti-47Al-3Cr alloy produced by mechanical alloying and Hot Isostatic Pressing.* Journal of Alloys and Compounds, Journal of Alloys and Compounds, 2000. **313**: p. 201-208.
109. T. G. Nieh, L.M.Hsiung, J. Wadsworth, *Superplastic behaviour of a powder metallurgy TiAl alloy with a metastable microstructure,* Intermetallics, 1999. **7**: p. 163-170
110. X. J. Xu, J. P. Lin, Y.L. Wang, J.F. Gao, Z. Lin and G.L. Chen, *Effect of forging on microstructure and tensile properties of Ti-45Al-(8–9)Nb-(W,B,Y) alloy*, Journal of Alloys and Compounds, 2006. **414**: p. 175-180.
111. X. J. Xu, J.P.Lin, Y.L. Wang, Z. Lin and G.L. Chen, *Deformability and microstructure transformation of pilot ingot of Ti–45Al–(8–9)Nb–(W,B,Y) alloy*, Material Science and Engineering A, 2006. **416**: p. 98-103.
112. T. Tetsui, K.Shindo, S. Kobayashi and M. Takeyama, *Strengthening a high-strength TiAl alloy by hot-forging,* Intermetallics, 2003. **11**: p. 299-306.
113. Z. H. Huang, *Workability and microstructure evolution of Ti–47Al–2Cr–1Nb alloy during isothermal deformation,* Intermetallics, 2005. **13**: p. 245-250.
114. E. A. Loria, *Quo vadis gamma titanium aluminide*, Intermetallics, 2001. **9**: p. 997-1001.
115. F. Appel, U. Brossmann, U. Christoph, S. Eggert, P. Janschek, U. Lorenz, J. Mullauer, M. Oehring, J. D. H. Paul, *Recent progress in the development of gamma titanium aluminide alloys,* Advanced Engineering Materials, 2000. **2**: p. 699–720.
116. V. V. Stolyarov, Y.T.Zhu, T. C. Lowe and R. Z. Valiev, *Microstructure and properties of pure Ti processed by ECAP and cold extrusion*, Materials Science and Engineering A, 2001. **303**: p. 82-89.
117. Vladimir V. Stolyarov, Y.T.Zhu, I. V. Alexandrov, T. C. Lowe and R. Z. Valiev, *Grain refinement and properties of pure Ti processed by warm ECAP and cold rolling*, Materials Science and Engineering A, 2003. **343**: p. 43-50.

118. S. M. L. Sastry, R. N. Mahapatra, *Grain refinement of intermetallics by severe plastic deformation*, Materials Science and Engineering A, 2002. **329-331**: p. 872-877
119. S. L. Semiatin, V. M. Segal, R. L. Goetz, R. E. Goforth and T. Hartwig, *Workability of a gamma titanium aluminide alloy during equal channel angular extrusion*, Scripta Metallurgica et Materialia, 1995. **33**: p. 535-540
120. H. Clemens, W. Glatz, and F. Appel, *Tensile properties and strain rate sensitivity of Ti-47Al-2Cr-0.2Si sheet material with different microstructures*, Scripta Materialia, 1996. **35**(3): p. 429-434.
121. P. R. Bhowal, H. F. Merrick, D. E. Larsen Jr, *Microstructure and properties of a creep-resistant, cast γ-titanium aluminide*, Material Science and Engineering A, 1995. **192-193**: p. 685-690.
122. J. Tang, B. Huang, W. Liu, Y. He, K. Zhou, A. Wu, K. Peng, W. Qin and Y. Du, *A high ductility TiAl alloy made by two-step heat treatment* Materials Research Bulletin, 2003. **38** p. 2019-2024.
123. J. N. Wang, K. Xie, *Grain size refinement of a TiAl alloy by rapid heat treatment*, Scripta Materialia, 2000. **43**(5): p. 441-446.
124. U. Brossmann, M. Oehring, F. Appel, *Structural intermetallics TMS*, 2001. Warrendale, USA, p. 191.
125. V. Guether, A. Otto, H. Kestler and H. Clemens, *Gamma titanium aluminides ,TMS*, 1999. Warrendale PA, USA, P. 225.
126. W. Smarsly, H. Baur, G. Glitz, H. Clemens, T. Khan and M. Thomas, *Structural intermetallics, TMS*, 2001. Warrendale PA, USA, p. 24.
127. Y. Song, Z. X. Guo, R. Yang, D. Li, *First principles study of influence of alloying elements on TiAl: cleavage strength and deformability*, Computational Materials Science, 2002. **23**: p. 55-61.
128. T. T. Cheng, M. R. Willis and I. P. Jones, *Effects of major alloying additions on the microstructure and mechanical properties of γ-TiAl*, Intermetallics, 1999. **7**: p. 89-99.
129. D. Hu, A. J. Huang, and X. Wu, *On the massive phase transformation regime in TiAl alloys: The alloying effect on massive/lamellar competition*, Intermetallics, 2007. **15**: p. 327-332.
130. W. H. Tian and M. Nemoto, *Effect of carbon addition on the microstructures and mechanical properties of [gamma]-TiAl alloys*, Intermetallics, 1997. **5**: p. 237-244.
131. B. Li, F. Kong, and Y. Chen, *Effect of Yttrium addition on microstructures and room temperature tensile properties of Ti-47 Al Alloy*, Journal of Rare Earths, 2006. **24**: p. 352-356.
132. G. X. Wang, M. Dahms, *Influence of Heat treatment on microstructure of Ti-35Wt%Al prepared by elemental powder metallurgy*, Scripta Metallurgica et Materialia, 1992. **26**: p. 717-722.
133. J. N. Wang, J. Yang, Y. Wang, *Grain refinement of a Ti-47Al-8Nb-2Cr alloy through heat treatments*, Scripta Materialia, 2005. **52** p. 329-334
134. M. Oehring, F.Appel, Th. Pfullmann, and R. Bormann, *Mechanical properties of submicron-grained TiAl alloys prepared by mechanical alloying*, Applied Physics Letters, 1995. **66**: p. 941-943.
135. M. Usta, H.Wolfe, D. J. Duquette, N. S. Stoloff and R. N. Wright, *Thermo-mechanical grain refinement in gamma (γ) based TiAl intermetallics*, Materials science and Engineering A, 2003. **359**: p. 168-177.

136. K. Nonaka, K.Tanosaki, M. Fujita, A. Chiba, T. Kawabata and O. Izumi, *Deformation and Fracture Behaviour of TiAl in compression Tests at Room Temperature,* Materials Transactions, JIM, 1992. **33**: p. 802-810.
137. D. M. Dimiduk, P. M. Hazzledine, T. A. Parthasarathy, M. G. Mendiratta and S. Seshagiri, *The role of grain size and selected microstructural parameters in strengthening fully lamellar TiAl alloys,* Metallurgical and Materials Transactions A, 1998. **29**: p. 37.
138. W. O. Soboyejo, K. Lou, M.McConnel, *Manganese Segregation and Intergranular fracture in gamma based titanium aluminides,* Scripta Metallurgica et Materialia, 1994. **31**: p. 63-68.
139. T. Kawabata, H. Fukai, O. Izumi, *Effect of ternary additions on mechanical properties of TiAl,* Acta Materialia, 1998. **46**: p. 2185-2194.
140. T. Kawabata, T. Abumia, O. Izumi, *Effect of Oxygen addition on the Mechanical properties of TiAl at 293-1273K,* Acta Metallurgica et Materialia, 1992. **40**: p. 2557-2567.
141. S. Yamauchi, H. Shiraishi, *Homogenity and Mechanical Properties of TiAl*, 1992. **A152**: p. 283-287.
142. B. Dogan, G. X. Wang, and M. Dahms, *Tensile properties and fracture behavior of Ti52Al48 and Ti50Al48Cr2 prepared from elemental powders*, Scripta Metallurgica et Materialia, 1993. **29**(7): p. 943-948.
143. W. O. Soboyejo, D. S. Schwartz, S. M. L. Sastry, *An Investigation of the fracture behavior of gamma-based titanium aluminides: Effects of annealing in the α + γ and α_2 + γ phase fields,* Metallurgical and Materials transactions A, 1992. **23**: p. 2039.
144. K. S. Chan, Y. S. Kim, *Microstructure and Property Relationships in Titanium Aluminides and Alloys, TMS symposium*. 1991. p. 176.
145. K. S. Chan, Y. W. Kim, *Influence of microstructure on the cracktip micromechanics and fracture behaviour of two phase TiAl alloys*, Metallurgical and Materials Transactions A, 1992. **23** p. 1663-1677
146. R. Cao, L.Li, J.H. Chen and J. Zhang, *Study on compression deformation, damage and fracture behavior of TiAl alloys: Part II. Fracture behavior* Materials Science and Engineering A, **Article in Press.**
147. J. B. McAndrew and H. D. Kessler, Ti-36%Al as a base for high temperature alloys, Journal of Metals, Transactions AIME, 1956. **10**: p. 1348.
148. T. Seishi, S. Mitao, and K. N. Minakawa, *Alloy modification of [gamma]-base titanium aluminide for improved oxidation resistance, creep strength and fracture toughness*, Materials Science and Engineering: A, 1992. **153**: p. 451-456.
149. P. L. Martin, M. G. Mendiratta, H. A. Lipsitt, *Creep deformation of TiAl and TiAl + w alloys*, Metallurgical and Materials Transactions A, 1983. **14**: p. 2170.
150. Y. Q. Yan, Z. Q. Zhang, G. Z. Luo, K. G. Wang and L. Zhou, *Microstructures observation and hot compressing tests of TiAl based alloy containing high Nb*, Material Science and Engineering A, 2000. **280**: p. 187-191.
151. J. Beddoes, High *temperature compression behaviour of near γ-titanium aluminides containing additions of chromium or tungsten* Materials Science and Engineering A, 1994. **184**: p. L11-L15.

152. H. Y. Kim, W. H. Sohn, S. H. Hong, *High temperature deformation of Ti–(46–48)Al–2W intermetalliccompounds*, Material Science and Engineering A, 1998. **251**: p. 216-225.
153. R. M. Imayev, G.A.Salishchev, O. N. Senkov, V. M. Imayev, M. R. Shagiev, N. K. Gabdullin, A. V. Kuznetsov and F. H. Froes, *Low-temperature superplasticity of titanium aluminides.* Materials Science and Engineering A, 2001. **300**: p. 263-277.
154. V. M. Imayev, R. M. Imayev, and G. A. Salishchev, On *two stages of brittle-to-ductile transition in TiAl intermetallic*, Intermetallics, 2000. **8**(1): p. 1-6.
155. P. R. Sneary, R. S. Beals, T. R. Bieler, *Cavitation in the neck of a deformed Ti-47Al-2Nb-2Cr creep specimen*, Scripta Materialia, 1996. **34**: p. 1647-1654.
156. M. Dahms, *Gamma Titanium Aluminide Research and Applications in Germany and Austria*, Advanced Performance Materials, 1994. **1**: p. 157-182
157. Y. Liu, B.Huang, Y. He, and K. Zhou, *Processing TiAl based alloy by elemental powder metallurgy*, Journal of Material Science and Technology, 2000. **16**: p. 605-610.

Chapter 2

Experimental Procedure

2.1 Powder Preparation

Elemental powders of titanium (99% pure, 100 mesh), aluminium (99% pure, average particle size 40 μm) and chromium (99% pure, -325 mesh), were added in required proportions according to Ti-47Al-2Cr (at %) composition. For 100 gms of powder mixture, 0.64 gms of stearic acid was added, which was used as a process control agent (PCA).

The powders were sealed in a hardened steel vial together with stainless steel balls of diameter 12.5 mm under argon atmosphere (oxygen content ~ 100 ppm) in a glove box. A ball to powder ratio of 5:1 was used for both mixing and milling operations. The powders were initially mixed for duration of 6hrs at 100 rpm speed without any interval, prior to high energy ball milling at a speed of 400 rpm. After mixing, the powders were milled for a net time of 6 hrs, with 30 minutes interval. The vial was opened in the glove box to collect a few grams of powder after mixing and 6 hrs of milling, for analysis. The 6hrs milled powder was further milled for another 6 hrs with an interval break of 30 minutes leading to a total net milling time of 12 hrs. Both the mixing and milling of the powders were carried out in a Retsch PM100 planetary mill. The image of the vial and the planetary mill used for preparing the powders is shown in Figure 2.1.

The sticking of the powder to the vial and the balls was observed after 6 hrs of milling, and the sticking was found to be more pronounced after 12 hrs of milling, in which almost all the powders were found to be stuck to the vial. A higher amount of PCA was not used, since it may increase carbon contamination, degrading the quality of the powder. After 12 hrs of milling the vial was opened in the glove box and ethyl alcohol was used to regain the powder, this was done by milling the stuck powder with ethyl alcohol for approximately 2 minutes. The

wet powder was then filtered and dried in an oven kept at 50^{o}C for 24 hrs before compaction. The yield of the powder after 12 hrs of milling, excluding the powder fractions taken at each stage was found to be around 93-95%.

Figure 2.1: The Retcsh Planetary mill with the stainless steel vial used for milling the powders.

2.2 Powder Compaction and Canning

The milled powders were uniaxially pressed using a hydraulic die press. The powders were compacted in a cylindrical die made of hardened H13 die steel with internal diameter of 34 mm respectively. Cold pressing was done for a duration of 10 minutes with a pressure of 35 MPa to produce a powder compact, and then the powder compact was cold isostatically pressed (CIPed) at 200 MPa pressure for 5 minutes.

Canning was done using 316 stainless steel tubes. The wall of the tubes was machined to make its thickness to be approximately 1 mm, and the internal diameter of the tubes to be around 34 mm. One end of each tube was covered by a round stainless steel plate, which was welded on to the tube, and then a green powder compact was slid into the tube to perfectly fit in the space, leaving a very small gap between the wall of the tube and the powder compact. A round stainless steel plate with a thin hollow tube welded on top was used to cover the other end of the tube. This was done by welding the plate and thin hollow tube assembly to the tube. The thin hollow tube was used for degassing purpose.

The degassing of the canned powder compacts was done by heating to 300^{o}C, and holding at this temperature and evacuating the can for one hour. The degassing set-up is shown in Figure 2.2(a). After degassing the thin tube was crimped using a fixture specially designed for this purpose, which is shown separately in Figure 2.2(b). After crimping, the outside portion of the thin tube was cut using a hacksaw and finally sealed by welding. The image of a degassed and sealed can ready for consolidation is shown in Figure 2.2 (c).

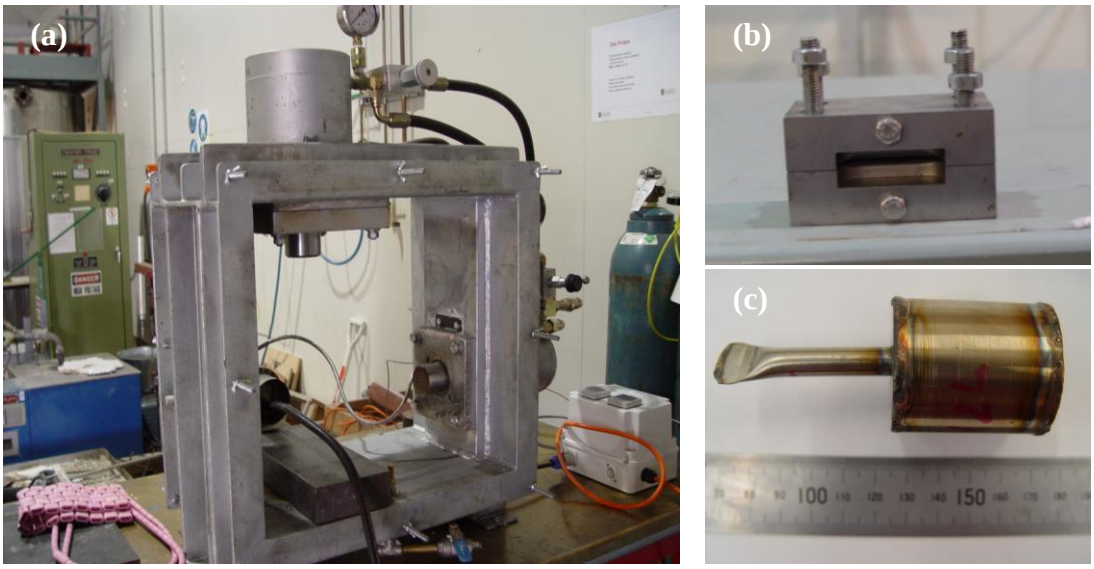

Figure 2.2: (a) the set up used for degassing of the canned compacts; (b) fixture used to crimp the tube of the can in order to seal it, and; (c) sealed can after welding ready for consolidation.

2.3 Powder Consolidation

2.3.1 Hot Isostatic Pressing

The powder compacts of 40 mm in height and 34 mm in diameter were canned and degassed as explained above. The CPSI SL-1, HIP system model in the University of Waikato was used to HIP the canned powder compact for producing HIP1 samples. On the other hand the HIP of the second set of samples HIP2 was conducted at American Hot Isostatic Presses Inc, Columbus, USA. The HIP cycle of the canned compacts used for the production of the HIP1 and HIP2 samples were shown in Figure 2.3. A heating rate of 6^{o}C/minute was used to reach 300^{o}C,

followed by a heating rate of 10°C/minute from 300°C to 1000°C. The pressure was applied at the rate of 4 MPa/minute, starting from 500°C, so that a pressure 200 MPa was assured at 1000°C. The compacts were HIPed at 1000°C for a duration of 2 hrs and 200 MPa pressure for HIP1 sample and for a duration of 3 hrs and 200 MPa pressure, for HIP2 sample respectively. Finally a cooling rate of 20°C/minute along with a pressure reduction of 5 MPa/minute was used to reach atmospheric conditions.

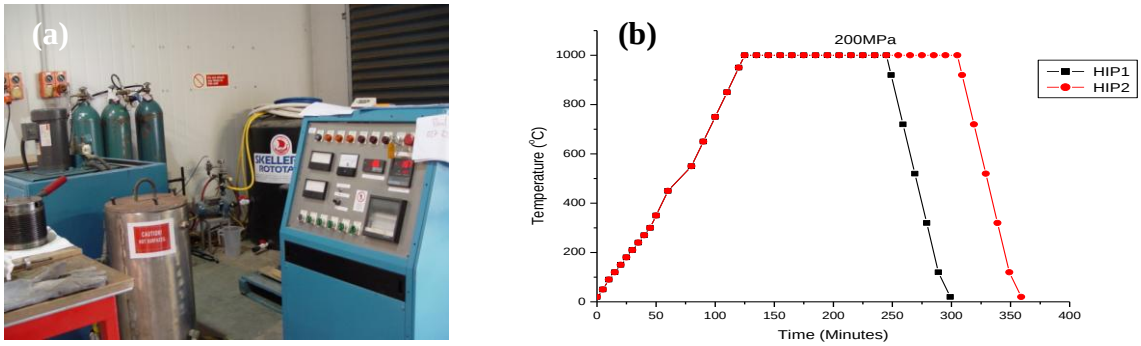

Figure 2.3: (a) HIP furnace used to produce HIP1 compact; (b) HIP cycle used during the process.

2.3.2 Powder Compact Forging

In the case of powder compact forging, the canning procedure used was the same as explained above. The two-step forging and one-step forging were both used. Press forging was done using a press of 500 ton capacity. Two-step forging was done as a trial experiment to produce consolidated bulk material (Forge-1 sample), for a preliminary study. In the two-step forging the sample was heated to 1200°C, using a heating rate of 14°C/min. The sample was took out, from the furnace after holding for 10 minutes at 1200°C, and then forged to reduce the height from 25 mm to 15.2 mm equivalent to an height reduction of 39% after first pass, using a crank press. The sample was then put back into the furnace and kept for 30 minutes, and heated back to 1200°C. The sample was then forged again to reduce the height from 15.2 mm to 8.4 mm, resulting in a further height reduction of 27%. A total height reduction of 67% was achieved in the two-step forging. While in the case of one-step forging (Forge-2, sample), the sample was heated to 1150°C, using a heating rate of 15°/minute. The sample was press forged from an initial

height of 40 mm to a final height of 12 mm, in one-step, resulting a total height reduction of 62%.

2.4 Sample Characterization

2.4.1 Particle Size Determination

The particle size distributions of the powders were determined using "Mastersizer S and MasterSizer 2000" particle size analyzers. Powders were dispersed ultrasonically in water and a few drops of 5% Nonidet P40 solution was used as a dispersant to avoid any agglomeration of the powders during the analysis.

2.4.2 Differential Thermal Analysis

Differential thermal analysis (DTA) of the powders was undertaken using a SDT 2960 instrument. The powders were loaded into an alumina crucible, and heating was done to 1000^{o}C, at a heating rate of 30^{o}/minute in an argon atmosphere.

2.4.3 X-Ray Diffraction

X-ray diffraction (XRD) was used to analyse the phases present in the powder and consolidated samples. The equipment used was a Philips X' Pert system, using a CuK_{α} radiation. The X-ray tube was set at 40 KV and 40 mA. Typical XRD scanning conditions were a scan range of 20 - 100^{o} 2θ at a scan speed of 1.2^{o}/minute. The results were interpreted using the PCPDF WIN software.

2.4.4 Oxygen analysis

The oxygen analysis on the bulk consolidated and the powder samples was done in the Central South University China. Oxygen analysis on a few specimens was also done in Durkee Testing laboratories USA.

2.4.5 Microscopy

The bulk samples for characterization were cut using either surface topography or cross sections of the powder particles and the bulk samples were studied using optical microscopy (Olympus BX60), scanning electron microscopy (SEM) HITACHI S4000SEM and HITACHI S4700SEM and transmission electron microscopy (TEM) using CM30 Philips operated at 200 KV.

For the SEM and optical microscopy the powder samples were prepared by cold mounting in the epoxy resin plus hardener. While in the case of bulk samples, mounting was generally not used. In the case of bulk samples, most of the samples for characterization were cut using an electro discharge machining (EDM) wire cutter shown in Figure 2.4, while a few were cut using diamond wheel cutting machine. The samples were subjected to a series of polishing steps as shown in Table 2.1. The initial polishing was done using 320 and 600 grit SiC papers, followed by intermediate polishing using 1000, 2000 grit SiC papers. Finally 4000 grit SiC papers were used, followed by Alumina dispersion to obtain the scratch free samples for microstructural analysis. In a few cases a grinding wheel was used to flatten the bulk samples before polishing. The polishing of the samples was done using a Rotopol-21 polishing machine.

Figure 2.4: The electro discharge machine used to cut the bulk consolidated samples

All the samples after polishing were ultrasonically cleaned and dried, before the microstructural examination. On the other hand etching using Krolls reagent was done on some samples. The Krolls reagent was prepared using 92 ml of distilled water, 6 ml of HNO_3 and 2 ml of HF, and the typical etching time used was 10-15 seconds.

The TEM specimens were prepared by cutting 3 mm disks from the bulk material and the samples were thinned down to ~ 100 μm and finally jet polishing was done using a mixture of 60% methanol, 35% Butanol and 5% perchloric acid. The quality of the specimens prepared using jet polishing was not good enough. A few of the TEM specimens for analysis was also prepared using focus ion beam technique (FIB) at the University of Birmingham (U K).

Table 2.1: The sample preparation, steps used for the microstructural analysis.

Steps	SiC Polishing Paper	Wheel rotation
Initial Polishing	320	300/150rpm
Initial Polishing	600	300/150rpm
Intermediate polishing	1000	300/150rpm
Intermediate polishing	2000	300/150rpm
Final Polishing	4000	300/150rpm
Final Polishing	Alumina dispersion (0.3μm)	300/150rpm

2.4.6 Density Measurement

The density of the powder compact was measured by dividing the weight of the compact in air by the volume of the compact, as shown in Equation 2.1.

$$Density\ of\ the\ powder\ compact = \frac{Weight\ of\ the\ compact}{Volume\ of\ the\ compact} \qquad (2.1)$$

The Archimedes method was used for measuring the density of the bulk consolidated samples using Equation 2.2 [1].

$$Density = \frac{Weight\ of\ the\ sample\ in\ air}{Weight\ of\ the\ sample\ in\ air - Weight\ of\ the\ sample\ in\ water} \quad (2.2)$$

2.5 Mechanical Testing

2.5.1 Microhardness testing

The microhardness testing, has been done using a LM700 microhardness tester, in which a square based diamond indentor was used, and the vickers hardness number (V H N) is defined as the applied load P divided by the surface area of the indent impression as per Equation 2.3 [2].

$$VHN = \frac{1854.4P}{(2a)^2} \quad (2.3)$$

Where P is the indentation load, and 2a the average diagonal measurement. The micro hardness in the present work was measured mostly by using a load of 100 gf and loading duration of 10 seconds and 25 gf and loading duration of 20 seconds.

2.5.2 Macrohardness testing

The macrohardness was measured on the consolidated samples using, LCR – 500 hardness tester. The Rockwell hardness on C scale (Rc) was measured using a diamond indentor using a load of 150 kgs.

2.5.3 Tensile testing

The samples for tensile testing were cut using EDM wire cutter, in which most of the wire cutting was done at the University of Waikato. The tensile specimens were polished using 600, 1000, 2000 and 4000 grit SiC polishing paper and ultrasonically cleaned and dried, before tensile testing. An INSTRON 4204 tensile testing machine was used for testing the samples both at room and elevated

temperatures. The set up used for room temperature tensile testing is shown in Figure 2.5(a). For room temperature tensile testing a cross head speed of approximately 0.05 mm/minute was maintained in most of the cases.

In the case of tensile testing at elevated temperatures the specimen along with the fixture was heated using a tube furnace. For all the elevated temperature tensile testing a heating rate of 6^{o}/minute was used to reach the testing temperature and a holding time of ~ 5 minutes was used at the testing temperature before starting the tensile testing. For all the elevated temperature tests, argon was purged from the top of the tube furnace. The set up used for elevated temperature tensile testing is shown in Figure 2.5 (b). The elevated temperature tensile testing was done using a cross head speed of approximately 0.096 mm/minute. Although the cross head speeds were kept almost constant for the room and elevated temperature tested samples, the strain rates differed due to the different specimen gauge lengths used for different samples.

For the HIP1 sample tensile testing samples of 16 mm gauge length, with a cross sectional areas of 2x1 mm^2 were used (Figures 2.6 (a) and (b)). Tensile testing at room temperature was done with a strain rate of $6x10^{-5}$/sec and at 800 ^{o}C, 900 ^{o}C and 1000^{o}C a strain rate of 1x 10^{-4} /sec was used. The tensile testing samples profile was changed, in order to avoid sharp corners as shown in the (Figure 2.7 (a)) which were cut from Forge-1 sample, with a gauge length of 14 mm and a cross sectional area of ~ 2x2 mm^2 was used with a strain rate of ~ 6 x 10^{-5}/sec at room temperature.

The sample size was slightly reduced in order to cut more samples for tensile testing, from Forge 2 sample. Tensile testing specimens with a gauge length of 6.5 mm (Figure-2.7(b)) were cut for room temperature testing and those with a gauge length of 8.5 mm (Figure 2.7(c)) for elevated temperature testing and strain rates of 1.4 x 10^{-4}/sec and $1.88x10^{-4}$/sec were used at room temperature and elevated temperature tensile testing (900^{o}C) respectively. The specimens for testing were cut from the central regions of the disk. In the case of HIP-2 sample, tensile samples with a 8.5 mm gauge length were used (Figure 2.7 (d)) and testing was carried out at room temperature, and at different elevated temperatures of 700 ^{o}C

750 ^{o}C and 800 ^{o}C. A strain rate of 1 x 10^{-4}/sec was used for tensile testing at room temperature, and a strain rate of 1.88 x 10^{-4}/sec was used for elevated temperature tensile testing.

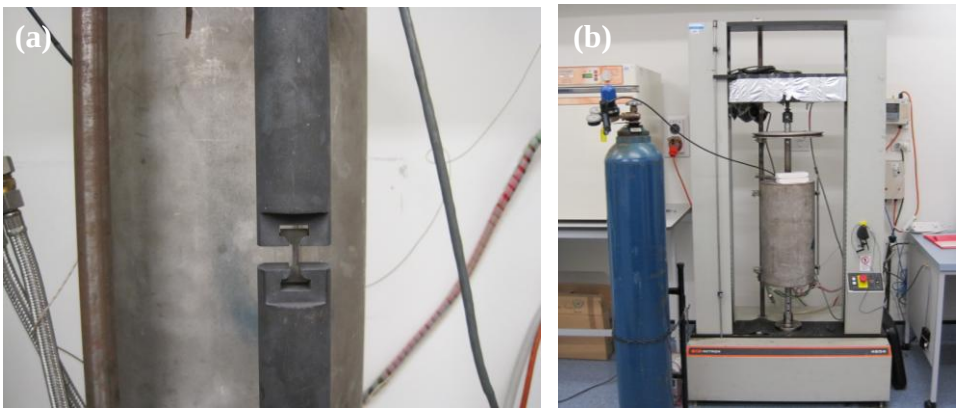

Figure 2.5: Tensile testing set up for (a) room temperature testing and; (b) elevated temperature testing.

(a)

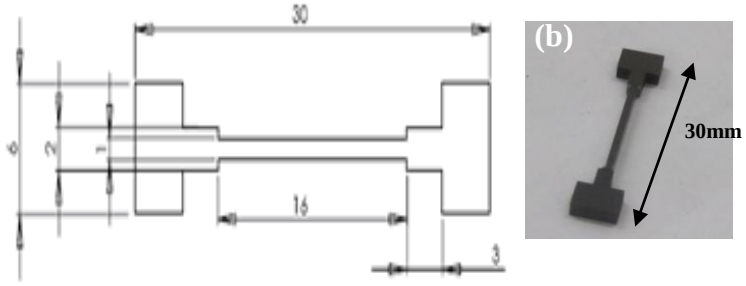

Figure 2.6: (a) schematic of the tensile sample cut from HIP1 sample, and (b) shape of tensile specimen

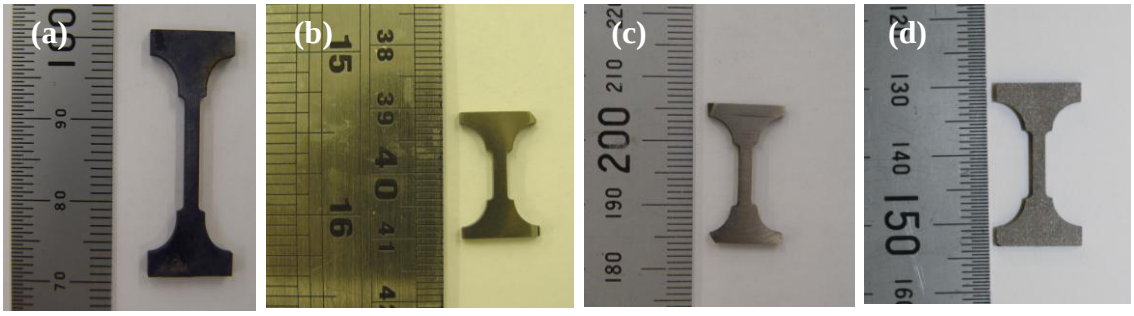

Figure 2.7: shape and size of the tensile specimens cut from: (a) Forge-1 sample; (b) and (c) Forge-2 sample; and (d) HIP-2 sample.

2.5.4 Compression testing

Compression testing was done both at room and elevated temperatures from the samples cut from HIP1 and Forge-2 materials. In the case of HIP1 sample, the compression samples of 6 mm diameter were cut using spark electrode cutting. The 6 mm diameter cylindrical bars were further cut into ~ 11 mm length, followed by grinding to make the end surfaces flat. Finally specimens of 6 mm diameter and 10.5 mm in height were used for compression testing at room temperature and at 900^{o}C respectively.

While in the case of Forge-2 sample, EDM wire cutting was used to cut compression test specimens of 4 mm in diameter and 7 mm in height for room temperature testing, and specimens of 8 mm in diameter and 10 mm in height for elevated temperature compression testing at 900^{o}C. The specimens were cut from the central region of the forged disk. After cutting the specimens into the required dimensions, they were made flat on both sides by grinding them.

Irrespective of the method of cutting the samples was polished using 2000 grit SiC paper, to avoid any scratches initiated while grinding. The compression samples cut from HIP-1 using spark electrode cutting and specimen cut from Forge-2 sample using EDM wire cutting for room and elevated temperature compression testing are shown in the Figures 2.8 (a), (b) & (c).

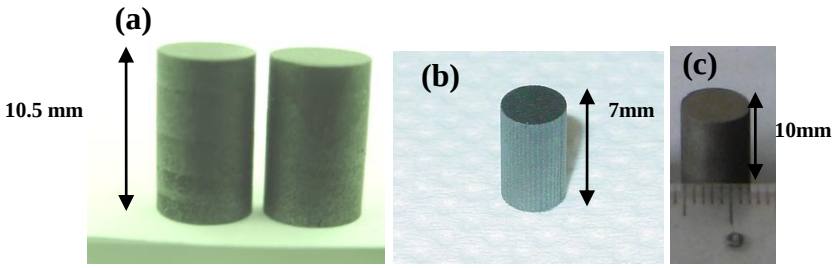

Figure 2.8: Compression samples cut from (a) HIP-1 using spark electrode cutting. Forge-2 sample using EDM wire cutting for (b) room temperature testing, & (c) elevated temperature testing.

In the case of HIP1 sample, the compression testing was done at room temperature, with a strain rate of approximately 8 X 10^{-5} /sec and a strain rate of 1.16 x 10^{-4} /sec was used at 900^{o}C. While for Forge-2 sample, the room temperature compression testing was done with a strain rate of ~ 1.2 x10^{-4}/sec and

the elevated temperature compression testing was done with a strain rate of 1.16x 10^{-4}/sec. The room temperature compression testing was done using INSTRON 4204 machine. For the room temperature compression testing, the specimen was placed in between small silicon carbide (SiC) cylinders of ~ 10 mm diameter and 10 mm in height on both sides, in order to protect the anvils made of H13 tool steel due to its high hardness. Since SiC was very brittle, high Cr steel was also tried, but was not useful, since the compression testing samples made an indent on the high Cr steel. So the experiments were done only by using SiC cylinders.

The experimental set- up used for the room compression temperature testing, is shown in Figure 2.9. The sample is kept in between silicon carbide cylinders and a plastic tube was used for safety, and also to collect the shattered pieces during the compression testing. High temperature compression testing was done by using a Gleeble thermo mechanical simulation machine in the Shanghai Jiaotong University, China. The compression testing was done with a strain rate of 1.16 x 10^{-4}/sec both for the specimens cut from powder forged (Forge-2) and HIPed (HIP1) materials. The testing was done in a vacuum atmosphere of 3.7 x 10^{-1} torr. During the experiment, the specimens were heated using electric heating, a heating rate of 300^{o}C/minute to reach 900^{o}C and a holding time of 2 minutes was used at 900^{o}C.

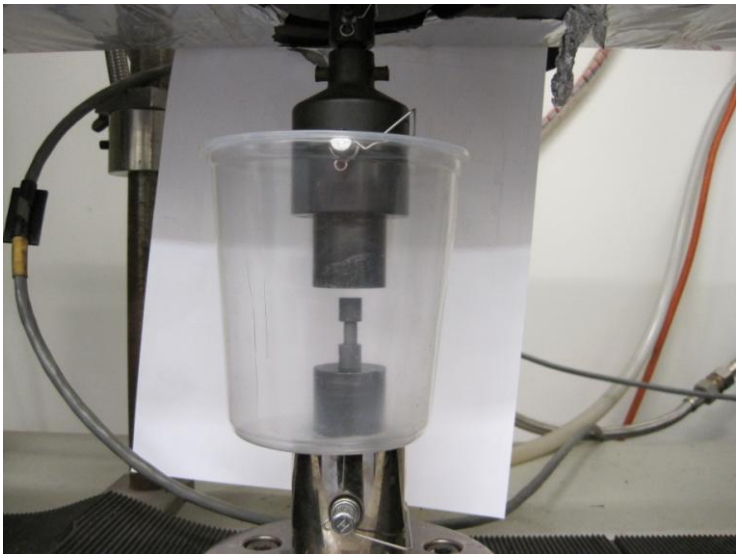

Figure 2.9: Set up used for the room temperature compression testing.

References

1. Roger B. Culver, “Facets of Physics, A conceptual Approach”, Chapter 7, Minneapolis/St. Paul, West Publication, 1993, p. 203.

2. George. E. Dieter, “Mechanical metallurgy”, Chapter 9, p. 337.

Chapter 3

Microstructures and Mechanical Properties of UFG Ti-47Al-2Cr (at %) Alloy Produced Using Mechanical Milling and Hot Isostatic Pressing.

3.1 Introduction

TiAl based alloys with UFG microstructures and good mechanical properties can be produced using a combination of high energy mechanical milling of powders and subsequent thermomechanical consolidation of these powders. The microstructures and phase distribution of the consolidated bulk materials were found to be dependent on initial powder condition of the powders used. Achieving a homogeneous microstructure with UFG structure is desirable to improve the mechanical properties, which is a great challenge, especially while using elemental powders as starting materials. This chapter describes and discusses the results of a study on the production of Ti-47-Al-2Cr (at %) alloy using a combination of mechanical milling and hot isostatic pressing (HIP), and elemental powders as starting material. The effect of processing conditions on the microstructures of the alloy and the mechanical behaviour of the alloy, both in tension and compression, at room and elevated temperatures has been studied.

3.2 Experimental Details

Elemental powders of Ti, Al, Cr were mixed to make up a composition of Ti-47Al-2Cr (at%), the powders were initially mixed for 6 hrs and the powder mixture was subsequently milled for 12 hrs in dry condition to produce a Ti/Al/Cr composite powder. The mixing and milling operations were done using Retsch planetary mill. The composite powder produced was cold pressed and cold isostatically pressed (CIPed) to produce a green compact of 40 mm in height and 34 mm in diameter. The CIPed compacts were canned using 316 stainless steel tubes, and the cans were degassed at 300^{o}C for one hour. HIP was performed at 1000^{o}C for a duration of 2 hrs. Tensile testing specimens of 16 mm gauge length,

with a cross sectional area of 2x1 mm^2 were cut using electro discharge wire cutting machine (EDM), while cylindrical compression test samples with 6 mm diameter and 10.5 mm height were cut using spark electrode cutting. Tensile testing was done at room temperature with a strain rate of $6x10^{-5}$/sec and at 800 ^oC, 900 ^oC and 1000^oC respectively with a strain rate of 1x 10^{-4} /sec. Compression testing was done at room temperature, with a strain rate of approximately 8 x 10^{-5} /sec and 1.16 x 10^{-4} /sec at 900^oC.

3.3 Microstructure and Thermal Behaviour of the Ball milled Powders

The XRD patterns of mixed and milled powders (Figure.3.1) showed only the Ti and Al peaks and no evidence of the formation of intermetallics during milling for up to 12 hours. With increasing milling time, the XRD peak intensities of both Ti, Al phases decreased, and the Al peaks became small after 12 hrs of milling. The XRD peaks of Ti and Al phases also became clearly more broadened with increasing milling time, indicating the grain sizes of both phases decreased significantly.

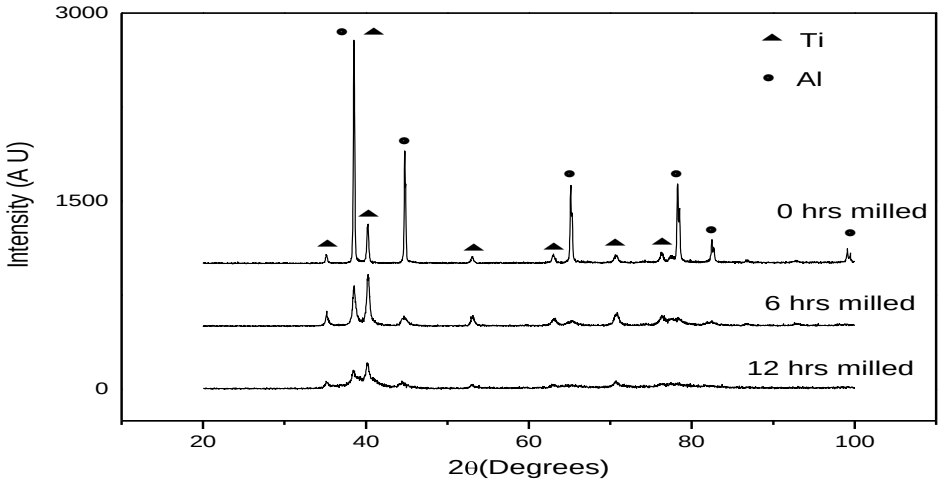

Figure 3.1: XRD patterns of the 0 hr, 6 hr and 12 hr milled powders

The average grain sizes of the Ti and Al phases were estimated using the Scherrer equation $t = 0.9\lambda / B\cos\theta$ [1], where t the diameter of the crystal, λ the wave length of the CuK_α radiation, B the broadening of diffraction line measured at half its maximum intensity and 'θ' the angle of the diffraction peak. The grain sizes,

calculated using the above equation were found to be approximately 42 nm for Ti, 35 nm for Al after 6hrs and 28 and 22nm after 12hrs of milling respectively. The cross sectional morphology of the mixed and milled powder particles as a function of milling time is shown in Figure. 3.2.

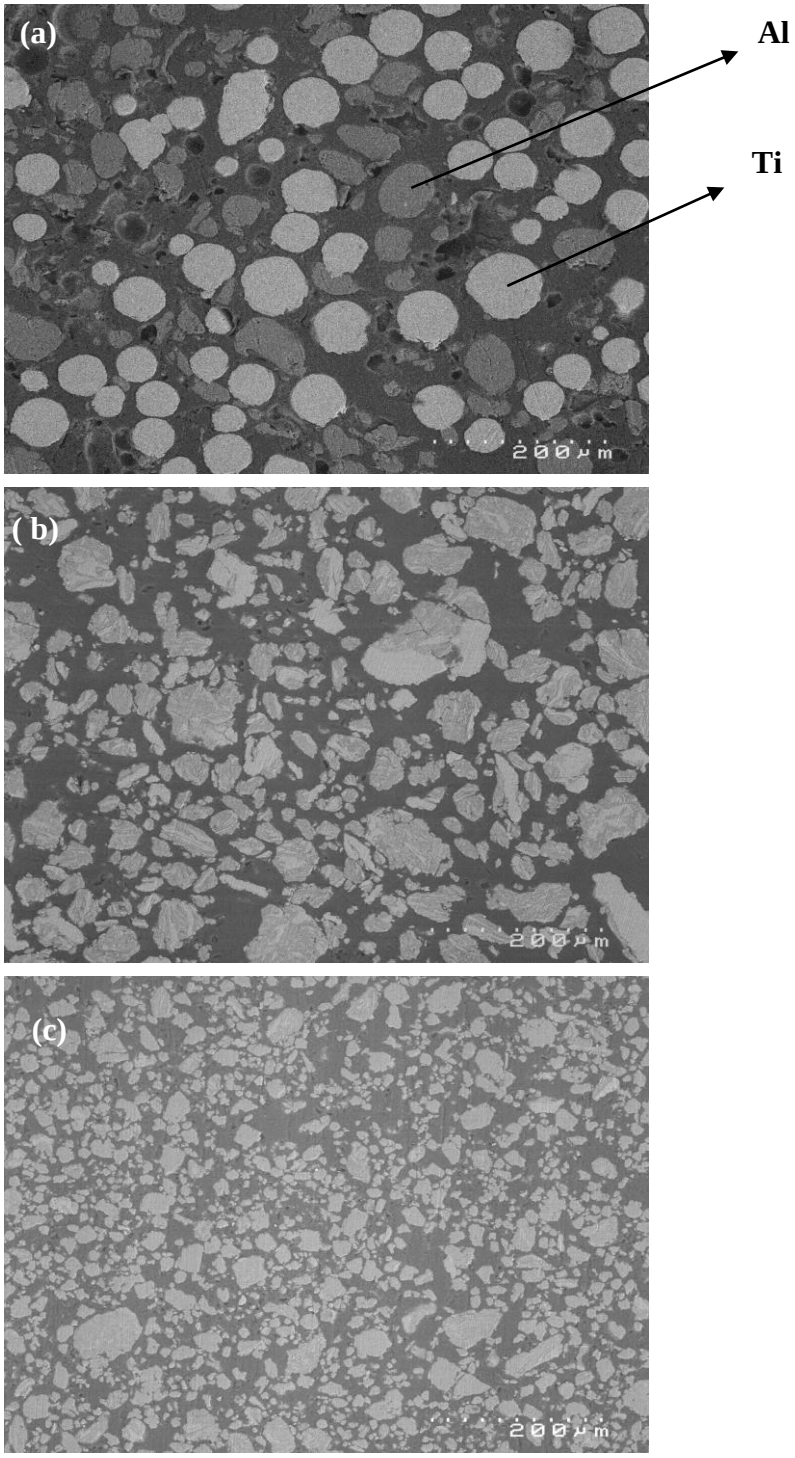

Figure 3.2: SEM back scattered electron images of the cross sections of the powder particles in (a) mixed powder; (b) 6 hours milled powder; and (c) 12 hours milled powder.

Ti and Al powder particles remained spherical after mixing for 6 hrs (Figure 3.2 (a)). The size and shapes of the powder particles changed after 6 hrs of milling, Al and Ti phases were incorporated into each of the powder particles (Figure 3.2 (b)). Further milling of the powder to 12 hrs led to a decrease in the sizes of the powder particles as shown in the Figure 3.2 (c). The effect of milling time on the composite particle structure has been explained below.

After 6 hrs of milling the powder particles consisted of two types of powder particles: (a) Layered composite Ti/Al/Cr composite; (b) Ti rich powder particles (Figure 3.3 (a) & (b)). Although the Ti rich powder particles were observed, the percentage of the layered composite particles was found to be slightly more after 6 hr of milling.

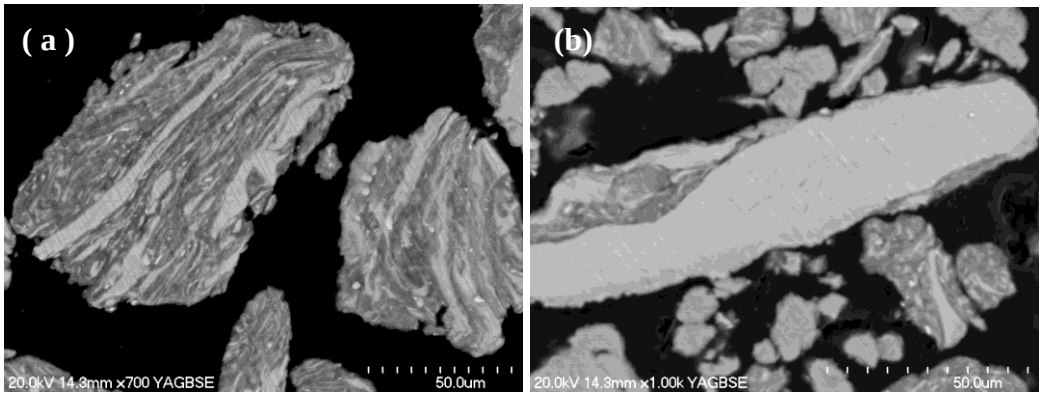

Figure 3.3: Cross section of 6hrs milled powder particle (a) layered Ti/Al/Cr composite powder particles; (b) Ti rich powder particles.

As the milling time increased to 12 hrs, the structure of the powder particles has changed considerably. The powder particles consisted of three types: (i) Layered composite Ti/Al/Cr composite; (ii) Composite powder particles in which no layered structure was observed; and (iii) Ti rich powder particles. The powder particles are shown in the Figure 3.4. It was observed that the increase in milling time to 12 hrs has resulted in the disappearance of the layered composite structure in most of the particles leading to the composite powder particles without layered structure. The sticking was found to be pronounced, after 12 hrs milling as compared to that after 6 hrs milling. After 12 hrs of milling a negligible amount of loose powder was observed.

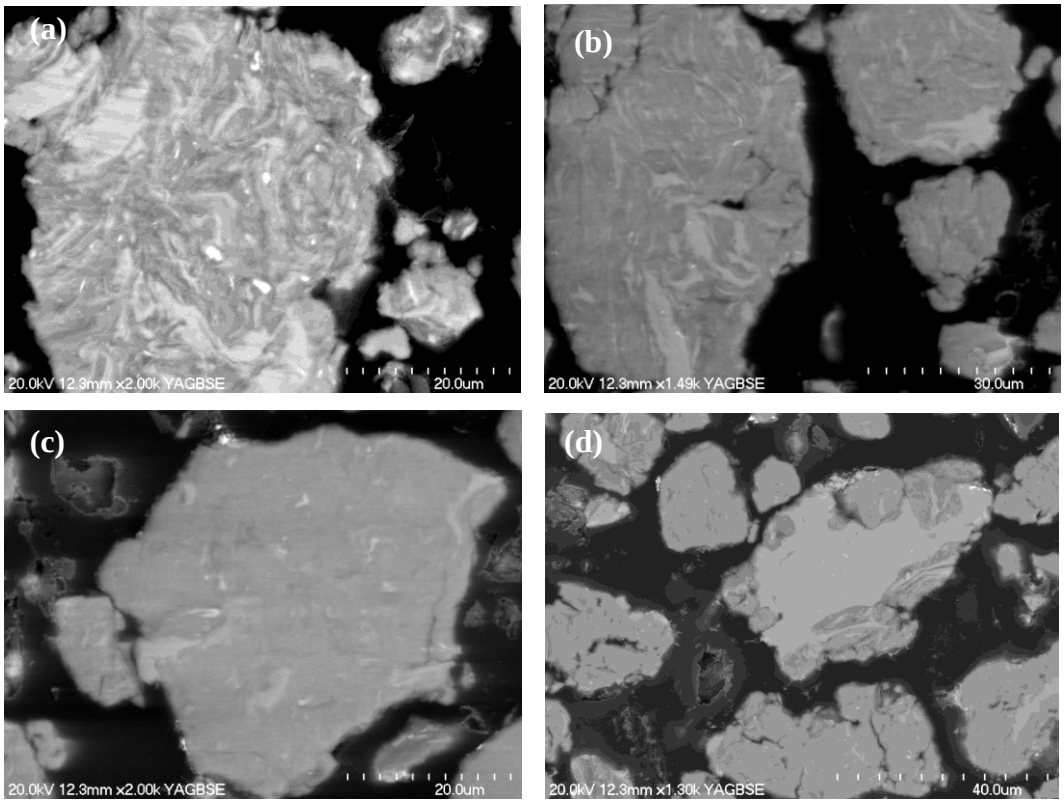

Figure 3.4: Cross section of 12hrs milled powder particle (a) & (b) layered Ti/Al/Cr composite powder particles; (c) composite powder particle without layered structure; and (d) Ti rich powder particle.

Further milling of the powders has not been done, due to the considerable amount of sticking which was observed after 12 hrs of milling. Although PCA was used, sticking of the powders was observed even after 6 hrs of milling, but the effect was much pronounced after 12 hrs of milling, in which a negligible amount of loose powder was found. The oxygen content in the samples was found to increase with milling time, being 0.3% after 0 hr milling and reaching 0.7% after 12 hrs milling. The increase in the oxygen content after different milling times is due to the particle size effect. Since the smaller the particle size, the larger is the surface area of the powder particle available for picking up oxygen during passivation of the milled powders. This resulted in higher oxygen content in the powders after 12 hrs milling.

The particle size distribution as a function of milling time (Figure 3.5) showed that the particle mean diameter D (V, 0.5) was 64.9 μm, 45.3 and 26.7 μm after 0, 6, 12 hrs of milling, respectively. The fraction of the particles above 75 μm also decreased drastically after 12hrs of mixing, which is in accordance with the

microstructural study of the powder particles, using SEM. Since a negligible amount of free powder was observed after 12 hrs milling the particle size distribution include the powder produced by wet milling of the material stuck on the wall of the milling vial.

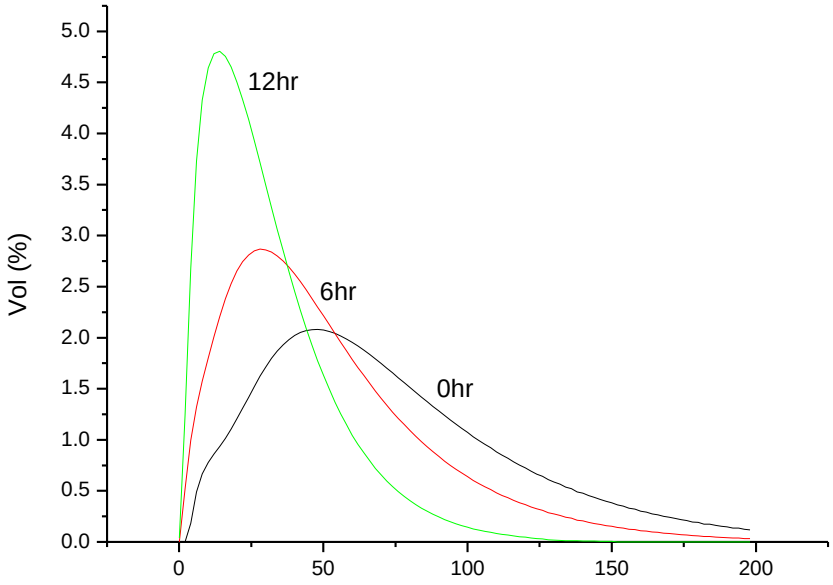

Figure 3.5: Particle size distribution of 0, 6 and 12 hrs milled powders.

The mechanical milling of the powders had a significant effect on the thermal behaviour of the powders as shown in the Figure 3.6. The DTA traces of the mixed powders showed an endothermic peak at approximately 660^{o}C, which is due to aluminium melting, and an exothermic peak at 810^{o}C resulting from the reaction between molten Al and Ti, which causes the formation of $TiAl_3$. While the DTA traces of the 6 hrs and 12 hrs milled powders showed no sharp peak. The solid state reaction occurred in the milled samples at much lower temperature, when compared to the unmilled samples. A broad peak in the temperature range of 300 – 650 °C was observed, but no endothermic peaks corresponding to the melting of Al (Figure 3.6), was shown. This confirmed that the Al was completely consumed by the reactions that occur during mechanical milling and heating. The large peak gave indication that a few exothermic reactions were occurring in that particular temperature range and was expected to be due to two reasons: (a) relaxation of stress due to strain hardening during milling; (b) solid state reaction between Al and Ti. The strain hardening in the as mixed powder was not expected

due to the low speed rotation (100rpm) used, resulting in the absence of high energy mechanical impacts. On the other hand the high energy mechanical milling for a duration of 6hr and 12hrs is expected to induce strain hardening in the sample, indicating that the broad peak is likely due to combination of solid sate reactions and the relaxation of the stresses caused by mechanical milling.

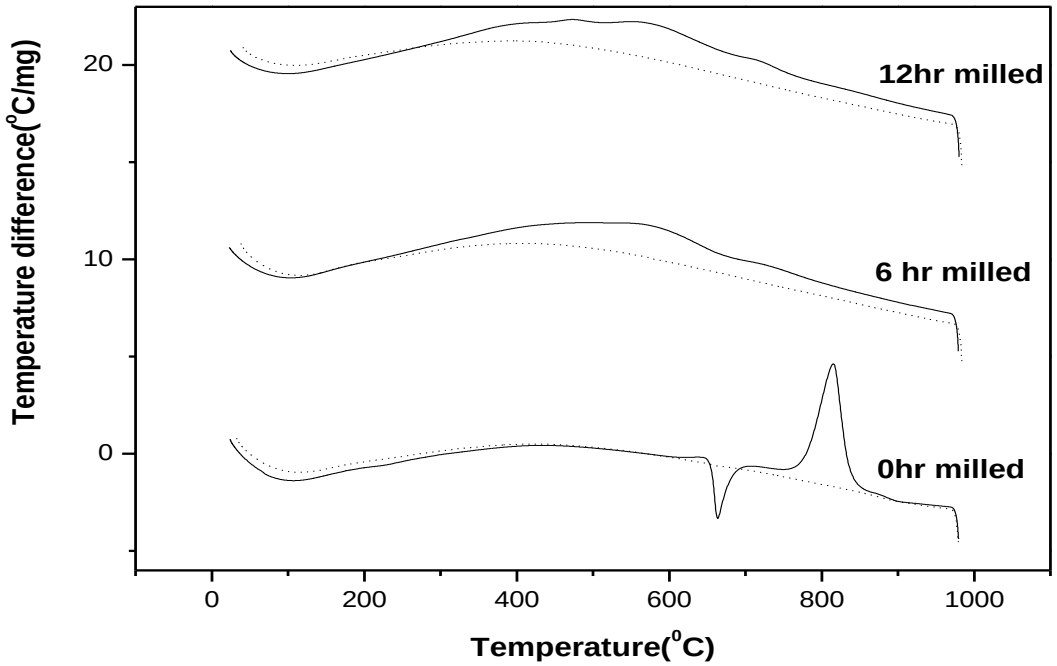

Figure 3.6: DTA curves of the 0, 6 and 12 hrs of milled powders (dotted lines are the DTA traces of the samples after the second run)

Although the reaction kinetics for the formation of TiAl during thermal treatment has been studied by a few researchers, the mechanism of the formation is still not clear. A few studies have demonstrated that the phase transition into the intermetallic TiAl phase proceeds through the formation of the disordered structure during milling, in which the reaction temperature depends on the Ti and Al grain size and the composite structure after milling [2, 3]. In the present case, the decrease in reaction temperature after mechanical milling can be attributed to the significantly refined Al/Ti composite structure obtained after milling. The reaction to form intermetallic phases was found to be complete, since no peaks were observed in the DTA traces of the samples after the second run, which are shown by the dotted lines in Figure 3.6. Since the formation and the refinement of composite structure during milling is essential to reduce the diffusion distance for the post milling reactions between Ti and Al, the finer structures are more

favourable for the reactions and diffusion during sintering [4]. In the present case the presence of Ti rich powder particles in the 12 hrs milled powder, which was used for consolidation, was found to affect the diffusion mechanism. The XRD patterns of the powders produced after DTA analysis of the unmilled powder (Figure 3.7) showed Ti, $TiAl_3$ and TiAl phases, but not Ti_3Al phase. The DTA analysis along with XRD results before and after DTA further confirmed that mechanical alloying did not occur during milling. The formation of composite structure after milling is found to be favourable to promote the formation of Ti_3Al phase instead of $TiAl_3$ phase. $TiAl_3$ phase is not acceptable in the final microstructure, because of its detrimental effect on the mechanical properties of TiAl based alloys.

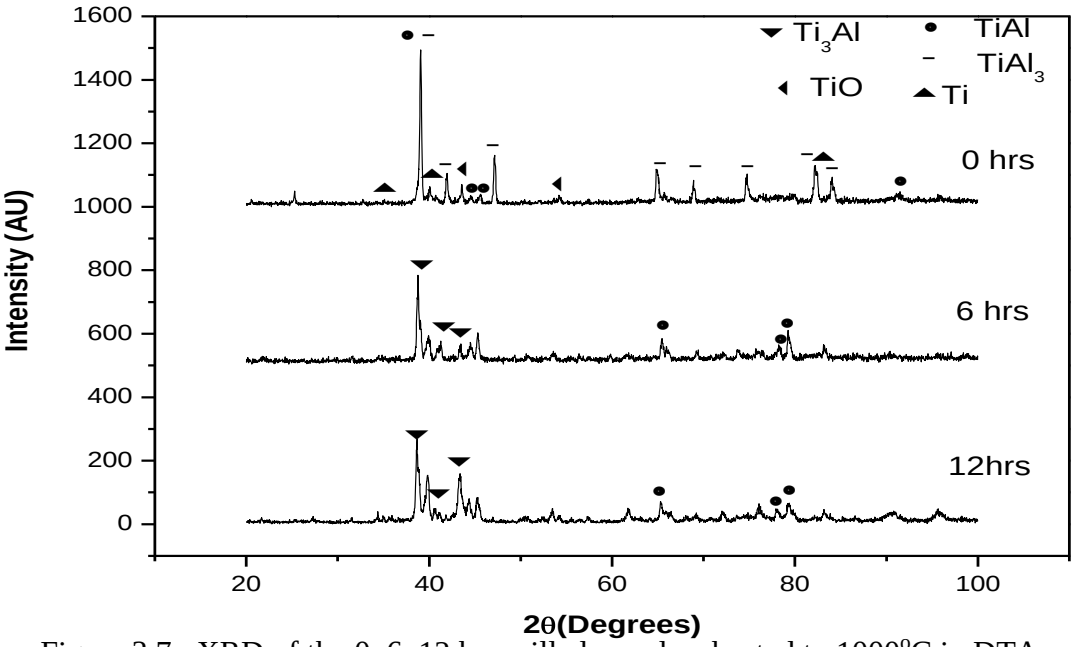

Figure 3.7: XRD of the 0, 6, 12 hrs milled powders heated to 1000^{o}C in DTA.

The microhardness of the Ti and Al phases in the mixed and milled powders were compared. The hardness values of the Ti and Al particles in the as mixed powders were 230 HV and 160 HV respectively. The microhardness increased as the milling time increased to 6 hrs, and was found to be in the range of 240 – 350 HV. This is attributed to the strain hardening caused by mechanical milling. Although some of the particles in the 12 hrs milled powder were rich in Ti phase, the hardness for most of the particles was found to be between 300-330 HV. This was mainly due to the increase in the fraction of the Ti/Al/Cr composite particles. The

hardness of the milled powder particles plays an important role in the consolidation characteristics of the material. The lower the hardness, the better are the consolidation characteristics of the material. The fairly low hardness values of the particles in the 12 hrs milled powder indicated that the powders were having good consolidation characteristics. A green density of 60% after cold pressing and 72% after cold isostatic pressing were achieved in powder compacting.

3. 4 Microstructural Characterization of as-HIPed Sample

The shapes of the can before and after HIP are shown in Figure 3.8. A 20% volume shrinkage of the can was noticed, indicting that the HIP was successful. After HIP, the can was chipped off easily, indicating no reaction between the stainless steel can material and the consolidated sample inside the can. The XRD pattern of the HIPed sample (Figure 3.9) showed γ, α_2 and Ti peaks. The XRD peaks were fairly broad indicating that the grains were at the ultrafine grained level.

The optical microscopy image of the microstructure (Figure 3.10) shows white, grey and dark regions which are Ti rich α_2 phase and the black background is γ phase. This assumption was made by measuring microhardness at different regions of the sample. The micro hardness of most white and grey regions was found to be between 780-820 HV, which was higher than that of dark regions, which had values ranging from 580-615 HV. A few grey regions were found to have same hardness values as that of dark regions. Although it was difficult to determine the fractions of different phases by this method, a preliminary understanding of the phases with different hardness values was obtained. While the macrohardness of the sample was found to be ~ 42 Rc, which is quite low, confirming the presence of porosity in the sample. The HIPed material was found to have a density of ~ 95%.

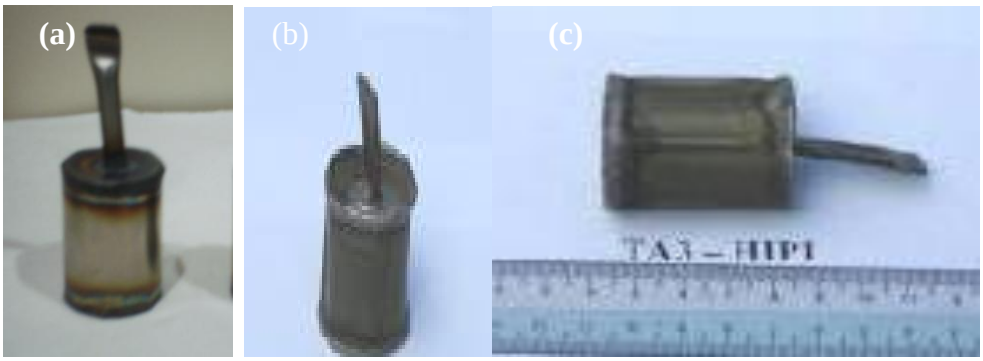

Figure 3.8: Images of the can; (a) before; and (b) & (c) after HIP

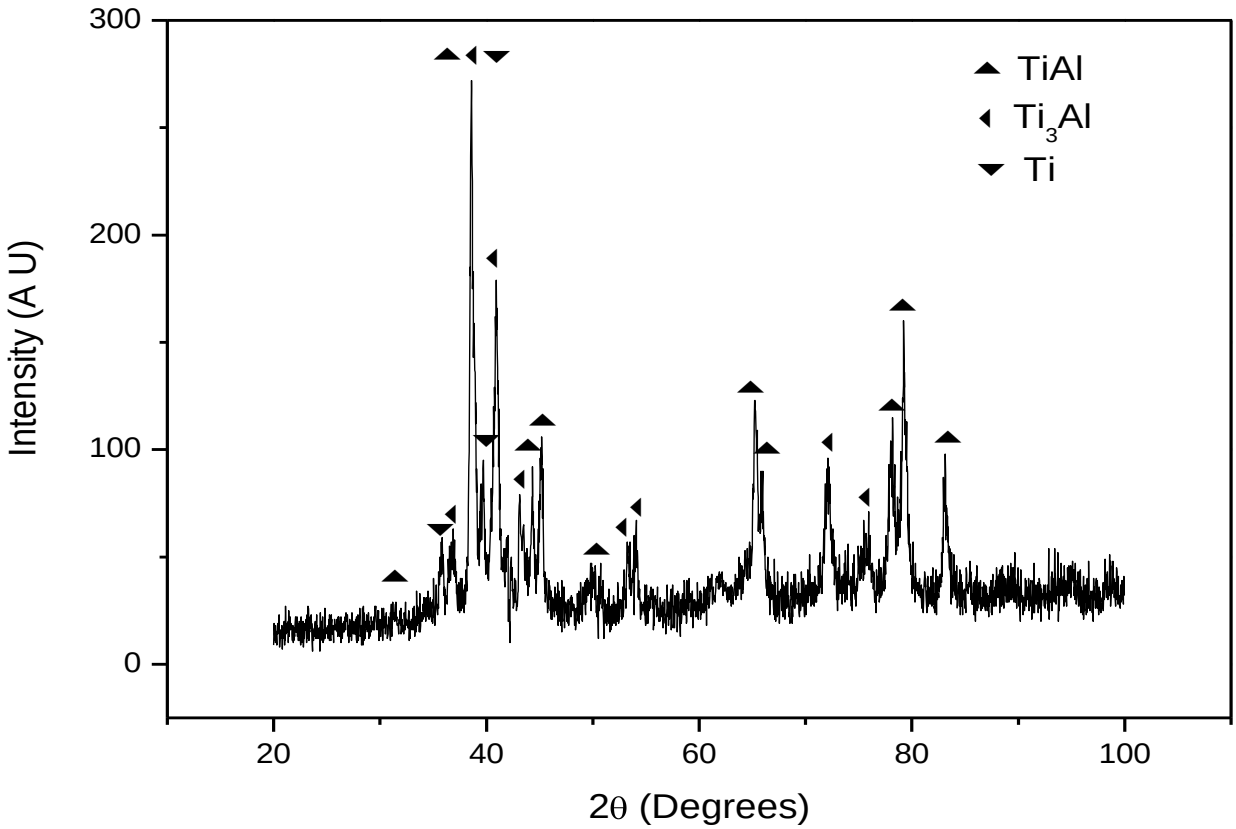

Figure 3.9: XRD of the as-HIPed bulk material (HIPed for 2hrs at 1000^{o}C).

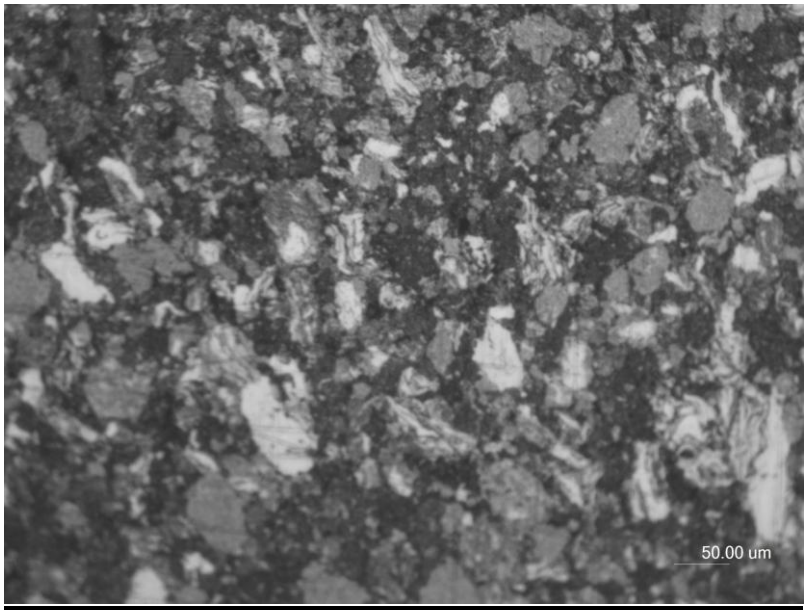

Figure 3.10: Optical micrograph of the etched surface of the as-HIPed sample

The SEM back scattered electron examination of the microstructure of the as-HIPed sample showed the presence of Ti rich regions and pores (Figure 3.11).

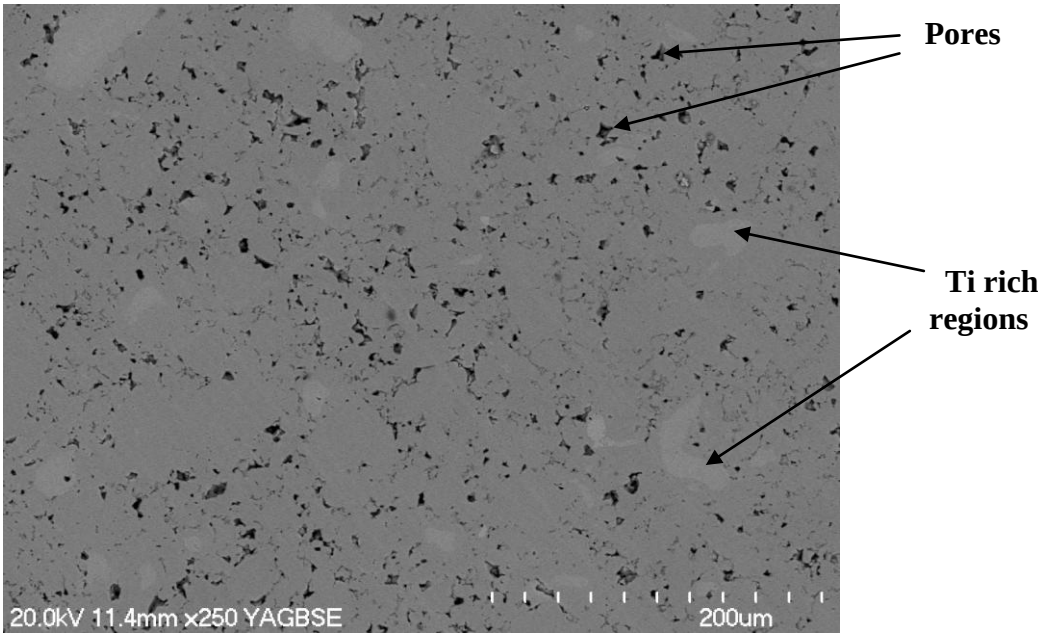

Figure 3.11: SEM Back scattered electron image of the as-HIPed sample showing the distribution of Ti rich regions and the pores.

The preliminary TEM examination of the microstructure of the as-HIPed sample have confirmed UFG microstructure of the alloy. Figure 3.12 shows a bright field TEM image of the specimen after room temperature compression test, which revealed that the sample had an UFG microstructure, with equiaxed grains, with

grain sizes in the range of 200 – 600 nm, a very small fraction of the grains were large being ~1 μm in diameter. Although trials have been done to produce TEM specimens from the as HIPed sample, using jet polishing technique, the quality of the TEM specimens produced was not sufficiently good. However, since room temperature compression testing is unlikely to cause any microstructural change, the microstructure shown in Figure 3.12 represents the microstructure of as-HIPed sample.

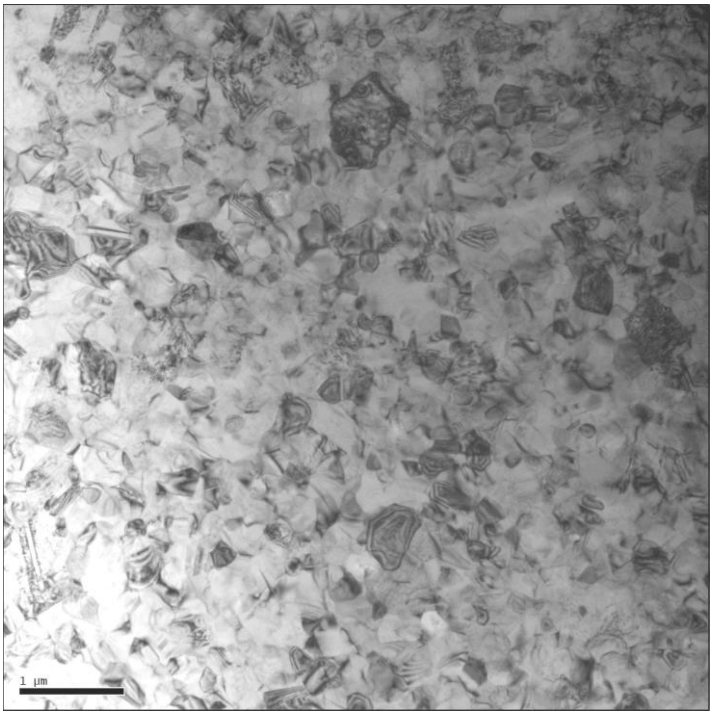

Figure 3.12: Bright field TEM image showing microstructure of the specimen after compression test at room temperature.

3.5 Mechanical Properties

3.5.1 Tensile properties

Room temperature (RT) tensile testing showed fracture strength of approximately 100 MPa, with no sign of yielding (Figure 3.13(a)). The tensile tests were also conducted at 800°C, 900°C and 1000°C. At 800°C the samples showed true strains between 0.38 to 0.43, with yield strengths between 84 - 90 MPa. Almost steady state flow was observed with negligible strain hardening at this temperature, Figure 3.13(b). While at 900°C, the sample started yielding at a considerably low stress, in the range of 55-58 MPa. The elongation to fracture

was in the range of 70-80%, indicating a true strain between 0.55-0.58. Slight work hardening was observed at this temperature (Figure 3.13 (c)). The samples tested at 1000°C, were heavily oxidised, and thus the elongation to fracture of the samples was only in the range of 0-12%, (Figure 3.13 (d)).

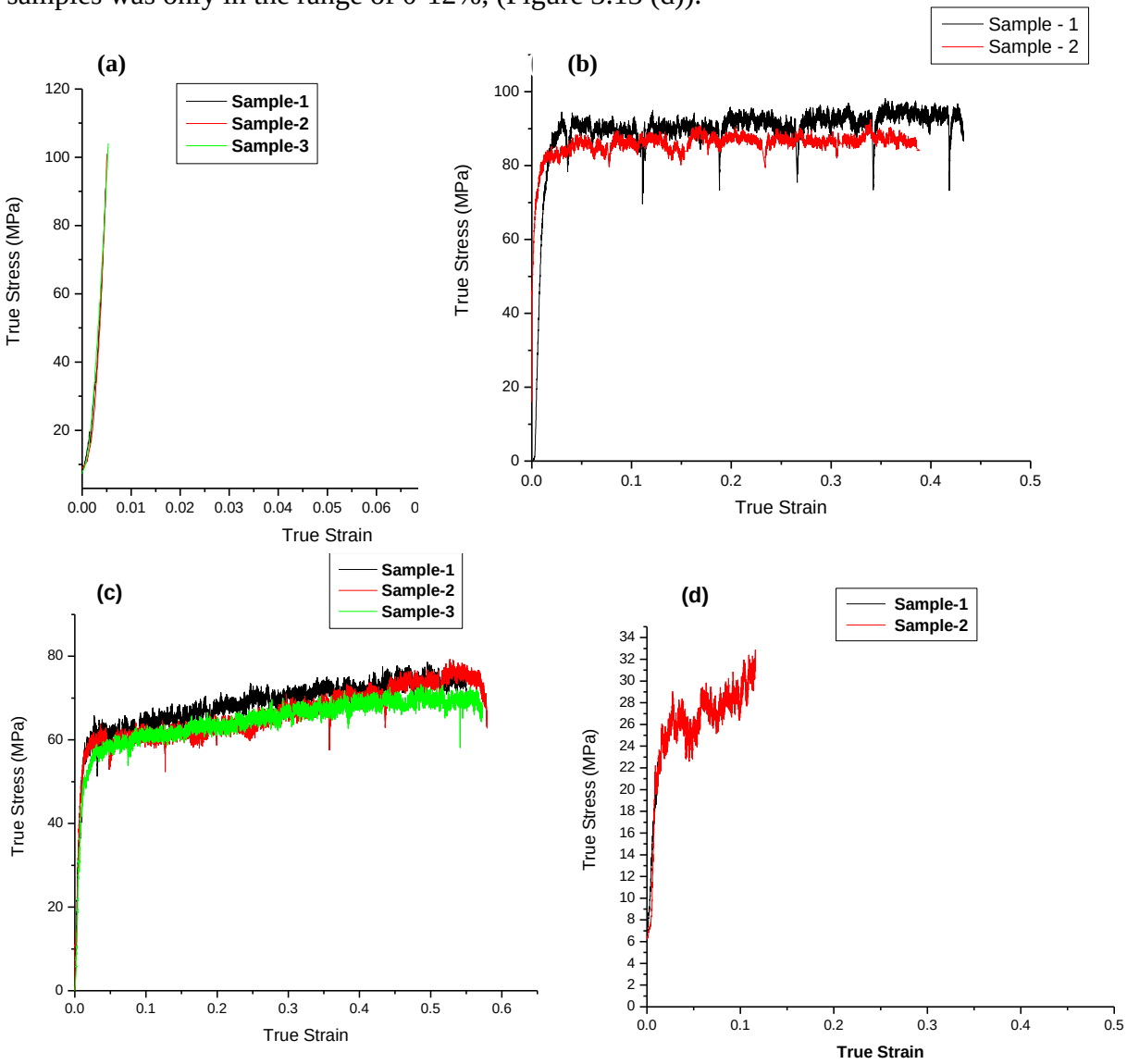

Figure 3.13: True stress true strain curves of the specimens tested at (a) room temperature (b) 800°C (c) 900° C (d) 1000°C.

As the oxidation resistance of the TiAl alloys is very poor at high temperatures (≥800°C) [5,6], the mechanical properties are affected adversely in most of the cases, particularly the TiAl alloys without Nb additions were found to be more prone to oxidation [7]. In the present study the tensile properties of the Ti-47Al-2Cr alloy tested at 1000°C, was found to be affected by oxidation, resulting in poor mechanical properties. The samples after tensile testing at

different temperatures are shown in Figure 3.14 (a)-(c) and the tensile mechanical properties at different temperatures are presented in Table 3.1.

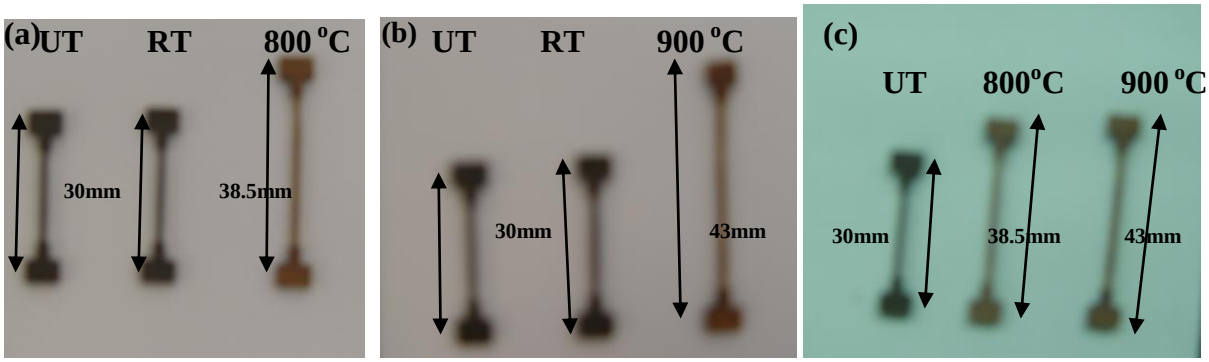

Figure 3.14: (a), (b) & (c) Specimens after tensile testing at different temperatures. (UT untested, RT room temperature tested)

Table 3.1: Tensile mechanical properties of the Ti-47Al-2Cr (at %) alloy tested at different temperatures

Property	Room temperature	800°C	900°C	1000°C
Yield Strength (MPa)	-	84-90 (MPa)	55-58 (MPa)	22MPa
True strain	0	0.38-0.43	0.55-0.58	0-0.1
True fracture Stress (MPa)	~ 100MPa	87-93(MPa)	65- 68 (MPa)	22- 32(MPa)

After tensile testing, the microstructure and the fracture surfaces of the tested specimens were examined to gain some understanding on how the material deforms and fractures. In the case of room temperature tensile tested specimens, the microstructure resembled the as-HIPped microstructure (Figure 3.15(a)). The morphology of the grains did not change and no noticeable amount of deformation was observed. It was observed that the fracture mode of the samples tested at room temperature was quasi cleavage type, which is more brittle in nature. The dark spots are pores ("A" in Figure 3.15(b)), which mainly acted as crack initiation and propagation points, and the dark regions ("B" in Figure 3.15(b)) are

likely the patches of original particle surfaces which were not atomically bonded to the neighbouring particles. It is expected that the easy separation of the powder particles associated with the lack of atomic bonding also assists formation of the pores under tensile stress which in turn accelerates crack propagation.

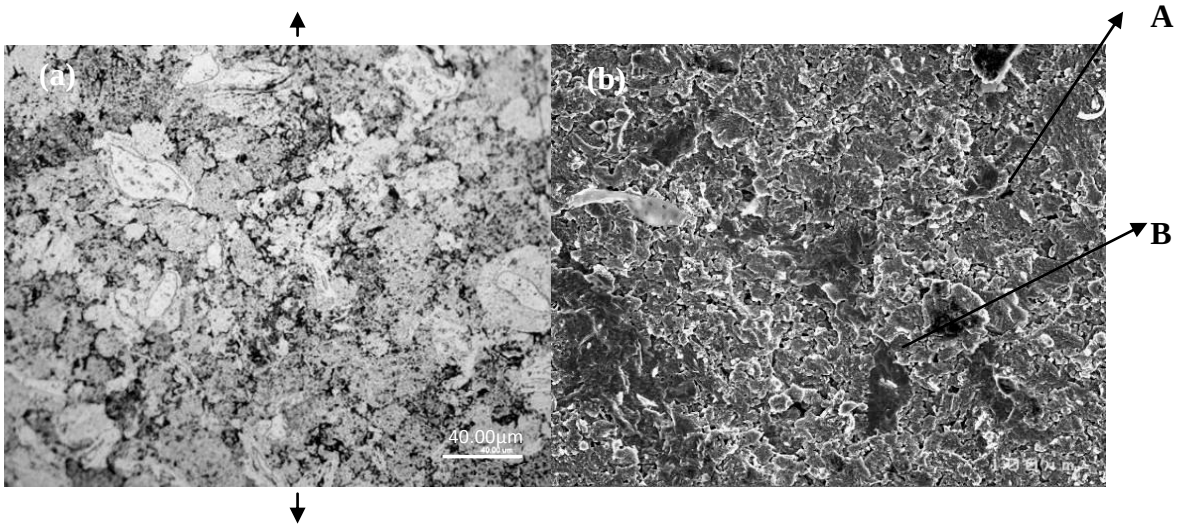

Figure 3.15: (a) Microstructure of the longitudinal section of the tensile tested sample; and (b) Fractured surface after room temperature tensile testing (arrows indicate tensile test direction)

In contrast, for the samples tested at 800 and 900°C, the longitudinal section showed that the grains and pores were elongated, indicating they were heavily sheared during tensile testing (Figure 3.16(a) & 3.17(a)). For the samples tested at 900^{o}C the elongated grains were aligned at 45° to the tensile axis. The resolved shear stress is expected to be at its maximum at 45°. The fracture surfaces of the samples tested both at 800^{o}C and 900 °C (Figures 3.16(b) & 3.17(b)) showed a fibrous type of fracture, which is ductile in nature. The sizes of the pores slightly increased with increasing testing temperature from 800 to 900^{o}C. This is expected due to the coalescence of the residual pores, and also thermally induced porosity cannot be ruled out.

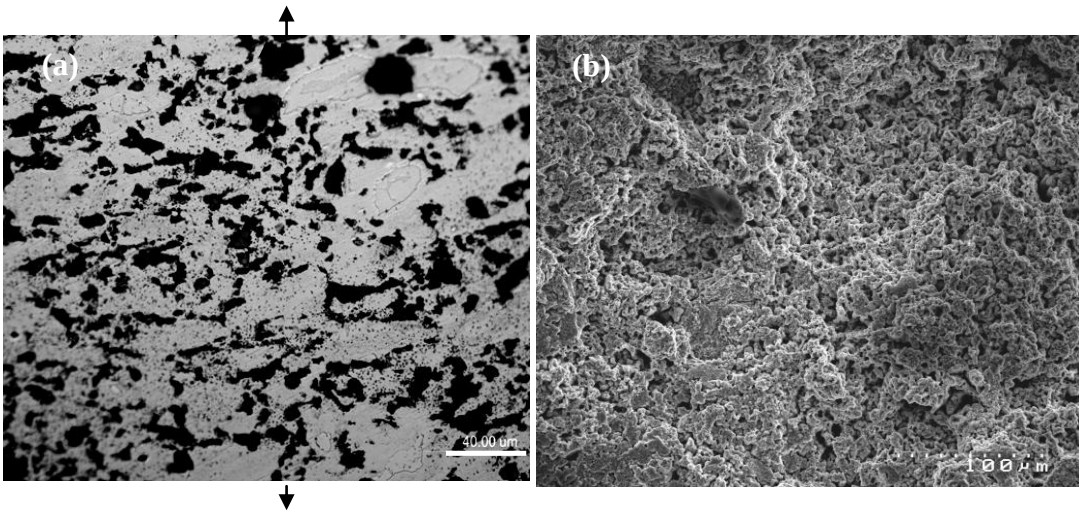

Figure 3.16: (a) microstructure of the etched longitudinal section of the tensile tested sample at 800^{o}C; and (b) fractured surface after tensile testing at 800^{o}C (arrows indicate tensile test direction)

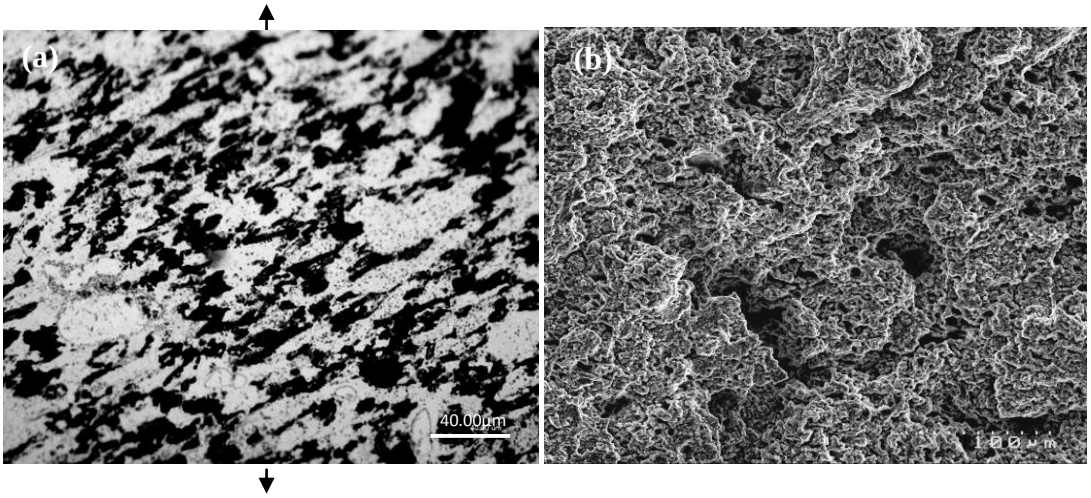

Figure 3.17: (a) microstructure of the longitudinal section of the sample tensile tested at 900^{o}C; (b) fractured surface after tensile testing at 900^{o}C (arrows indicate tensile test direction)

The low room temperature tensile strength is probably due to the following factors. Firstly the geometry of the tensile sample, which is originally designed for high temperature testing, may have caused some stress concentration and thus premature fracture. This is evidenced by the fracture site of all room temperature test samples fractured at the edge of the grip, as indicated by the arrow in Figure 3.18 (a), but the high temperature tensile tested samples fractured inside the gauge length as shown in Figure 3.18 (b). The corner at the locations where the width of the sample changes acted as a notch which introduces a triaxial state of stress. Secondly the high porosity level present in the samples obviously decreased the

tensile strength. Thirdly, the low level of atomic bonding between particles in the sample assists the formation of cavities for crack propagation.

On the other hand, the low elevated temperature tensile strength of the alloy likely resulted from the high porosity level and low level of atomic bonding between powder particles, but not from the geometry of the tensile sample. Although the geometry of the sample was not expected to affect elevated temperature tensile strength, but it is expected to slightly affect the ductility at elevated temperatures. This paved the way to modify the tensile sample profile, having a sharp corner to a curvy corner. The modified design of the tensile samples have been used in the experiments presented in Chapters 4 and 5.

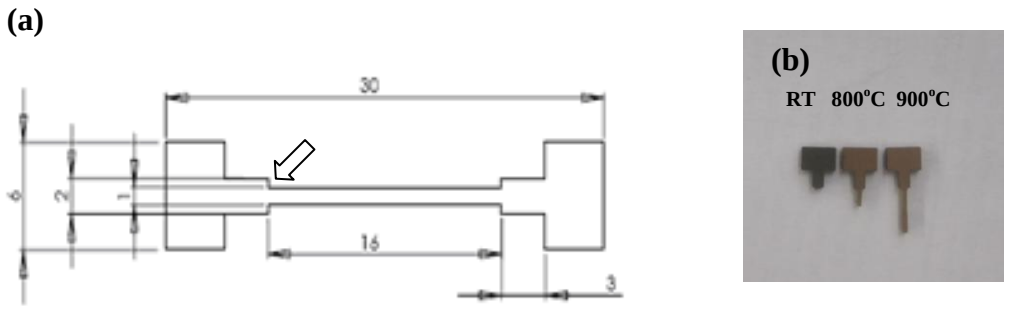

Figure 3.18: (a) Profile of the tensile tested samples; and (b) Fractured sites after tensile testing

3.5.2 Compressive mechanical properties

The RT compression testing of the specimens cut from the HIPed sample showed that the sample had a compressive strength of around 1580 MPa, with yield strength of 1410 MPa and a plastic strain to fracture of around 1%. The true compressive stress strain curves are shown in the Figure 3.19(a). During compression testing the specimens were broken into multiple pieces, with a loud sound. The high compressive strength observed in the samples is mainly due to the UFG structure of the material. The samples before and after compression testing are shown in the Figures 3.19 (b) & (c). At 900°C the behaviour of the sample changed totally, showing an decrease in true compressive yield strength to around 33 MPa (Figure 3.20(a)). The samples were easily deformed to a true strain of ~ 0.7 without fracturing (Figure 3.20 (b)).

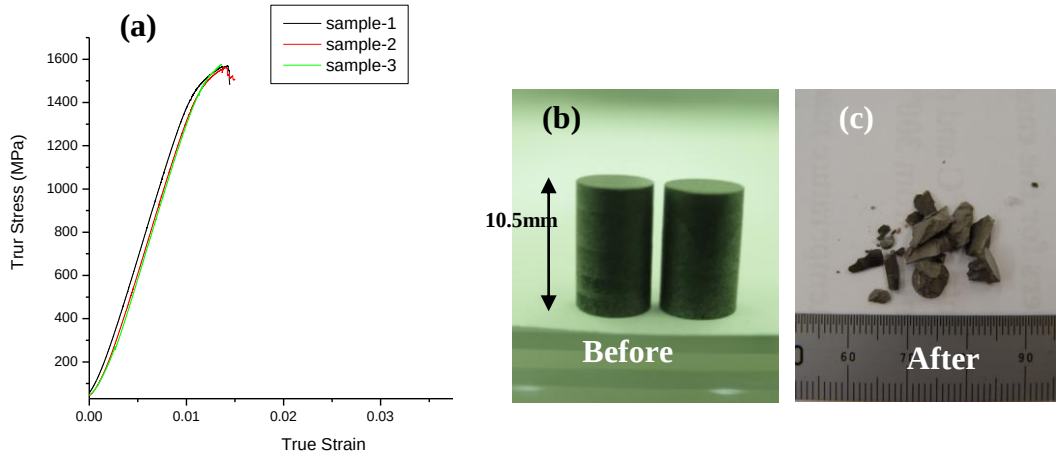

Figure 3.19: (a) compressive true stress true strain curves of the specimens tested at room temperature; (b) image of the sample before room temperature compression testing; and (c) fractured pieces after room temperature compression testing.

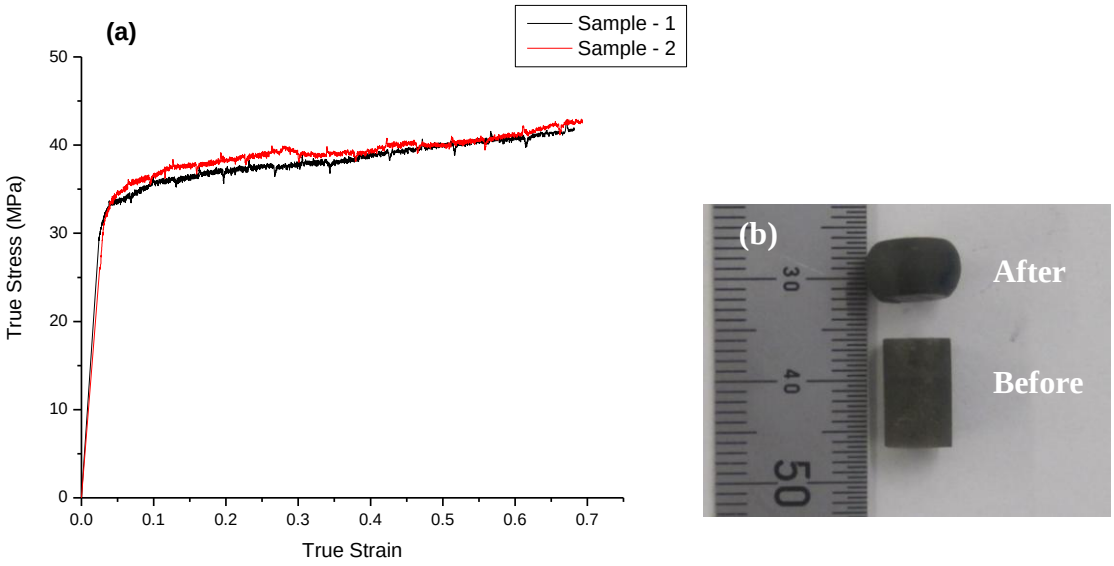

Figure 3.20: (a) compressive true stress true strain curves of the specimens tested at 900^{o}C; and (b) image of the specimens before and after compression testing at 900^{o}C.

A slight strain hardening was observed during the compression testing, and no cracking was observed in the samples after 50% height reduction, as shown in the Figures 3.21(a) & (b).

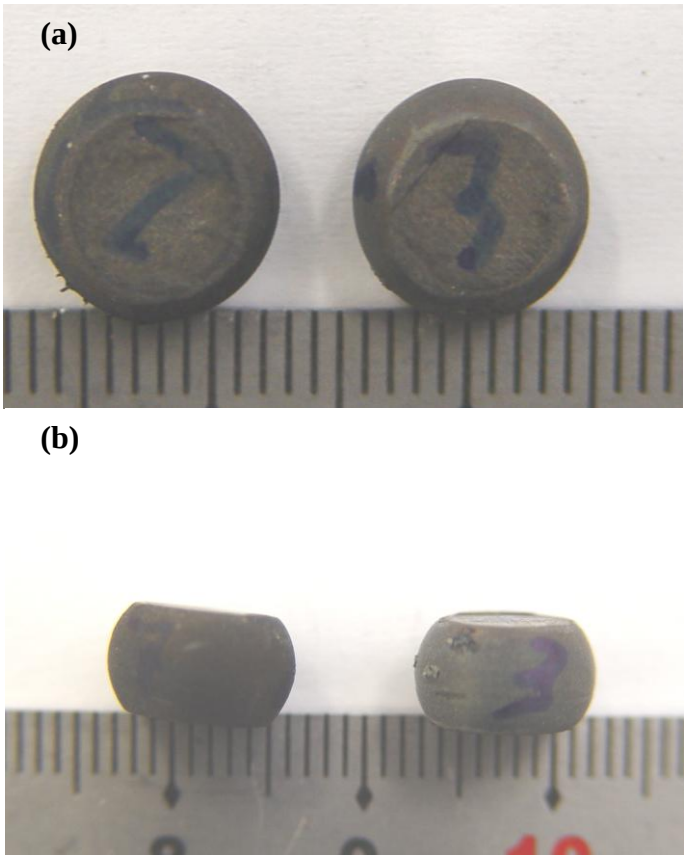

Figure 3.21: (a) & (b) images of the specimens after compression testing at 900^{o}C.

The microstructures of the cross sections of the samples after compression testing at room temperature resembled that of as-HIPed material (Figure 3.22(a)). However, a few regions have shown a tendency to elongate more as compared to other regions, indicating localized deformation. A mixture of elongated and equiaxed regions indicated that the material had certain phase regions, that underwent plastic deformation. After elevated temperature compression testing, the phases were found to be elongated in a direction normal to the compressive axis (Figure 3.22(b)). The shape and morphology of pores changed after compression testing. The pores were found to coalesce after room temperature compression testing, which played an important role in the fracture of the specimens, while at elevated temperatures, the size of the pores decreased, this behaviour is explained in section 3.5.3.

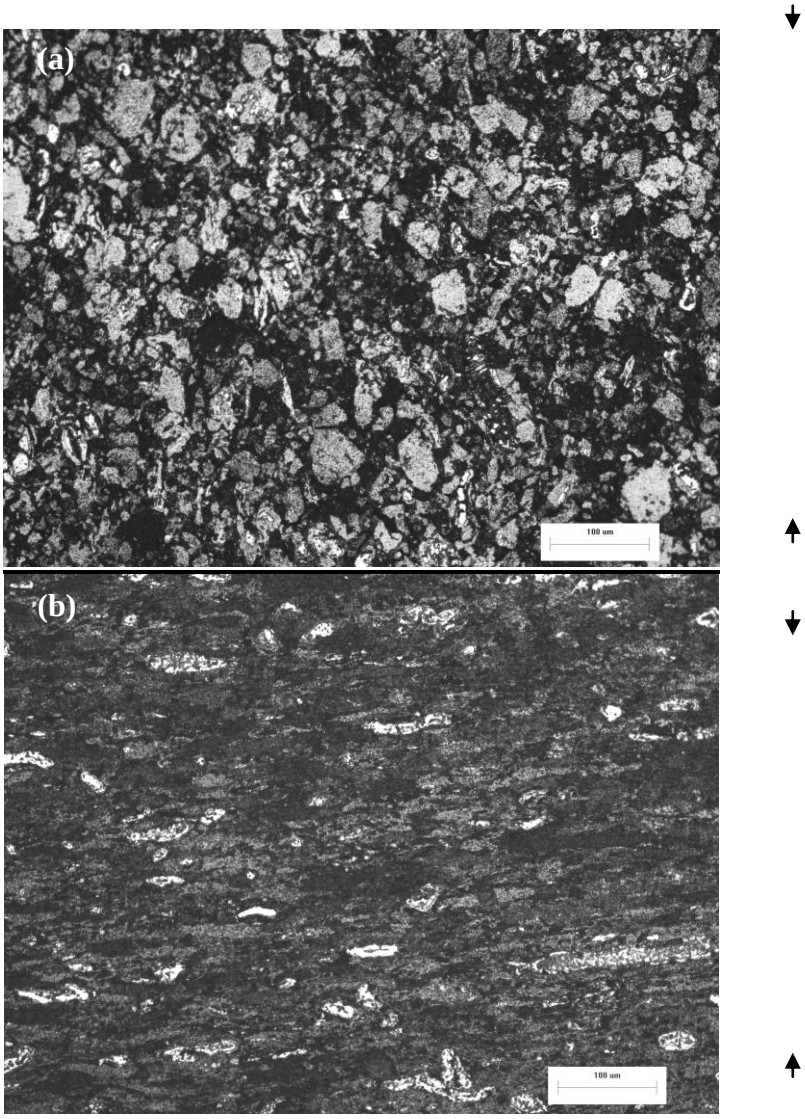

Figure 3.22: Images of the etched cross sections of the specimens after compression testing at (a) Room temperature and (b) $900^{O}C$ (arrows indicate direction of the compressive force)

As discussed above, the RT compression test, resulted in fracture of the samples into multiple pieces, with a little bit of plastic deformation. The fracture in the present case is depicted to originate from the microcracks in the specimen and then propagate resulting in specimen fracture. This is due to the microcracks which nucleate at pores, weak interparticle bonding sites and other defects, Figure 3.23, shows a crack running from inside to the outer surface. The cracks were found to propagate parallel to the compressive axis with applied load increasing. Some cracks were expected to propagate to the main crack or propagate and connect with each other and finally induce the specimen fracture. The multiple fracture paths observed, indicating that a lot of cracks were created prior to the

fracture. The fracture surface examination of the samples in some areas revealed river markings indicating a cleavage type of fracture (Figure 3.24(a)) and in some regions revealed a quasi cleavage type of fracture (Figure 3.24 (b)). Also a few regions revealed a fibrous type of fracture (Figure 3.24(c)), indicaing that in some regions plastic deformation recurred at microscopic scale.

At low temperatures the UFG based materials are characterized by high values of hardness and compressive yield strength, which can be explained by the classical Hall-petch equation and ultrafine grains. As the grain size decreases, the dislocation gliding and twinning as the prevailing deformation mechanisms are hampered by the fine meshed grain boundaries, present in the UFG alloys. At elevated temperatures, the behaviour has changed completely, the smaller the grain size of the specimen, the more and sharper the drop in the yield strength upon raising the temperature [8]. The decrease in the yield strength at elevated temperature has indicated favourable conditions for hot working of these materials in compression.

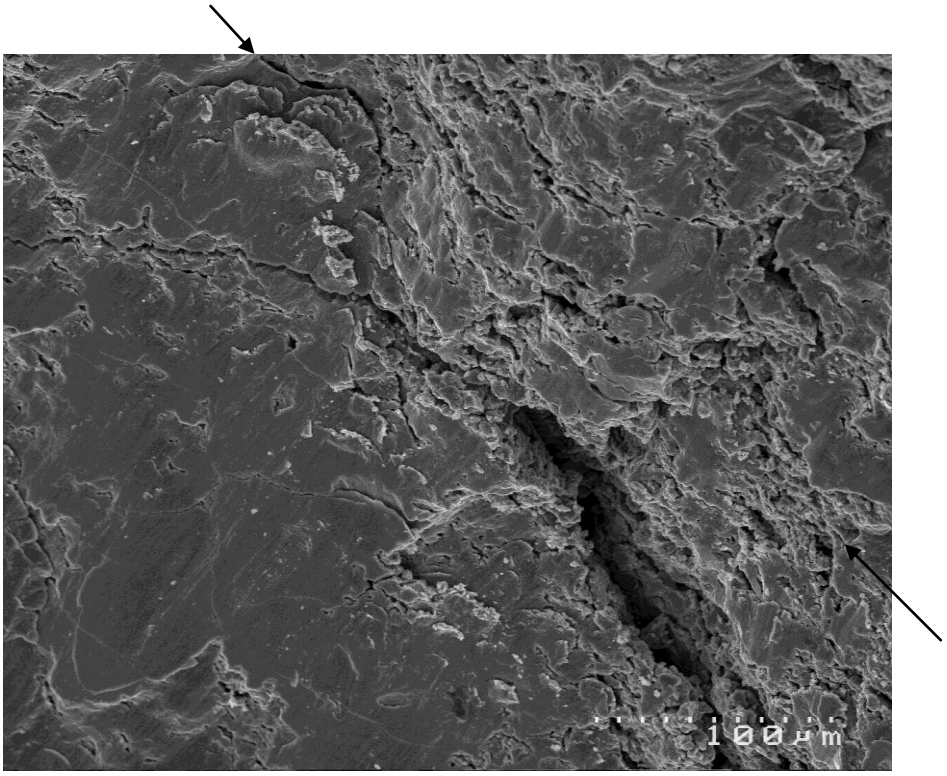

Figure 3.23: Fractured surfaces of the samples after compression testing showing crack propagation (arrows indicate the compressive direction).

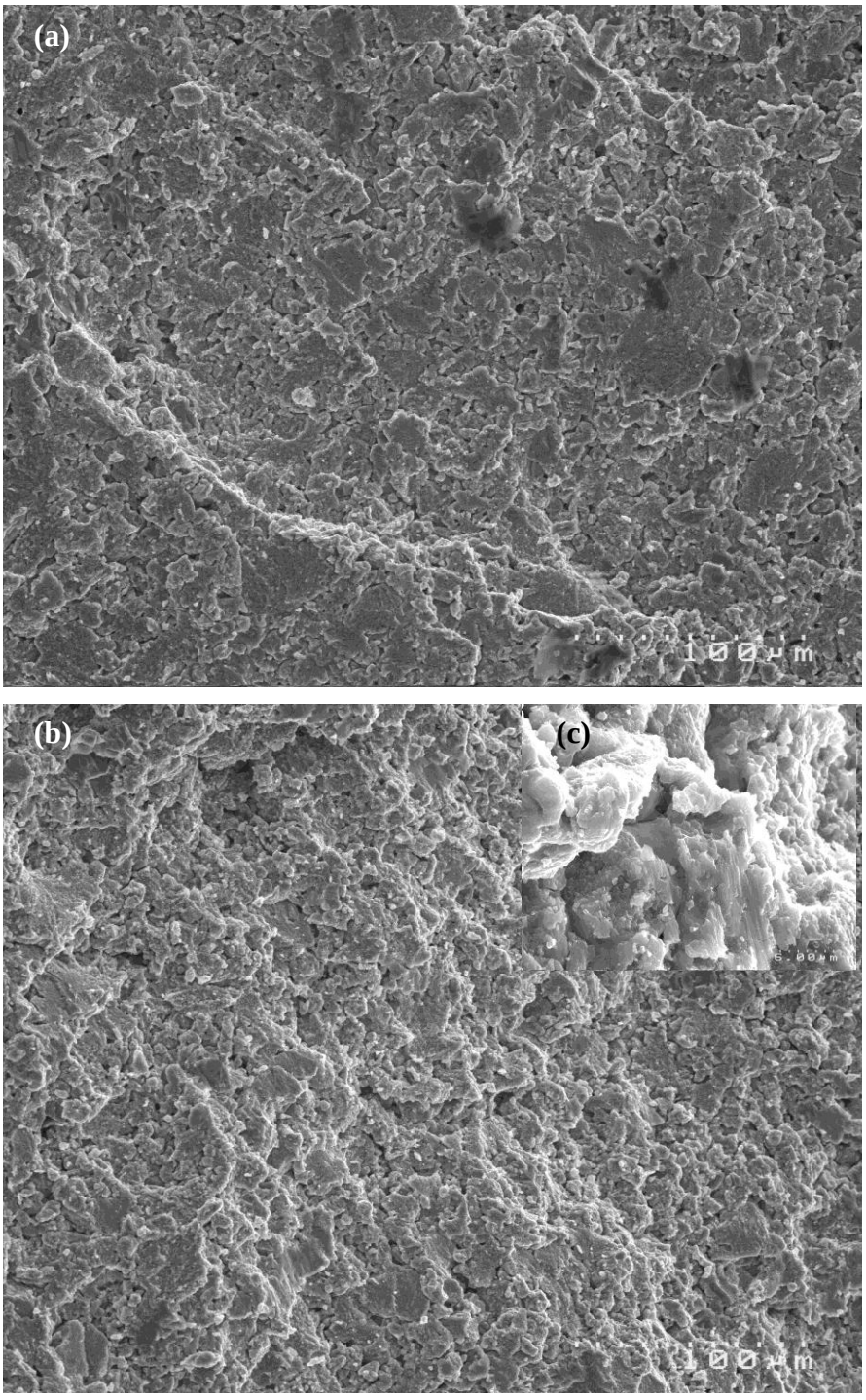

Figure 3.24: Fractured surfaces of the samples after compression testing: (a) quasi cleavage type of fracture; and (b) regions showing ductile behaviour; (c) ductile region.

3.5.3 Effect of porosity on the mechanical behaviour

The microstructures of the samples after deformation in compression and tension are compared with that of as-HIPed microstructure (Figure 3.25(a)). In the samples which are tested in tension at room temperature Figure 3.25(b), the pores size and distribution did not change when compared to as-HIPed microstructure, but the morphology changed after the RT compression testing (Figure 3.25(c)). Pores size has increased, which is expected due to the coalescence of the initial residual pores. Also a few cracks were developed due to the large amount of compressive load applied during the deformation, since a very small flaw inside the material is sufficient to fracture the material having high yield strength.

So the initial residual pores acted as crack initiation points, resulting in a premature failure in room temperature compression testing. After the yield point, the samples have deformed until the cracks have reached a critical size, after which macroscopic fracture was observed. This can be explained by the observation of an increase in the size and distribution of the cracks, in the sample which was subjected to a compression upto the maximum load which does not cause fracture.

After tensile testing at 900 ^{o}C the shape of the pores remained irregular, but the size was found to be slightly increased (Figure 3.25(d)) and to be aligned 45^{o} to the tensile force direction. After elevated temperature compression testing almost all the pores were closed, and the shape of remaining pores changed to spherical. This indicated that the shape of the pores changed from an initial irregular shape to a combination of irregular and elliptical shape after RT compression, and finally to a spherical shape after compression testing at 900^{o}C (Figure 3.25(e)). This indicated that pores in compressive deformation tend to take spherical shape.

In tensile testing the shape of the pores remained irregular after room temperature and high temperature tensile testing, but the sizes of the pores tend to increase slightly after tensile testing at 900^{o}C, which is expected due to the coalescence of residual pores.

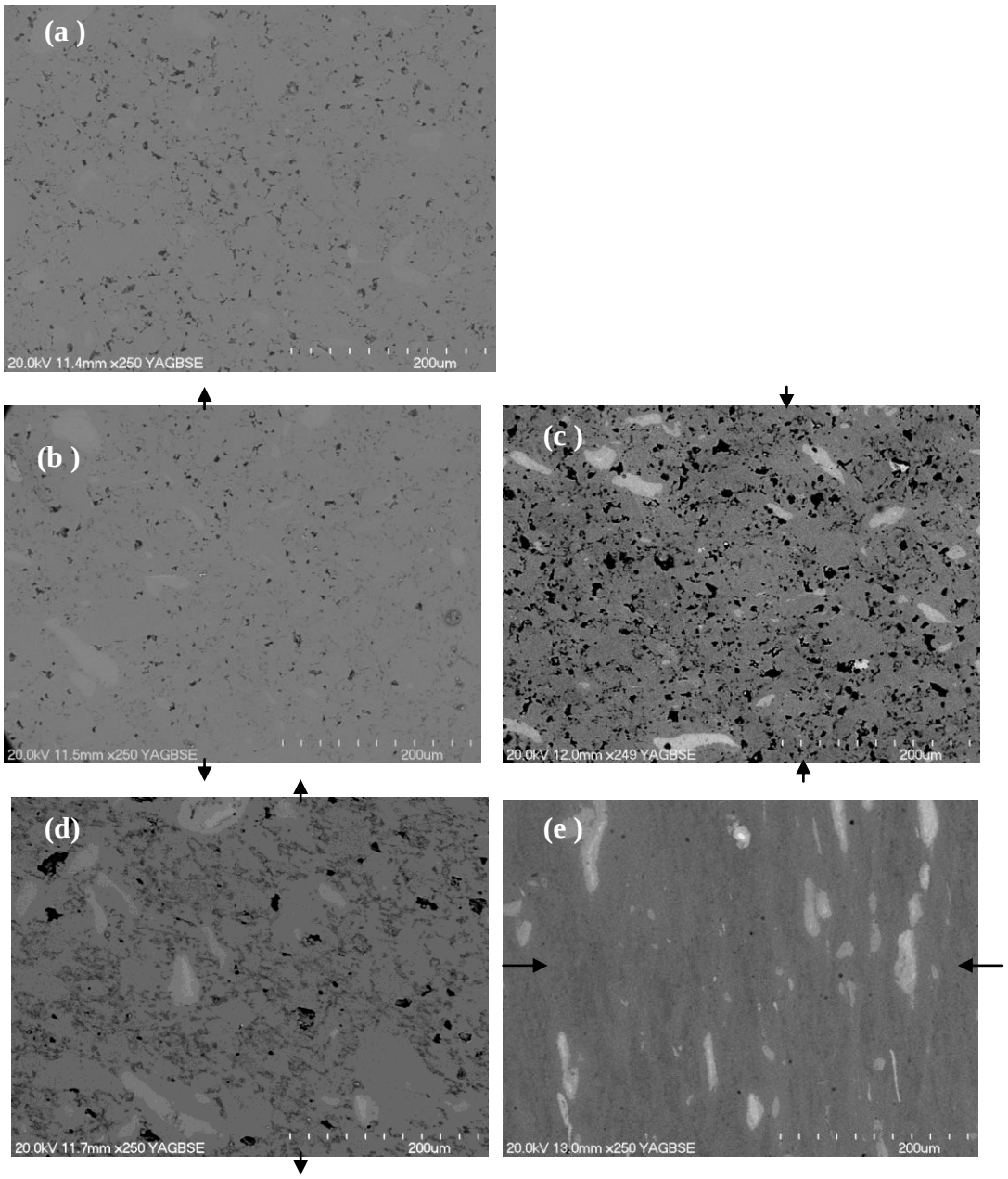

Figure 3.25: Back scattered secondary electron images of **(**a) as-HIPed; (b) longitudinal section of room temperature tensile tested; (c) cross section of room temperature compression tested sample; (d) longitudinal section of tensile tested sample at 900^{o}C; (e) cross section of compression tested sample at 900^{o}C.

3.6 Discussion

3.6.1 Effect of Powder Preparation on Consolidation Characteristics

The high energy ball milling of elemental powders resulted in fine layers of Ti/ Al/ Cr composite structure after 12 hrs of milling. The powder particles showed Ti layers embedded in a matrix of Al, and no evidence of the formation of

intermetallics, indicating that mechanical alloying has not occurred during milling. Despite the slight increase in hardness with milling time, due to the strain hardening occurring during milling, the powder particles were found to be having good consolidation characteristics. The overall microstructure of the powder was found to be homogeneous, with an average particle size of around 26.7 μm. Although a homogeneous microstructure was obtained after milling, the oxygen content in the samples increased with milling time. The main source of oxygen was found to be from the milled powders, due to the large surface area of the milled powder particles, finally resulting in a bulk material with high oxygen content.

As for reducing the oxygen content in the consolidated samples, a high degassing temperature should be used, since the degassing temperature, used in the present case is not sufficiently high. In the meantime, it is also necessary to transfer the milled powders directly into the powder compacting and canning steps without exposing them to air. The porosity in the bulk consolidated material was found mainly due to the insufficient time, used during HIP consolidation. On the other hand, the low interparticle bonding is expected to be from the mechanical milling process since it is evident from ref [9], that mechanical alloying increases contamination of the powders, resulting in oxides on the surfaces of powder particles and thus low interparticle bonding after consolidation using HIP.

3.6.2 Effect of phase composition

The microstructure of the as-HIPed sample consisted of Ti rich islands distributed inhomogeneously, and a few of the Ti rich regions were found to be a mixture of Ti_3Al and Ti, indicating that the diffusion is not complete. The presence of Ti_3Al in these alloys is expected from the phase diagram, a higher percentage of the phase affects the ductility in an adverse way. Although a small fraction of Ti_3Al phase is expected to absorb interstitials, and improves the ductility of the alloy. A few investigations also reported that the Ti_3Al phase with high amount of interstitials makes the alloy brittle [10].

According to suggested by Chan and Kim [11], the maximum ductility of TiAl based alloys, is obtained when the Ti_3Al phase content is between 10 – 15%. The XRD and SEM studies indicated that the Ti_3Al phase content in the TiAl alloy prepared from the present study was slightly higher than this range.

3.6.3 Comparison between mechanical properties in tension and compression

At room temperature the compression tested samples showed a very high yield strength of around 1410 MPa and a compression strength of about 1580 MPa with an overall plastic strain of 1% after compression testing. The sample shattered into multiple pieces. The samples tested in tension showed a very low fracture strength of 100 MPa, and no ductility. The low room temperature tensile fracture strength of the samples is likely to be due to the low level of interparticle bonding, and the high amount of porosity in the samples. The high compression strength of the alloy was comparable to those reported by Bohn et al [8] and slightly lower to that reported by Oehring et al [14], which is a typical character of the UFG materials, but the compressive ductility was much less than the reported value [8]. This is expected mainly due to the high amount of oxygen in the sample, which was found to be around 0.87%.

The main factor responsible for reducing room temperature compressive strength is the low level of the interparticle bonding, based on the examination of the fractured samples from the compression tests, which showed some unbonded interparticle boundaries and pores. The effect of porosity is less pronounced in compression as compared to that in tension, since the stress to initiate microcracks in compression is much higher. The high oxygen content and low interpaticle bonding of the HIPed sample were found to affect the room temperature ductility adversely. The behaviour of samples in the present alloy study is likely to be due to the low interparticle bonding, and the presence of brittle phase regions in the alloy. Although pores showed a tendency to close up, the above factors affected the pore closure mechanism adversely. Inspite of all the above reasons, the alloy has shown a yield strength and fracture strength comparable to that observed from the literature, because of the UFG microstructure. The residual pores were found

to affect the strength adversely more severely in tension, than in compression, due to the different type stress conditions in tension and compression.

The true stress-strain curves of the samples tested at 900^{o}C in compression and tension respectively, showed a different behaviour. A yield stress of 55 -58 MPa was found in tension, while 33 MPa yield stress was found in compression. The samples tested in tension showed uniform elongation until fracture without necking. After testing the pores were found to incline towards 45^{o} to the tensile direction. The pores are expected due to the residual porosity and thermally induced porosity in the sample at elevated temperatures [13]. Grain boundary sliding is the dominant mechanism of deformation of UFG TiAl based alloys at temperatures above 800^{o}C (12, 14), and through this mechanism, the deformation strain is accommodated by diffusion flow or dislocation glide across the neighbouring grains to avoid cavitation and therefore premature fracture. In the present case the sliding strain was better accommodated at 900^{o}C.

While in the sample which was compressed to a true strain of 0.69 at 900^{o}C, the porosity level in the sample along direction decreases and the Ti_3Al rich regions become elongated perpendicular to the compression axis. The unreacted Ti regions were found in the samples even after compression testing at 900^{o}C, which indicated that it is essential to get an initial homogenised microstructure, since it is found to be difficult to eliminate unreacted Ti, once it is found in the microstructure of the as consolidated material.

3.6.4 Grain size and temperature dependence of mechanical properties

It is a well known fact that the yield stress is strongly dependent on the grain size and temperature. The effect of grain size on yield stress can be explained with the Hall-Petch relationship, in which the yield stress is proportional to the $1/\sqrt{d}$ of the grain size *d*. So the UFG alloys based on γ TiAl are characterized by high values of hardness and compressive yield strengths at low temperatures. This is due to the fact that the fine meshed net of grain boundaries present in UFG alloys

hamper the dislocation glide and mechanical twinning, leading to an increase in hardness and strength.

According to Clemens et. al [15] the yield strength of near gamma alloys fullfill a Hall-Petch relationship, in which 60-70% of the yield stress arises from the long range interactions of dislocations with the grain boundaries, and the stress part is assumed to be the same as long as the related microstructure is not significantly changed. In the present case, although the grains are at UFG level, the above phenomena are not valid due to the low interparticle bonding and porosity, resulting in a brittle material. The material may fracture pre-maturely. In this case, fracture strength is lower than yield strength.

The mechanical properties of the UFG Ti-47Al-2Cr alloy in the present study are compared with ternary alloys of near gamma composition (Figure 3.26). It can be seen that the tensile yield strengths of the fine grained alloys are higher at room temperature than the UFG TiAl based alloy produced in the present study. On the other hand the yielding at room temperature was observed in compression and the yield strength was comparable to the literature results (Figure 3.27). Hence it can be said that the porosity and low level of interparticle bonding have less significant effect in compression at room temperature, and the UFG Ti-47Al-2Cr alloy followed Hall- Petch relation. However the presence of defects (pores and low interparticle bonding) in the present alloy affected the room temperature compressive ductility adversely.

While at elevated temperatures, the relations changed completely due to the structural changes occurring at high temperatures, during which the UFG materials become very soft. The smaller the grain size, the higher the drop in the yield strength will be upon raising temperature. The ternary Ti-47Al-2Cr (at %) alloy in the present study showed the same kind of behaviour indicating the favourable conditions for hot working. The elevated temperature ductility of the samples is much higher as compared to the samples produced by IM processes [18] and comparable to that of UFG and fine grained alloys produced using other powder metallurgy routes [8].

The yield strength in compression testing, from the present study reduced drastically to 33 MPa at 900^{o}C, and it was found that at higher temperatures, true strains of around 0.69 can be easily achieved. The same type of behaviour was reported by Oehring et. al [14] with Ti-48Al alloy and Tokizane et. al [19] with Ti-50Al alloy produced using mechanical alloying and consolidation. Even though slight strain hardenening was observed from compressive deformation in the present case, which is slightly contradicting the above works, the material exhibited good formability at elevated temperature.

The yield strength in compression at elevated temperature was found to be much lower than that of coarse and fine grained materials produced from different processing routes as shown the Figure 3.27. As far as literature is concerned, the lowest elevated temperature yield strength was expected to be from the present work.

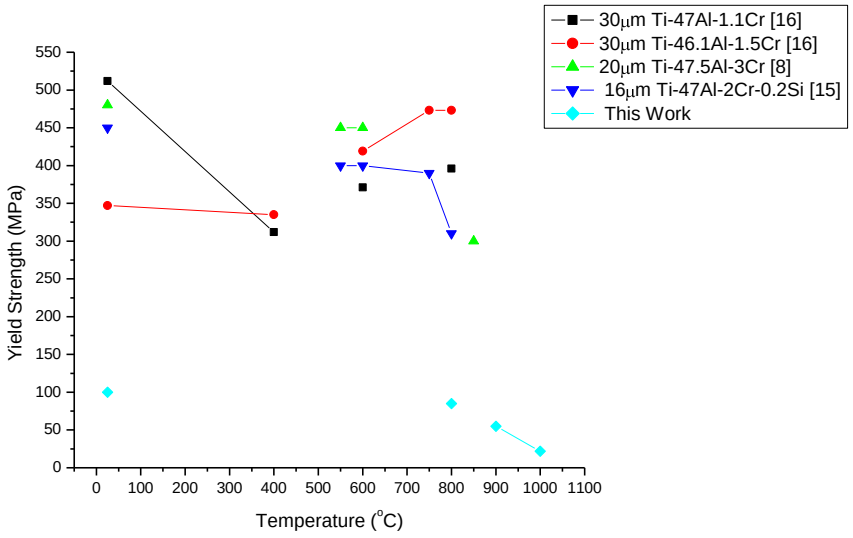

Figure 3.26: Yield strength in tension as a function of grain size and temperature

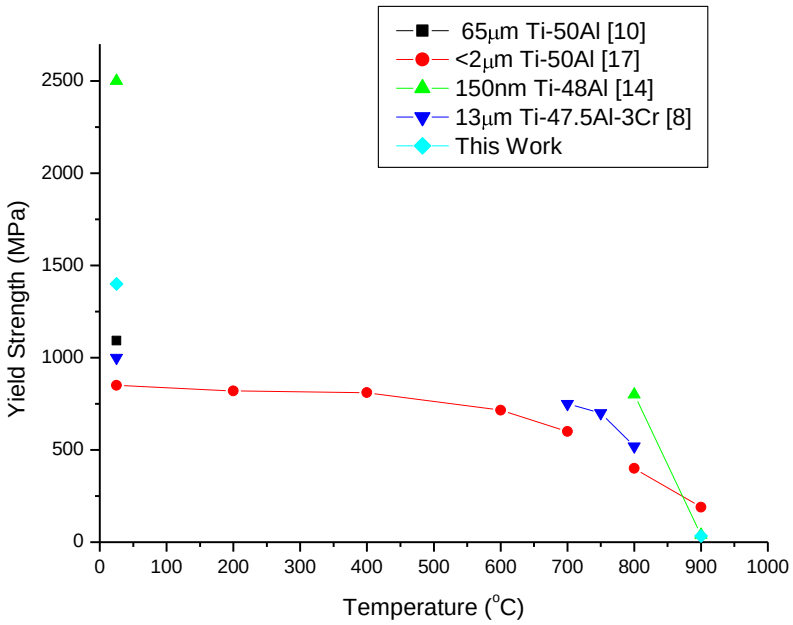

Figure 3.27: Yield strength in compression as a function of grain size and temperature

3.7 Summary

This study has clearly demonstrated, that UFG Ti-47Al-2Cr (at%) can be synthesized by a combination high energy mechanical milling and HIP. The as-HIPed bulk material was found to have porosity of approximately 5% with a slightly non-homogeneous microstructure, consisting of Ti rich regions. The Ti rich regions consist of elemental Ti phase, embedded in the Ti rich island, indicating that the diffusion is not complete. The high oxygen content of the as-HIPed material is due to the high oxygen content of as milled powders and the low degassing temperature used.

The room temperature mechanical properties of the material, especially in tension was affected by the low inter particle bonding, and porosity, but in compression the material showed good strength with some plasticity due to the UFG microstructure of the alloy. On the other hand the high oxygen content in the sample is responsible for the low ductility at room temperature both in tension and

compression. At elevated temperatures, the behaviour of the material has totally changed, showing good formability both in tension and compression. It was determined that the best hot working temperature of the alloy from the present study was 900^{o}C. The yield strength of the material at elevated temperatures, in compression was very low, as compared to that in tension, indicating that the material is more easily formable in compressive type of deformation, rather than in tension. The considerable amount of ductility of the consolidated alloy samples despite their high porosity level suggests that the formability of the material for secondary processing is very high, leaving a large space for improvement of the quality and microstructure of the alloy. It should be noted that the UFG microstructure of the consolidated samples is the primary reason for the good ductility and formability of the consolidated alloy.

References

1. B. D. Cullity, "Elements of X – Ray Diffraction", Addison-Wesley Pub. Co., c1978, Chapter 9.

2. C. Suryanarayana, G.E. Korth and F.H. Froes, Metallurgical and Material Transactions. *A*, 1997. **28**: p. 293–302.

3. N. Forouzanmehr, F. Karimzadeh, and M. H. Enayati , Journal of Alloys and Compounds, 2009. **471**: p. 93-97

4. S. Qu, X. Li, Y. Li, L. Hu and E. Wang, Rare Metals, 2006. **25**: 21-26.

5. A. Rahmel, W.J. Quadakkers and M. Schütze, Material Corrosion, 1995. **46**: p. 271–285.

6. X. Lu, X.B. He, B. Zhang, X.H. Qu, L. Zhang, Z.X. Guo and J.J. Tian, Journal of Alloys and Compounds, 2009. **478**: p. 220-225.

7. M. Yoshihara and K. Miura, Intermetallics, 1995. **3**: p. 357–363

8. R. Bohn, T. Klassen, R. Bormann, Intermetallics, 2001. **9**: p. 559-569.

9. M. R. Shagiev, O. N. Senkov, G. A. Salishchev and F. H. Froes, Journal of Alloys and Compounds, 2000. **313**: p. 201-208.

10. K. Nonaka, K. Tanosaki, M. Fujita, A. Chiba, T. Kawabata and O. Izumi, *Materials Transactions*, JIM , 1992. **33**: p. 802-810.

11. K. S. Chan, Y.S. Kim, Microstructure and Property Relationships in Titanium Aluminides and Alloys, in Proceedings of TMS symposium, 1991. p. 176-196.

12. R.M. Imaev, V. M. Imaev, and G. A Salishchev, The Physics of Metals and Metallography, 2005. **100**: p. 307-317.

13. P.R. Sneary, R.S. Beals and T. R. Bieler, Scripta Materialia, 1996. **34**: p. 1647-1654.

14. M. Oehring, F. Appel, Th. Pfullmann, and R. Bormann, Applied Physics Letters, 1995. **66**: p. 941-943.

15. H. Clemens, W. Glatz and F. Appel**,** Scripta Materialia, 1996. **35**: p. 429-434.

16. In-Sung Lee, S. K. Hwang, W.K. Prak, J.H. Lee, D. H. Park, H. M. Kim and Y. T. Lee, Sripta Metallurgical et Materialia, 1994. **31**: p. 57-62.

17. E. Paransky, E. Y. Gutmanas, I. Gotman and M. Koczak, Metallugical and Materials Transactions A, 1996. **27**: p. 2130-2138.

18. C. T. Liu, J. H. Schneibel, P. J. Maziasz, J. L. Wright and D. S. Easton, Intermetallics, 1996. **4**: p. 429-440.

19. M. Tokizane, Y. Takaki, and K. Ameyama, Metal Powder Industry Federation, Princeton, NJ, 1992, 7, 315.

Chapter 4

Microstructures and Mechanical Properties of Ti-47Al-2Cr (at %) Alloy Produced Using Powder Compact Forging of a Mechanically Milled Ti/Al/Cr Powder

4.1 Introduction

Development of innovative techniques to produce gamma TiAl based alloys, with good mechanical properties, while still maintaining ultra fine grain sizes can be rewarding, but is also a great challenge. Numerous investigations showed that the microstructures and mechanical properties of TiAl based alloys are highly dependent on the processing techniques used in the production of the bulk material [1]. In this chapter, the direct powder forging of powder compacts to produce bulk consolidated material has been explained in detail. A Ti-47Al-2Cr (at %) alloy has been produced by directly forging green powder compacts of a Ti/Al/Cr composite powder produced by high energy mechanical milling of a mixture of elemental Ti, Al, Cr powders. Initially the experiments were performed to produce a bulk consolidated material using direct powder forging followed by characterization of the sample to get a preliminary understanding of the process. Further experiments were done to produce bulk material to analyze the microstructure and mechanical properties of the material in detail. The mechanical properties in tension and compression and at room and elevated temperatures were studied respectively.

4.2 Experimental Procedure

Elemental powders of Ti, Al, Cr were put together to make up a composition of Ti-47Al-2Cr (at %) composition. The powders mixture was initially mixed for 6 hrs without any interval under high purity argon using a Retsch planetary mill with spherical stainless steel balls of diameter 12.5 mm. The mixed powders were subsequently milled for a net time of 12 hrs using the same vial, balls and the mill, but with a speed of 400 rpm. The milled powders were cold pressed using a die to

produce green compacts of 25 mm in height, 34 mm in diameter and 40 mm in height, 34 mm in diameter, respectively. The green compacts were further densified using cold isostatic pressing (CIP). The CIPed compacts were canned using 316stainless steel tubes, and the cans were degassed at 300^{o}C for a duration of 1 hour. Forging was done on the powder compacts heated to 1200^{o}C (Forge-1) and 1150^{o}C (Forge-2) respectively, using an industrial scale 500 ton crank press, followed by air cooling (for Forge-1) or oil quenching (forge-2). The oxygen analysis has been done on the specimens cut from different locations of the Forge-2 sample.

Tensile test specimens with a gauge length 14 mm were cut from Forge-1 sample. A strain rate of ~ 6 x 10^{-5}/sec was used for room temperature testing. In the case of Forge-2 sample, tensile testing specimens with a gauge length of 6.5 mm were cut for room temperature testing and with a gauge length of 8.5 mm for elevated temperature testing. The specimen cutting was done using a electric discharge machining (EDM) wire cutter. Strain rates of 1.4 x 10^{-4}/sec and 1.88x10^{-4}/sec were used at room temperature and elevated temperature tensile testing at 900^{o}C respectively.

Compression testing specimens were cut from Forge-2 sample. Specimens of 4 mm in diameter and 7 mm in height were used for room temperature testing. The room temperature compression testing was done with a strain rate of ~ 1.2 x10^{-4}/sec. Specimens of 8 mm in diameter and 10 mm in height were used for elevated temperature compression testing at 900^{o}C. The elevated temperature compression testing was done with a strain rate of 1.16x 10^{-4}/sec.

4.3 Powder Characterization

After 12 hrs of milling the particle size distribution of the powder samples have shown the same trend for both of the Forge-1 and Forge-2 samples. A mean particle size of ~ 35 µm was observed (Figure 4.1 (a)). After 12 hrs of milling, sticking of the powder to the wall was pronounced, with negligible amount of loose powder being left. Also ~ 15% of the particles were found to be above

75 µm. The morphology of the powder particles used for Forge - 2 are shown in the Figure 4.1 (b). The mechanical milling of elemental powders resulted in three types of powder particles; (i) Ti/Al/Cr layered composite structured particles; (ii) particles consisting of a mixture of Ti and Al in which layered structure is not observed and (iii) Ti rich powder particles, as shown in Figures 4.1 (b) - (f). This suggested that the composition of powder particles after 12 hrs milling was not homogeneous.

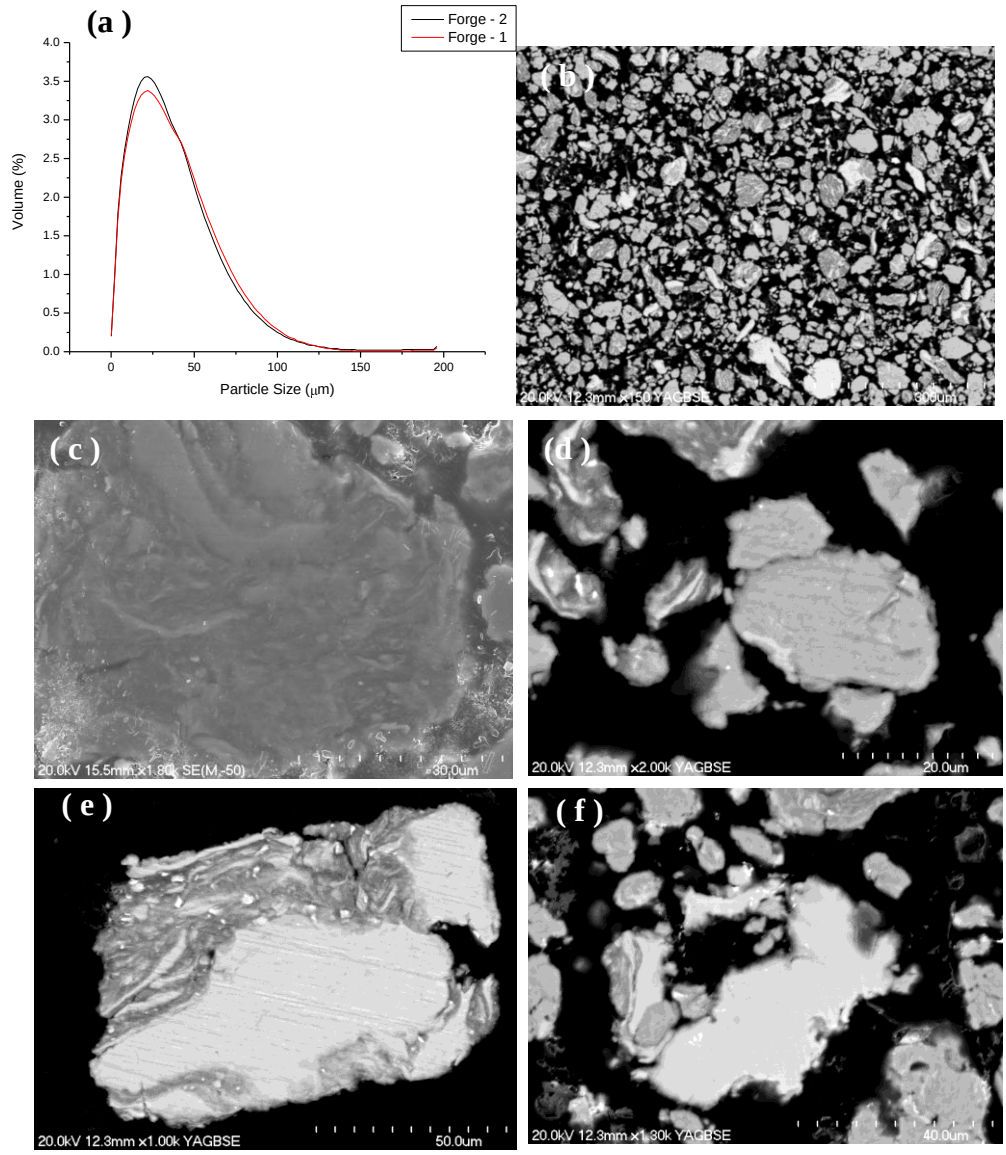

Figure 4.1: (a) Particle size distribution curves of 12 hrs milled powders used for Forge-1 and Forge-2; and SEM backscattered images of the 12 hrs milled powders used for powder compact forging of Forge-2 sample; (b) showing morphology of the powder particles; (c) layered composite particle; (d) composite powder particle, in which no layered structure was observed, consisting of both Ti and Al; (e) and (f) Ti rich particles.

The same powder particle morphology was observed for the 12 hrs milled powder used to consolidate Forge-1 sample. The fraction of Ti/Al/Cr composite with no layered structure was higher as compared to that of layered composite structure after 12 hrs of milling. The green density of the powder compacts after cold isostatic pressing was found to reach ~ 67- 69%. The thermal behaviour and XRD patterns of the 12 hrs milled powders used for consolidation indicated that the formation of the intermetallic phases, after 12 hrs of milling was not evidenced, as explained in Chapter 3.

4.4 A Preliminary Study

Initially, experiments were done to produce consolidated bulk material using direct powder forging to produce Forge-1 sample using two-step forging. The powder compact was heated to 1200^{o}C, using a heating rate of 14^{o}C/min. After holding for 10 minutes at 1200^{o}C, the sample was taken out and forged to achieve an initial height reduction of 39%. A further height reduction of 27% was achieved in the second pass, which was done after the forged powder compact was heated back to 1200^{o}C. A total height reduction of 66% was achieved in two passes. The canned Ti-47Al-2Cr compact and the sample produced after two step forging are shown in Figure 4.2.

After forging the can was found to have small cracks on the surface, and a consolidated sample of approximately ~30 mm in diameter and 6.5 mm in thickness was produced after removing the can. The surface of the can was black, indicating heavy oxidation of the samples, and also loose powder particles were found on the surface. A layer of approximately 1.5 mm in thickness on each side was removed to obtain the actual material. The density of the bulk alloy was ~ 94.5 in the centre region and the 82.5% at the periphery. The XRD patterns of the bulk consolidated sample showed Ti, $Ti_{3.3}Al$ and TiAl phases (Figure 4.3).

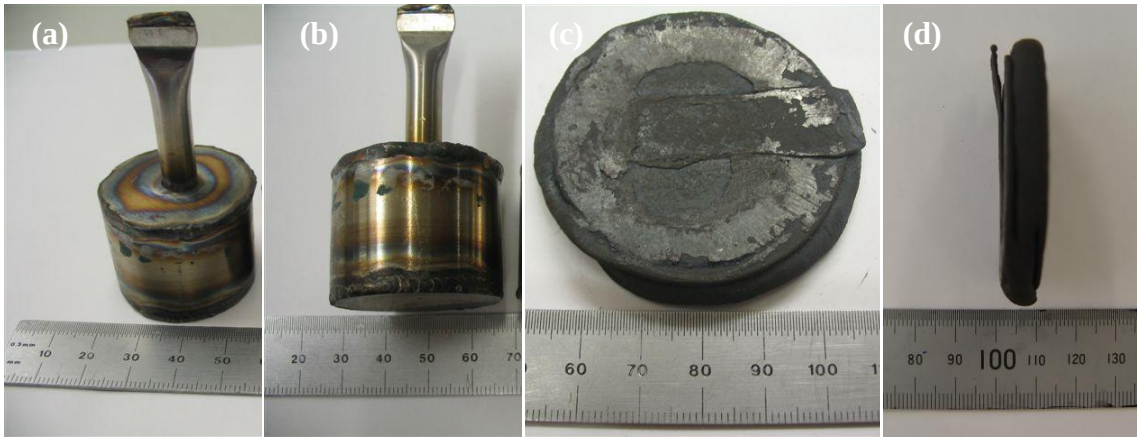

Figure 4.2: Canned compact (a) and (b) before; (c) and (d) after powder compact forging

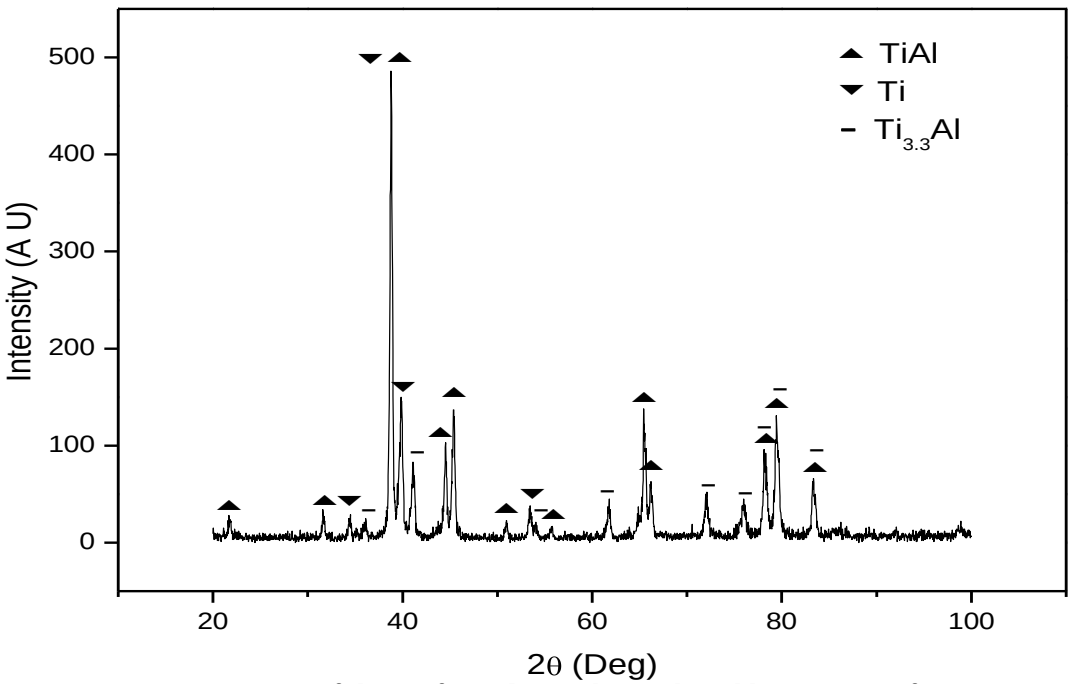

Figure 4.3: XRD pattern of the as-forged sample produced by two step forging.

The microstructure of the alloy in the centre region and near the edge are shown in the Figure 4.4, respectively. The level of porosity was higher near the edge as compared to the central regions of the disk. The alloy consisted of Ti rich regions distributed randomly in the bulk alloy. The distribution of Ti rich regions in the bulk alloy is shown in Figure 4.5.

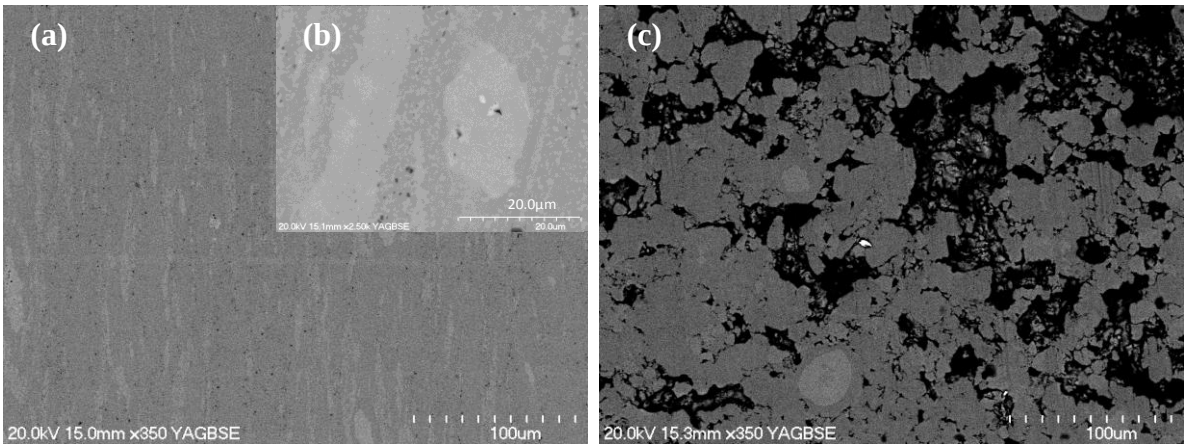

Figure.4.4: SEM back scattered electron images of the cross sections of the as forged material; (a) and (b) at the centre; (c) at the edge.

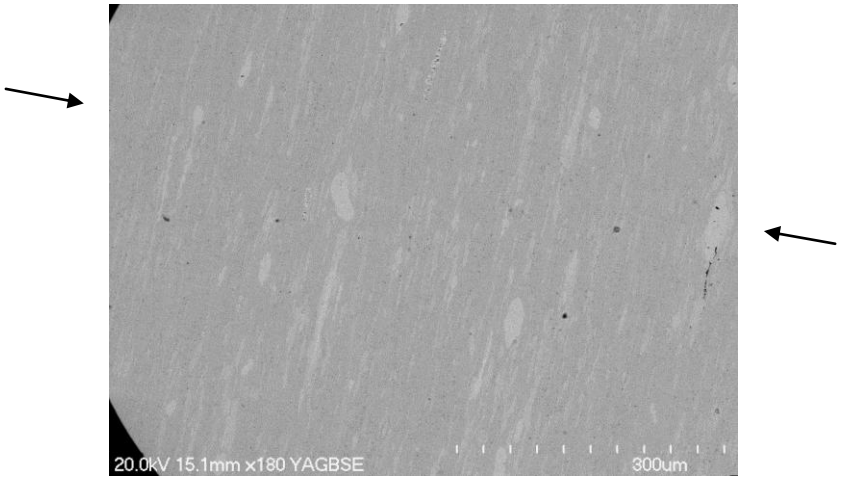

Figure 4.5: SEM back scattered electron images of the cross section of the as forged material at the centre, showing the phase distribution. (Arrows indicate forging direction)

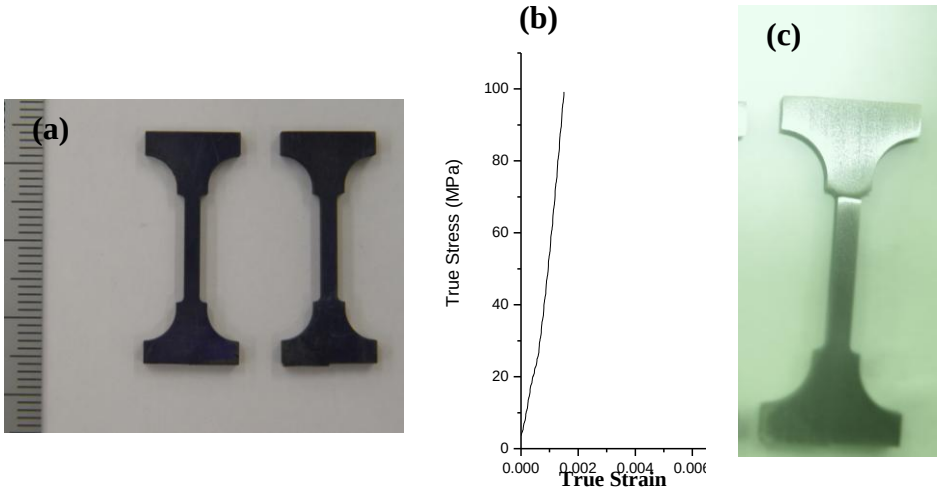

Figure 4.6: (a) profile of the tensile testing specimens; (b) tensile true stress true strain curve; (c) tensile tested sample showing fracture at the edge.

The amount of consolidated material produced in this forging experiment was only sufficient to cut two tensile testing specimens, which can be seen in Figure 4.6(a). Although RT tensile testing was done on both specimens, the data of only one sample was usable, because the other specimen fractured outside the gauge length. The true stress-stain curve of the specimen (Figure 4.6 (b)) revealed fracture strength of 100 MPa, and no yielding was observed. The fractured site of the specimen (Figure 4.6 (c)) revealed the brittle nature of the sample.

The preliminary study has revealed that a bulk consolidated material can be produced by the direct forging of the powder compact. However the surface quality of the bulk material produced using two-step forging, was not good enough, because of the high amount of surface oxidation. In order to prevent the oxidation, one-step forging and quenching in oil was done on another canned powder compact in the second forging experiment.

4.5 Consolidated sample Produced by One Step Forging Process

4.5.1 Quality and Microstructure

One step forging of a canned powder compact was done using a crank press which gives a high strain rate during forging. The sample was reduced from an initial height of 40 mm to a final height of 12 mm, in one step, resulting in a total height reduction of ~ 62%. The external appearance of the can before and after forging and the consolidated material inside the can is shown in the Figures 4.7(a)-(d). The can and the consolidated material had cracks. This was likely due to the high strain rate imparted during forging and a large amount of deformation in one pass. After forging, a consolidated bulk alloy disk of 46 mm diameter and 12 mm thickness as shown in Figure 4.7(d) was produced. This was sufficient to cut samples for mechanical testing and characterization.

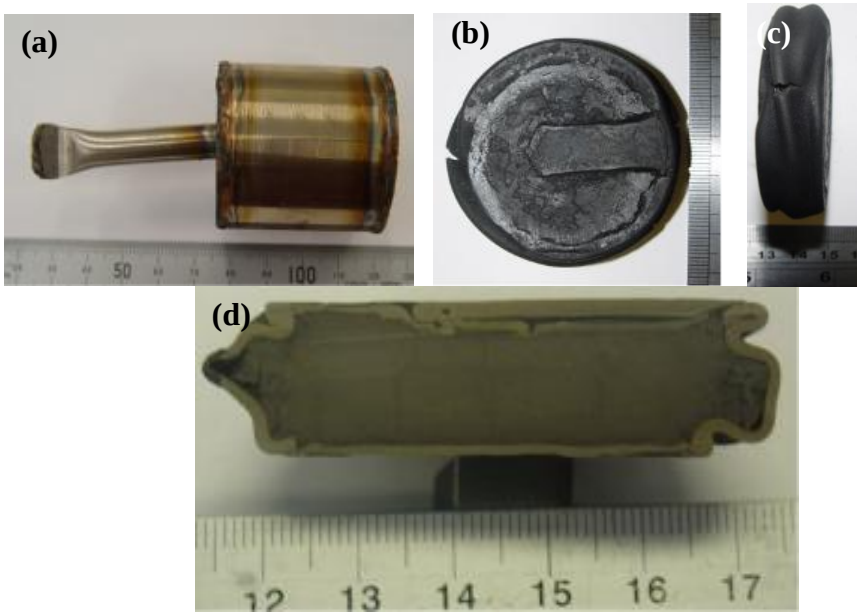

Figure.4.7: Canned compact (a). Before forging (b), (c) after forging and (d) cross section of the bulk alloy produced after powder compact forging.

Density measurement at five different locations in the forged sample showed that the average density in the central region was ~ 95%, and around 84.6% near the edge, as shown in Figure 4.8. The oxygen content of the sample was measured to be approximately 1.1% and it varied little from the centre to the periphery as shown in the Figure 4.9. SEM backscattered electron images (Figures 4.10(a) & (b)), showed that the central region of the sample had a significantly lower level of porosity than the region near the edge. This confirmed that the can was not effective in constricting the material flow properly during forging both in one step and two step forging methods. This may be due to the relatively low green density (69%) of the powder compacts.

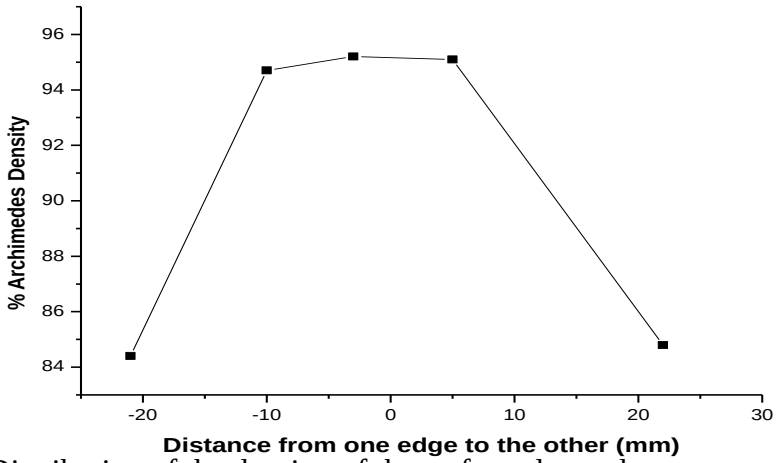

Figure.4.8: Distribution of the density, of the as-forged sample

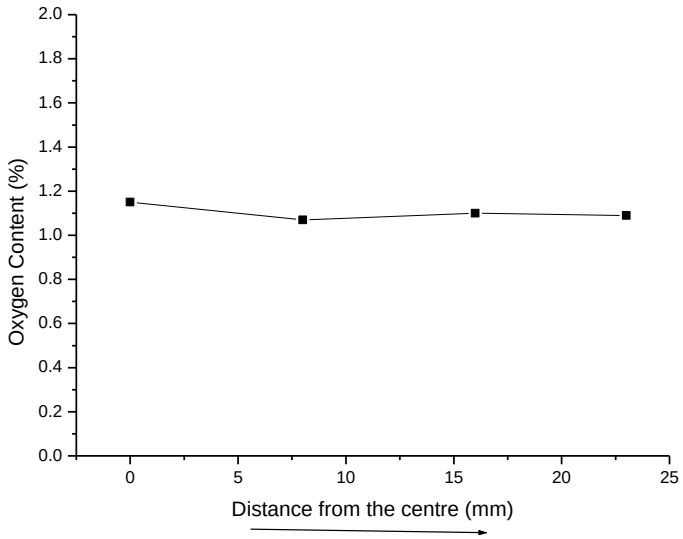

Figure 4.9: Oxygen variation in the sample from the centre to the periphery

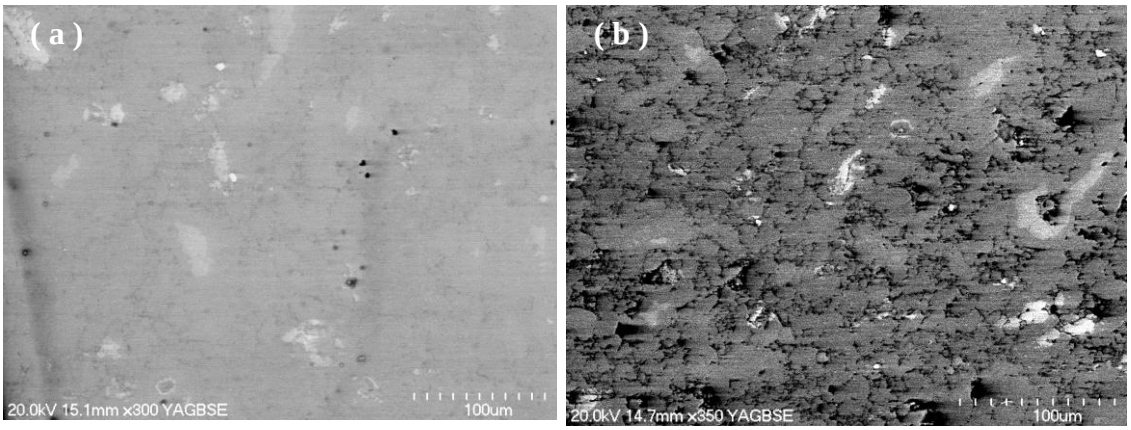

Figure.4.10: SEM back scattered images of the cross sections of as-forged alloy; (a) at the centre (b) at the edge

The XRD pattern of the bulk alloy (Figure 4.11), showed TiAl, Ti, $Ti_{3.3}Al$, phases, and a slight broadening of the XRD peaks of the different phases indicated that the grains were at ultrafine level. SEM examination combined with EDS showed that white regions were rich in Ti, and the dark background is TiAl, some Cr rich regions were also observed (Figure 4.12).

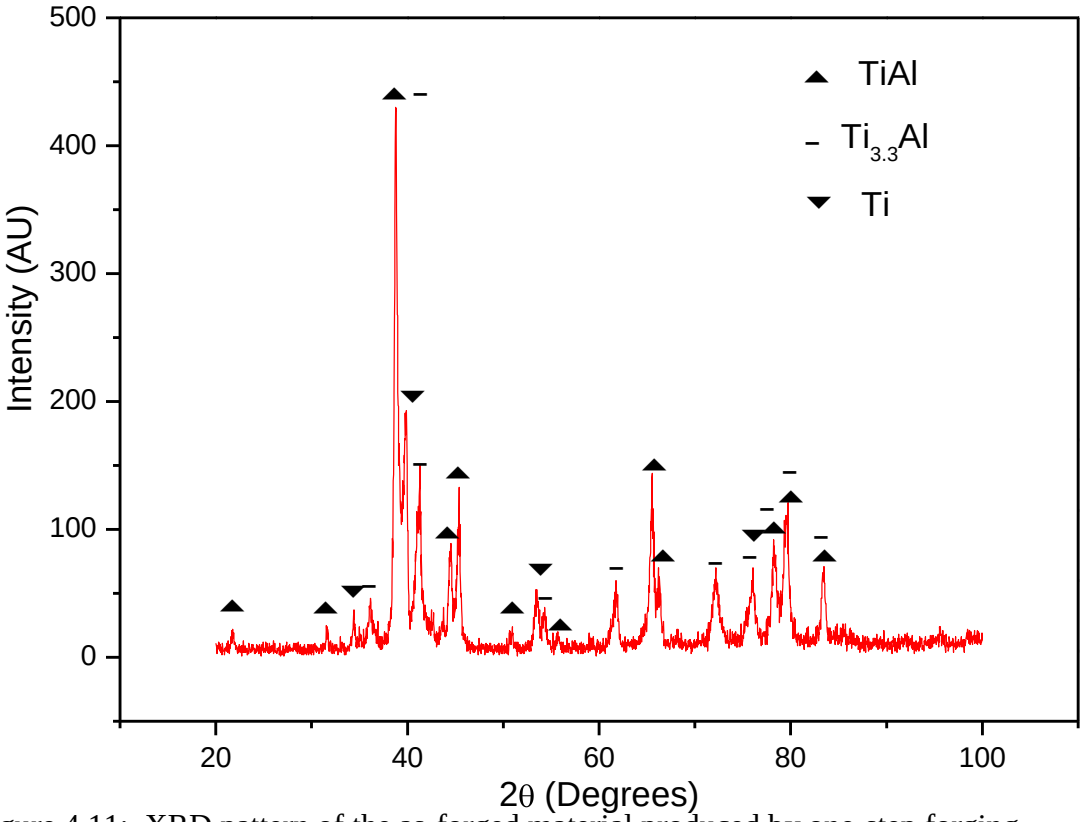

Figure 4.11: XRD pattern of the as-forged material produced by one-step forging.

The Ti and Cr rich regions are likely due to the compositional inhomogenity of the particles composition in the initial powder. As shown in Figure 4.1(b), a fraction of the Ti/Al/Cr composite particles had much higher Ti fraction than that required for the formation of TiAl through reacting Ti and Al. The short holding time at 1150^{o}C was not sufficient and to homogenize the composition of the forged disk. The distribution of the Ti rich regions in the sample varied slightly from one region to another as shown in Figures 4.13 (a) and 4.13 (b).

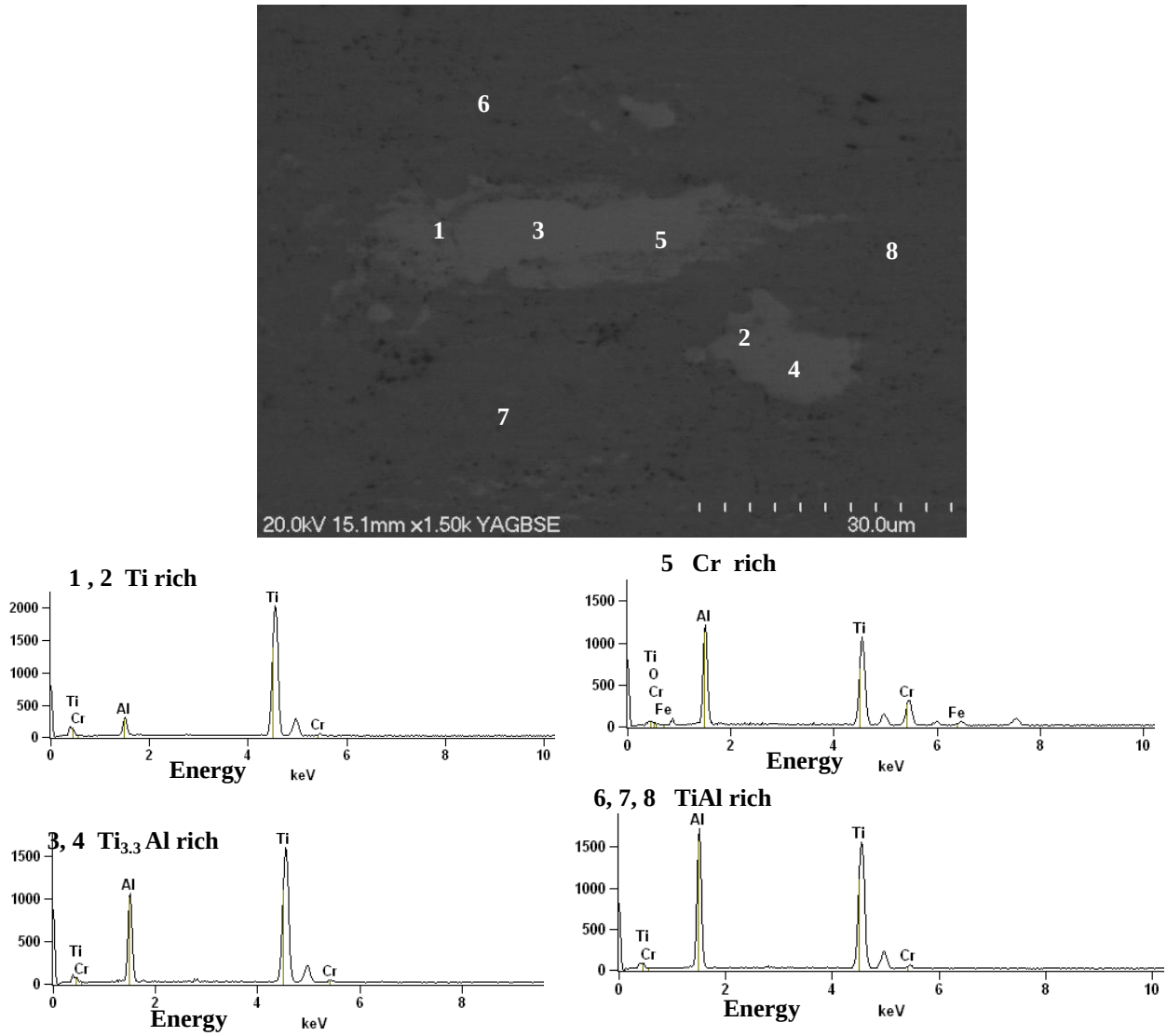

Figure 4.12: SEM back scattered image showing high magnification Ti rich region and EDS analysis.

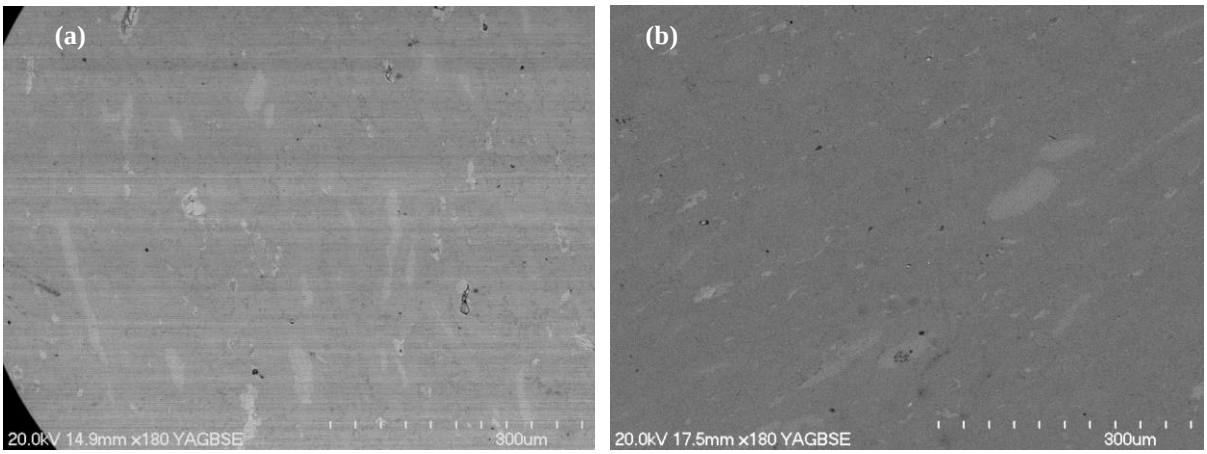

Figure 4.13: (a) and (b) SEM back scattered images showing the distribution of Ti rich regions from different areas in the as-forged sample.

Microhardness testing carried on the planar section at different locations showed that the sample had a high hardness of ~ 520 HV in the central region and a much lower hardness of ~ 230 HV near the edge of the sample as shown in Figure 4.14. However some locations of the sample between the centre and the periphery (data point 2 from the Figure 4.14(c)) were found to have comparable hardness to that at the centre, which is expected due to the inhomogeneous pores distribution along the cross section of the sample. The graph was plotted on the basis of average reading values took from different regions from the centre to the periphery of the samples.

The microhardness values of the central region of powder forged sample were comparable to those of the as-HIPed material described in Chapter 3. In addition to the porosity and the Ti rich regions, the bulk consolidated alloy was also found to have low level of interparticle atomic bonding. The particle boundaries in the material were clearly visible Figure 4.15, which was also confirmed by the fracture analysis of the room temperature tested samples.

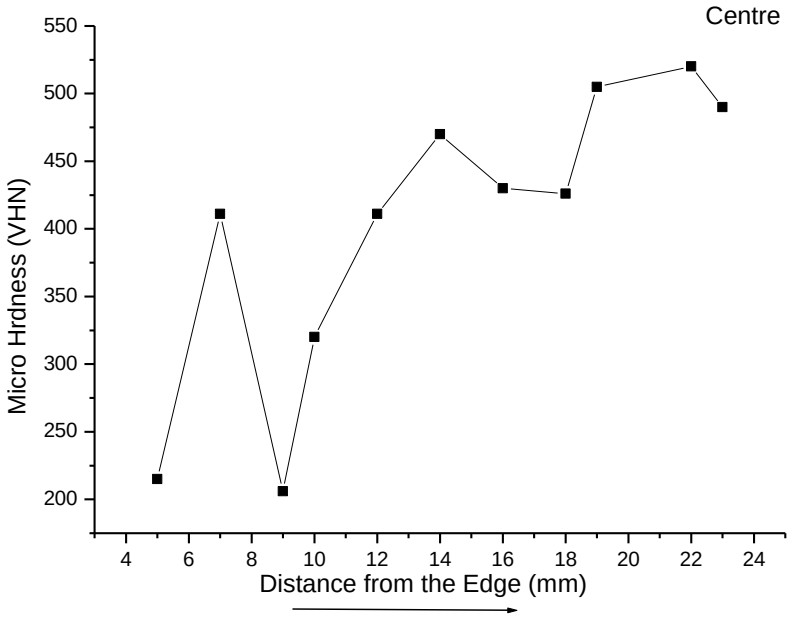

Figure 4.14: Microhardness distribution of the sample from the periphery to the centre.

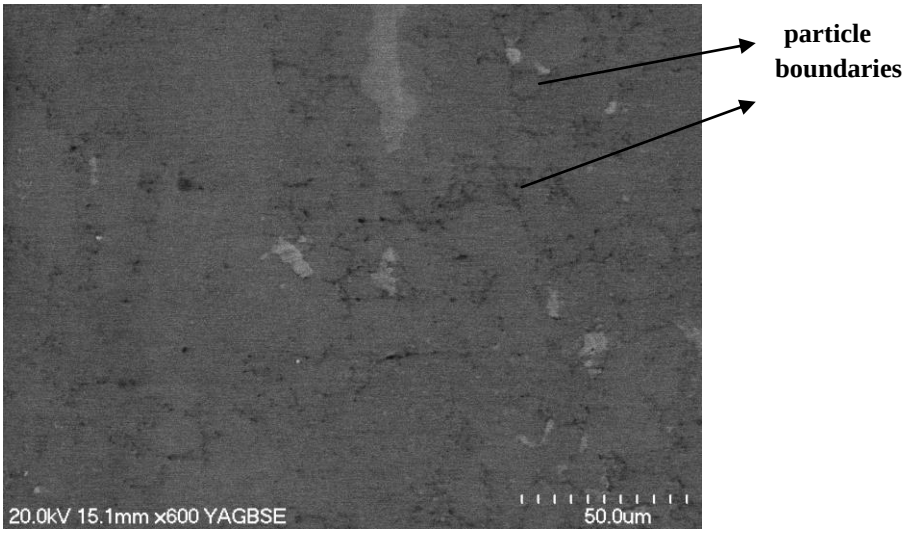

Figure 4.15: SEM back scattered electron Image showing interparticle boundaries in the as-forged bulk alloy.

4.5.2 Mechanical Properties of the as-forged material

4.5.2.1 Specimen cutting

Tensile testing and compression testing specimens were cut from the central region with a density of ~95%. The locations from which the tensile and compression specimens were cut and the tensile and compressive testing directions with respect forging direction are shown in Figures 4.16(a) and 4.16(b).

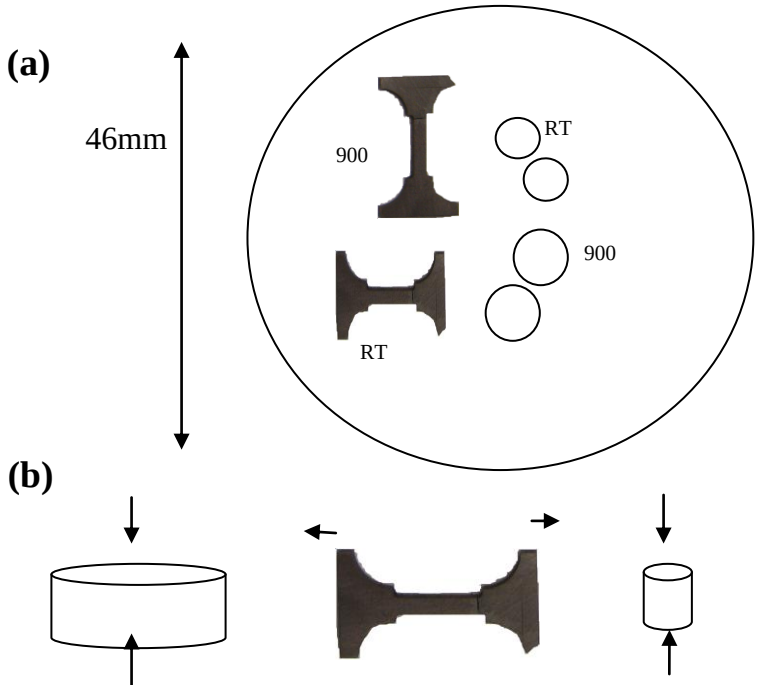

Figure 4.16: (a) Locations of the tensile and compression tested samples cut from the bulk alloy disk for room temperature and elevated temperature tensile and compression testings; (b) forging, tensile and compressive force directions.

4.5.2.2 Tensile Properties

The tensile true stress-strain curves of the specimens tested at room temperature are shown in Figure 4.17(a). Room temperature tensile test results showed a small variation in tensile strength, ranging 115 – 132 MPa and no ductility was observed. All the room temperature tensile tested specimens, fractured at the location of width change of the specimens as shown in Figure 4.17 (b), indicating a brittle nature of the samples.

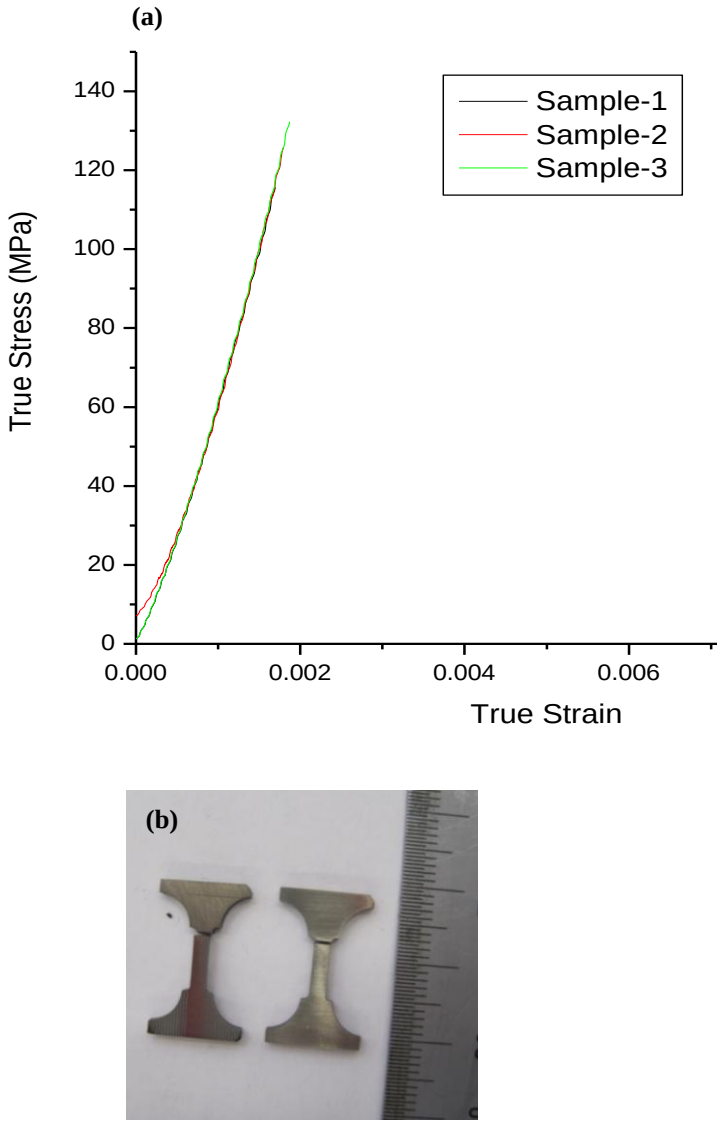

Figure 4.17: (a) room tempertaure true stress true strain curves of tensile tested specimens; (b) fractured specimens.

The specimens tested at 900^{o}C showed a yield strength in the range of 70-90 MPa, an elongation to fracture in the range of 80-165%, and a true strain to fracture in

the range of 0.6 to 0.96 (Figure 4.18(a)). It appeared that the specimen with lower yield strength had a larger elongation to fracture. All specimens showed a slight strain softening, which can be attributed to cavitation. Although the specimens were tested in flowing argon, after testing their colour turned into pale yellow indicating that oxidation had occurred during testing (Figure 4.18(b)).

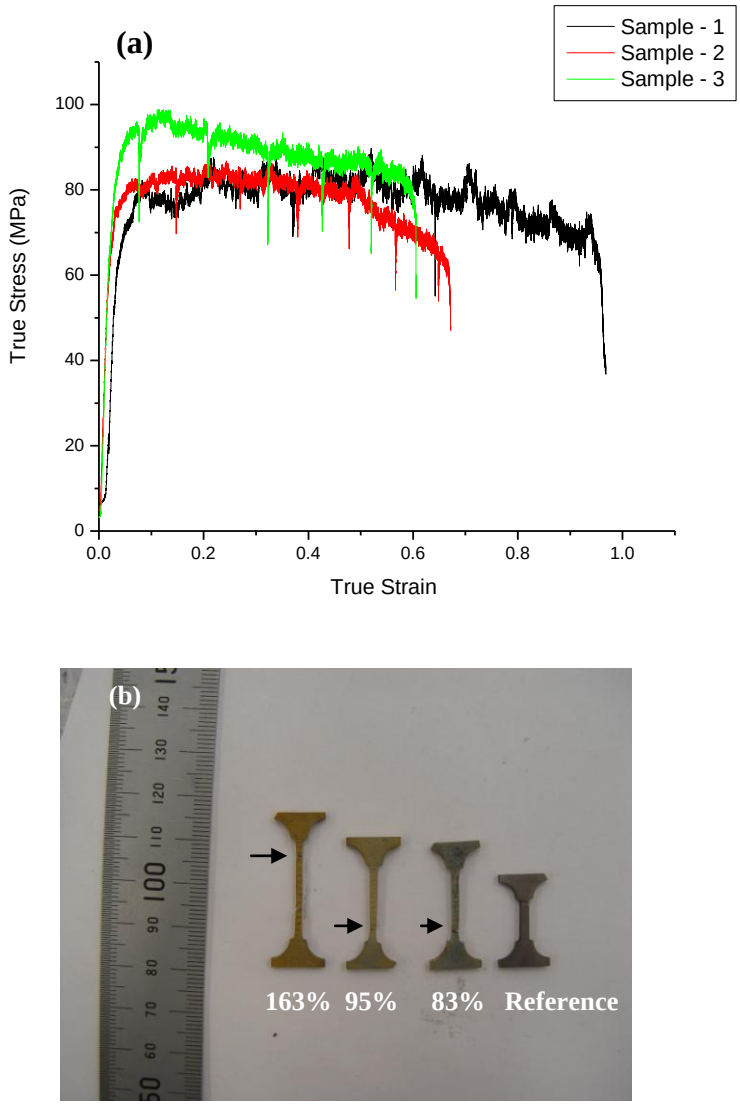

Figure 4.18: (a) true stress true strain curves of tensile tested samples at 900^{o}C; (b) fractured specimens after tensile testing at 900^{o}C (arrows indicate fractured sites).

After room temperature tensile testing the porosity near the fracture end and the microstructure in the gauge section were similar to the as-forged state (Figures 4.19 (a) and (b)). On the other hand the low magnification images of the fracture surface indicated quasi cleavage type of fracture (Figures 4.20(a) and (b)). Some

individual particles can be clearly seen from the fractured surface (Figure 4.21(a)), Some particles were separated during tensile testing due to low interparticle bonding. Some regions of the fracture surface showed microscopic dimples (Figure 4.21(b)). The SEM EDS analysis on these regions indicated that the regions were mainly TiAl phase. Overall the specimens exhibited a brittle type of fracture during room temperature tensile testing.

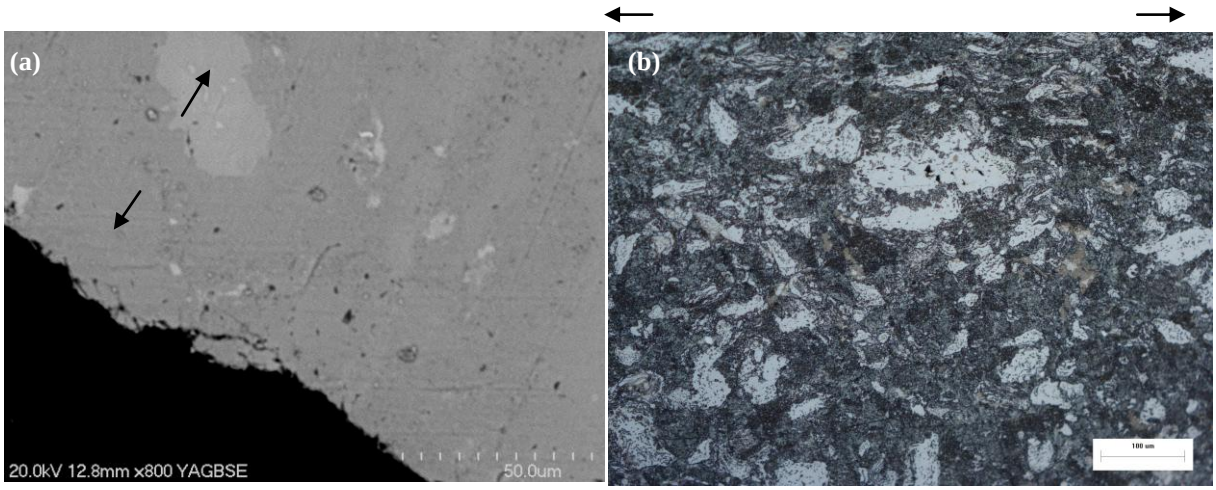

Figure 4.19: (a) SEM back scattered electron image of the longitudinal section of the specimen near the fracture end after tensile testing at room temperature, (b) optical micrograph of etched longitudinal section of the tensile tested sample. (Arrows indicate the direction of the tensile force).

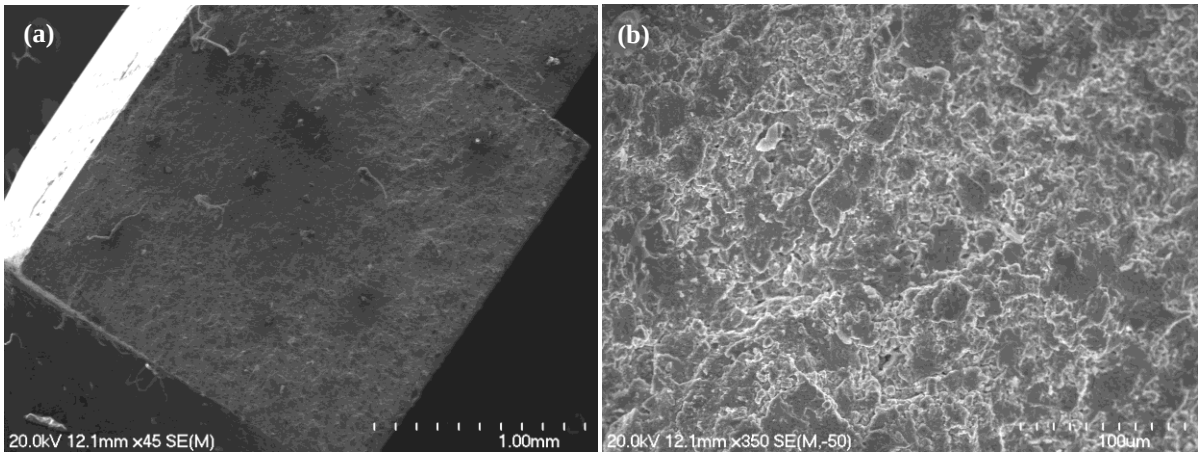

Figure 4.20: (a) & (b) fractured surface of the sample after room temperature tensile testing.

Specimens tested at 900^{o}C showed cavitation. A large fraction of cavities were clearly observed in the gauge section of each specimen that was tensile tested at 900^{o}C. The area fraction and the size of the cavities were higher near the fracture surface, as shown in Figures 4.22(a) and (b).

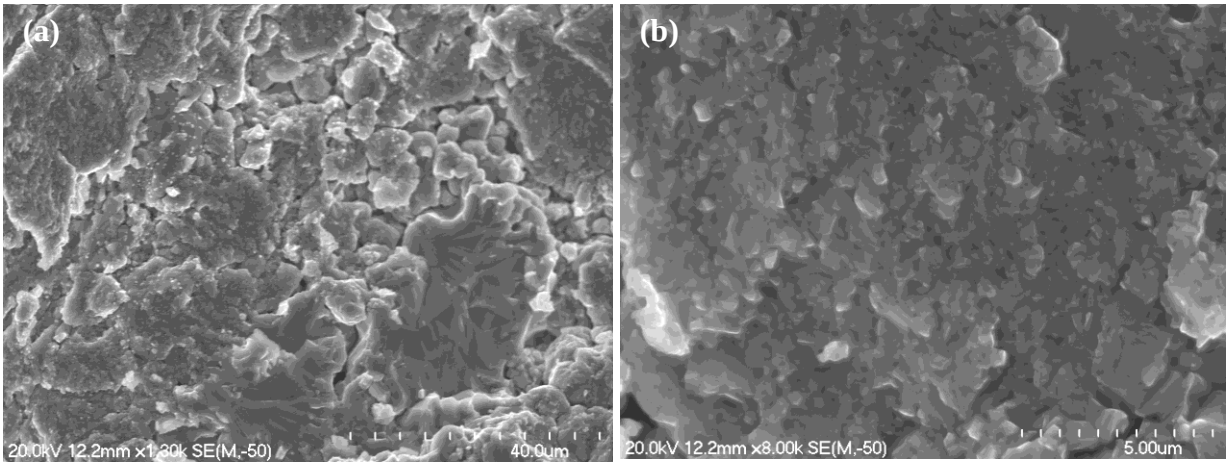

Figure 4.21: SEM back scattered images of room temperature tensile tested specimens showing: (a) the individual particles; and (b) a few regions on the fracture surface showing fibrous nature.

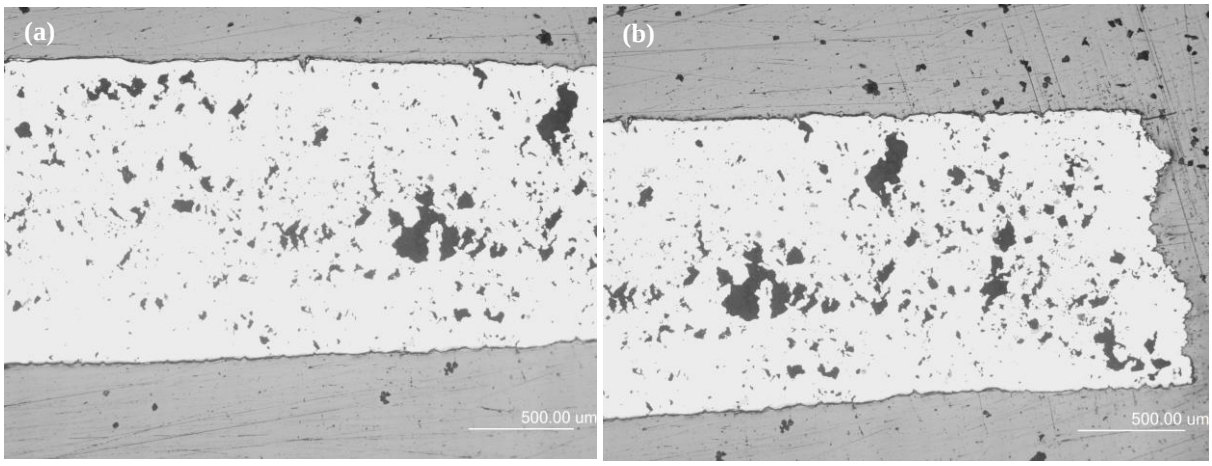

Figure 4.22: Optical micrographs of longitudinal cross sections of specimens tensile tested at 900^{o}C; (a) within the gauge length and away from the fracture; (b) near the fracture surface.

After elevated temperature tensile testing, a ductile fracture surface with a large density of dimples was observed. A number of cavities were observed on the fracture surface. The fracture strain was expected to be controlled by the number of cavities and their coalescence. Since fracture occurs at the point where the

accumulation of cavities is maximum, the holes observed on the fractured surface (Figures 4.23 (a) and (b)) which formed through cavity coalescence, may act as the initiation points, for the ductile fracture.

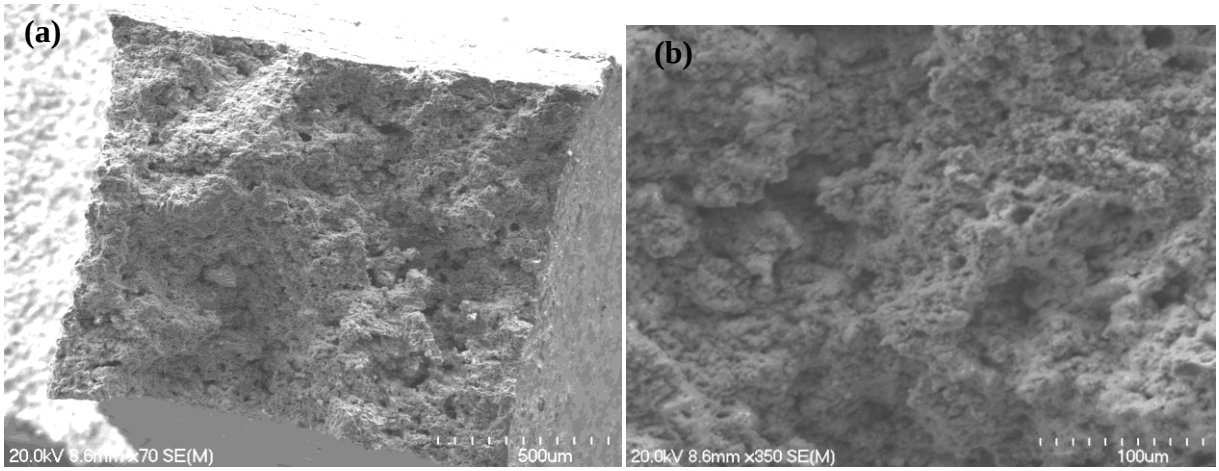

Figure 4.23: SEM back scattered images of the fracture surface of a tensile tested specimen at 900^{o}C; (a) low magnification; and (b) high magnification.

The cavities were found to be aligned at 45^{o} from the tensile force direction (Figures 4.24(a) and (b)).

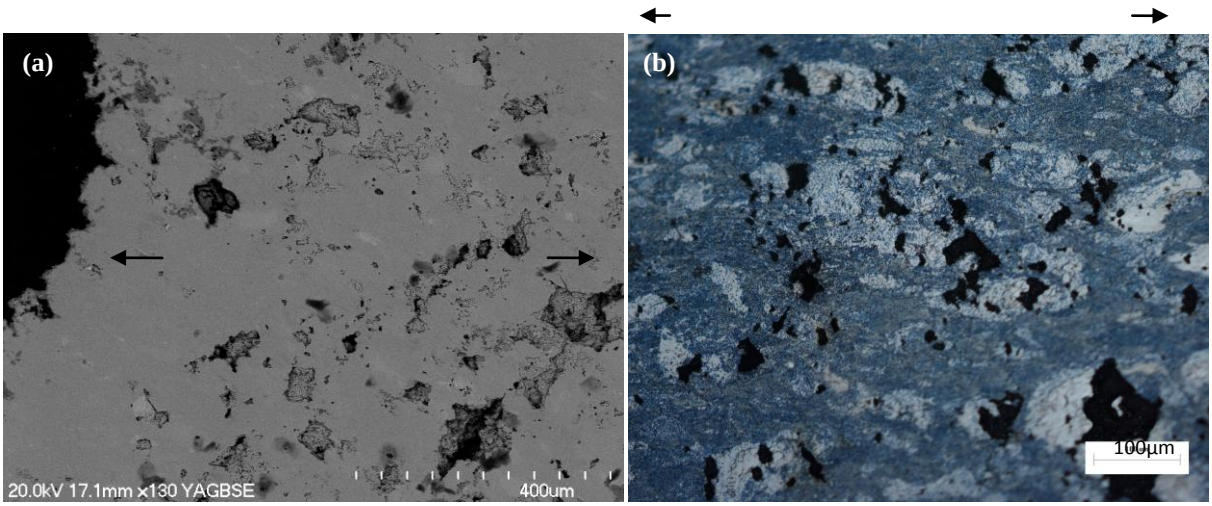

Figure 4.24: SEM back scattered images; (a) near the fracture end and; (b) optical micrograph of etched longitudinal section of tensile tested sample after elevated temperature tensile testing (900^{o}C). (Arrows indicate tensile test direction)

4.5.2.3 Mechanical properties in compression

The true stress-true strain curves of the compression testing specimens tested at room temperature are shown in Figure 4.25(a). At room temperature the specimens fractured in a brittle manner at the onset of yielding, at a stress of ~ 1400 MPa. The specimens were broken into pieces (Figure 4.25(b)), which was similar to the room temperature compression behaviour of the HIPed material shown in (Chapter 3).

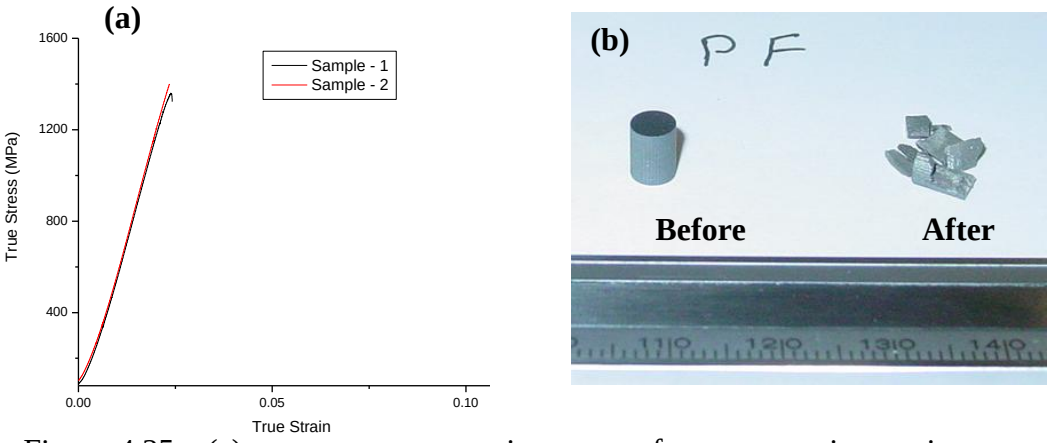

Figure 4.25: (a) true stress true strain curves after compression testing at room temperature; (b) sample before and after room temperature compression testing.

The true stress-true strain curves of the samples tested at 900^{o}C are shown in the Figure 4.26(a)). The compression test was stopped when the height of the specimen was reduced by ~ 50% which was equivalent to a true strain of 0.69 (Figure 4.26(b)). Work hardening during compression of the specimens was almost negligible. The two specimens tested, showed yield strength of ~65 MPa, and almost identical plastic flow curves after yielding.

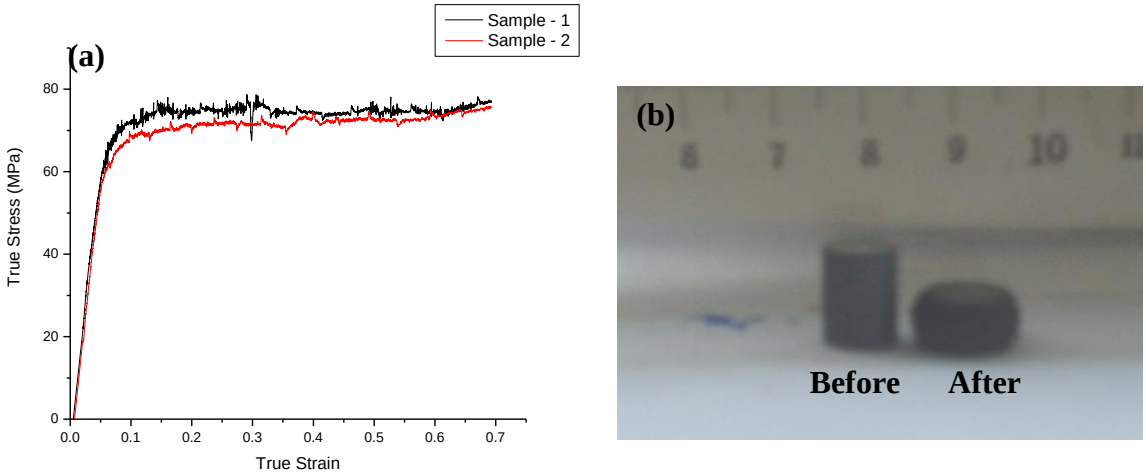

Figure 4.26: (a) true stress strain curves after compression testing at 900^{o}C; and (b) specimens before and after elevated compression testing (900^{o}C).

During compression testing at 900^{o}C, the specimens were very deformable, and there was no sign of cracking in the specimens during the whole process, as shown in Figure 4.27. The surface groves observed on the specimens were caused by EDM wire cutting of the original test specimens, and not due to the compression testing. These results indicated that the variation of the porosity level and the level of interparticle atomic bonding between specimens has less effect in compressive deformation than in tensile deformation.

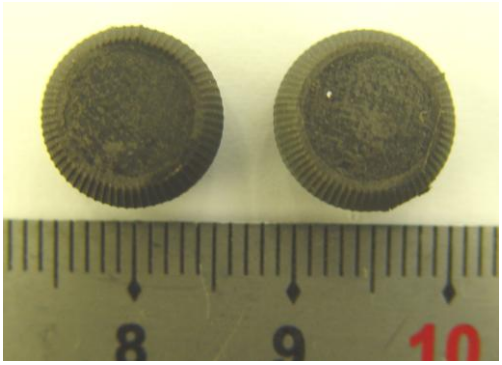

Figure 4.27: Compressed samples after elevated compression testing at 900^{o}C.

In addition, the residual pores in the as-forged state were closed after compressive deformation which can be seen by comparing Figs. 4.28 (a) and 4.28 (b).

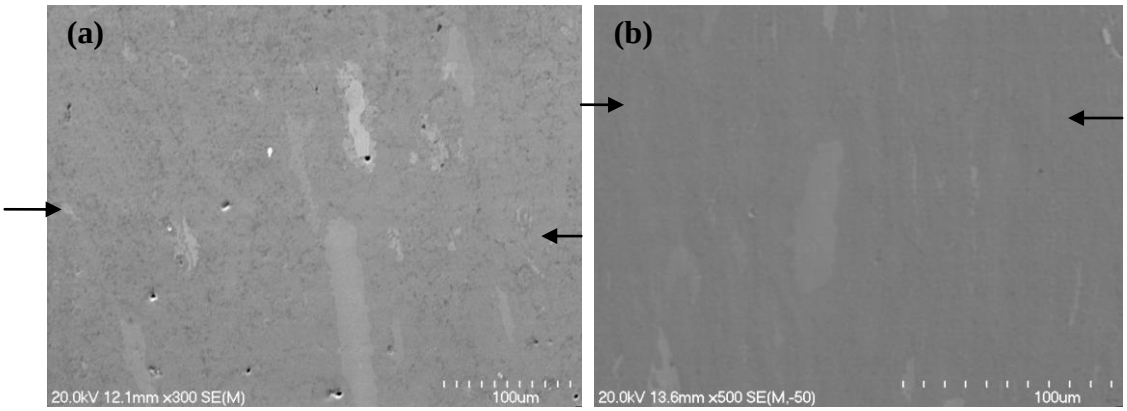

Figure 4.28: SEM secondary electron images of (a) cross section of as forged disk; (b) cross section of the sample after compression testing at 900^{o}C (Arrows indicate direction of forging and the compressive force)

The microstructure of the specimen after room temperature compression testing was not studied in the present case, since the specimens fractured without any yielding. The cross sections of the samples after elevated temperature compression have shown the same kind of orientation as that of as forged material, since the forging and compression testing directions are the same, except that the elongated phase regions were found to be thinner in the compression tested samples (Figures 4.29(a) and (b)), showing a higher amount of deformation during compression testing. The fracture analysis of the compression tested samples showed a cleavage type of fracture (Figure 4.30(a); also a few regions at high magnifications have shown signs of ductile fracture (Figure 4.30(b) and (c)). This indicates that at a few locations of the specimen the compressive load is accommodated in a ductile manner. Although a few ductile regions are found in the sample, the residual porosity and low interparticle bonding likely control the deformation process, resulting in a brittle fracture. In addition the high oxygen content in the present sample reduced the ductility of the sample to zero.

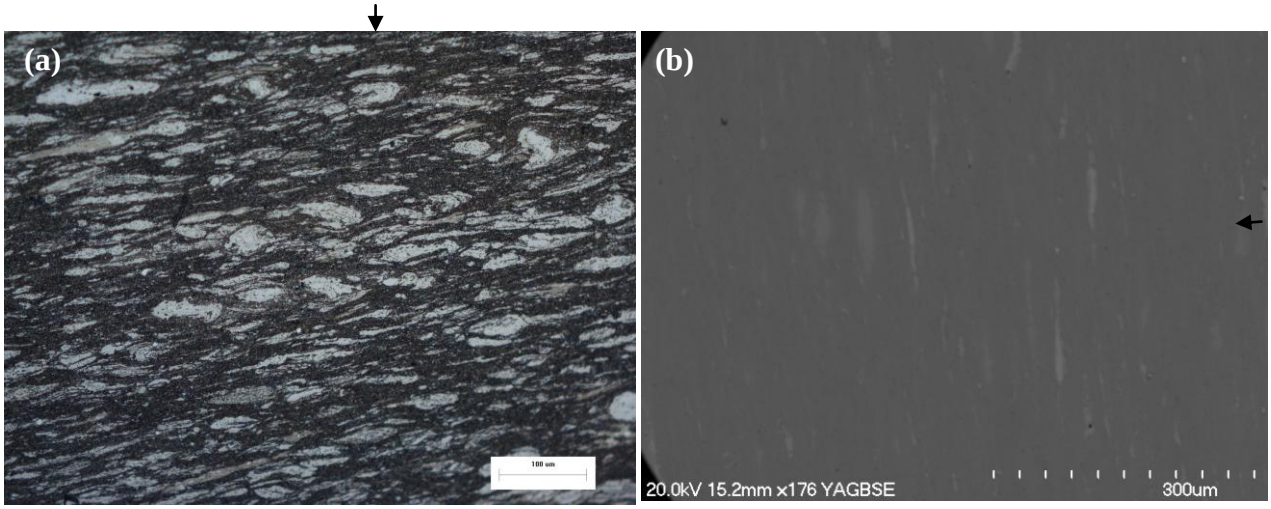

Figure 4.29: (a) optical micrograph of etched cross section showing the flow of the material after elevated temperature compression testing; (b) SEM back scattered electron image showing the preferred orientation after elevated temperature compression testing.

The individual particles which are debonded during compression testing can be seen from the fracture surfaces (Figure 4.31 (a)). The cracks in the present case are expected to propagate by the interlinking of microcracks, which nucleate at the precracks, residual pores, low interparticle sites and other defects. The crack

propagation, shown in Figure 4.31 (b), was found to be parallel to the compressive axis, which is similar to the behaviour described in Chapter 3.

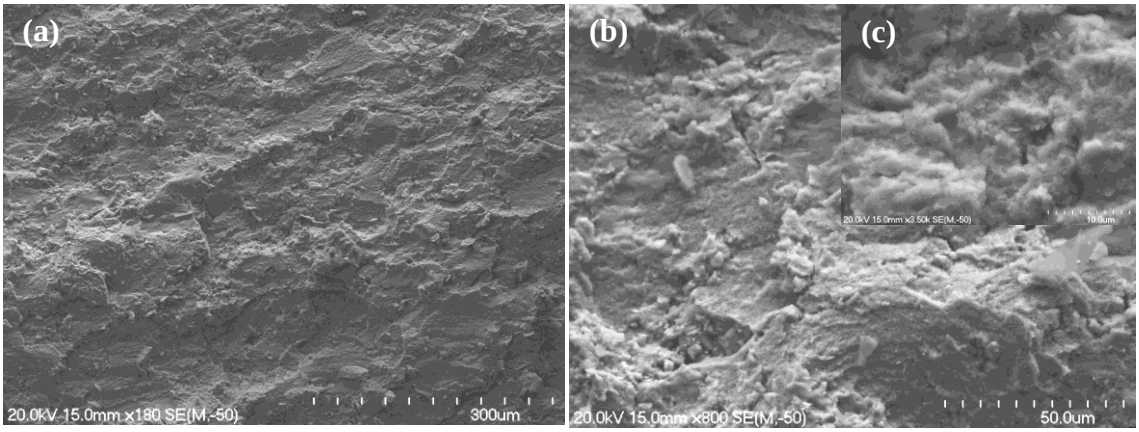

Figure 4.30: Fracture surfaces of compression tested samples tested at room temperature showing, (a) cleavage type of fracture, (b) and (c) ductile regions.

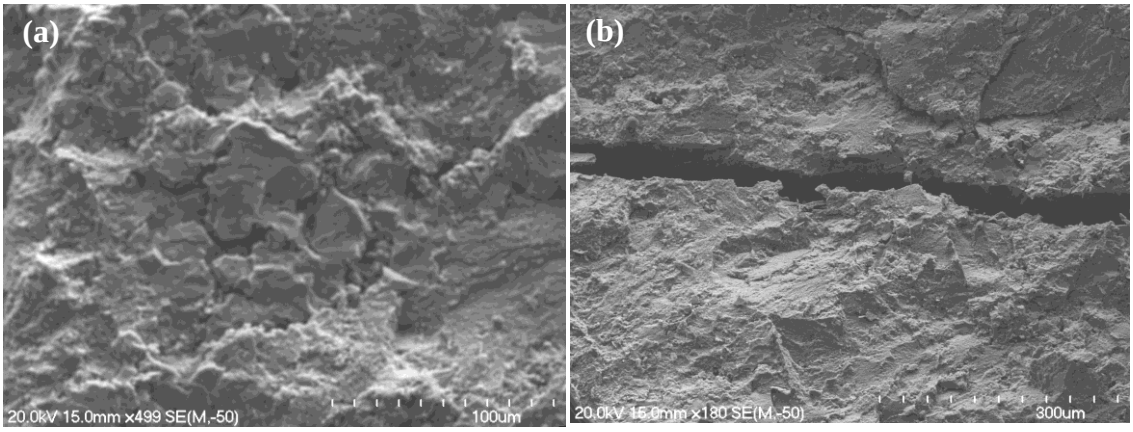

Figure.4.31: Fracture surfaces of the compression tested samples tested at room temperature showing, (a) debonded individual particles, and (b) crack propagation.

4.6 Discussion

4.6.1 Control of the powder forging process

The material production using powder compact forging encountered some difficulties. It was difficult to maintain homogeneous plastic flow during the forging process, due to the low density of the green compacts. This resulted in variation of pressure distribution on the can during forging, which in turn affected the consolidation characteristics of the material. It has been proven that canning of

the consolidated material improves the forging process in three ways: (i) forging of the canned consolidated material improves the efficiency of the forging process by constricting the material flow, resulting in a uniform distribution of the material; (ii) a large height reduction can be achieved by using one step deformation; and (iii) the temperature decrease caused by the heat loss during forging can be reduced, especially if stainless steel is used as canning material [2]. This indeed confirmed that the important factor which affected the powder compact forging process is the density of the green compact. It is expected that the increase in the density of the green compact will result in an uniform material flow, which in turn assists the deformation process.

So the canning of the powder compact in the present case was not effective in constricting the material flow, since while using green compacts having low density, it was found to be difficult to control the material flow homogeneously. Also the cooling mechanism of the sample after forging was found to have much effect on the quality of the sample. As in the case of one-step forging (Forge-2), the surface oxidation in the sample was found to be negligible, as compared to that of Forge-1 sample, which was expected due to shorter exposure time at elevated temperature. Although the effect of strain rate was not studied in the present case, it was found to be essential to control the strain rate to improve the homogeneous flow during the process.

On the other hand, canning of powder compacts means that decanning after forging and degassing before forging are needed. These operations can be time consuming. Therefore instead of canning, use of a controlled atmosphere to produce bulk material by powder compact forging can be beneficial. While using canned powder compacts, the one-step forging was expected to be more promising to produce UFG TiAl alloy, due to the low exposure times at elevated temperatures, provided that the strain rate is controlled properly.

The microstructure of the forged disk is mainly dependent on the initial condition of the powder particles. The inhomogenity of the powder particle composition of the composite powders, used for powder forging accompanied by the short

processing times during forging, resulted in an incomplete diffusion reaction between Ti and Al, and incomplete homogenization of the microstructure.

4.6.2 Mechanical Properties

The microstructure of the alloy after powder compact forging was found to have much effect on the mechanical properties of the alloy. Since the distribution of the pores varied from the centre to the periphery in the forged pancake [3], the location from which the tensile and compression testing specimens were cut (Figure 4.16(a)), played an important role.

4.6.2.1 Room temperature properties

At room temperature, all the tensile tested samples, fractured at the edge, without yielding, indicating the brittle nature of the samples. The low room temperature tensile strength and the brittle nature of the samples was believed to be due to the porosity and lack of very high level of atomic bonding between particles. The high oxygen content in the alloy also further affected the ductility in an adverse manner. Although the profile of the tensile samples cut from the forged disk did not have sharp corners, all the tested samples, still fractured at the locations of width change. This indicates that no matter which thermomechanical processing process is used for the production of Ti-47Al-2Cr (at %) alloy, porosity and weak interparticle bonding affect room temperature mechanical properties of the alloy. The room temperature tensile strength observed in the powder forged alloy was found to be far below to that reported in the literature [4 - 8].

In compression at room temperature, the strength of the sample was found to be ~ 1400 MPa without any ductility, indicating the brittleness of the samples in compression at room temperature. According to Oehring et. al [9], the material with high yield strength may fracture due to very small flaws in the specimen. In the present case the main reason for fracture was expected to be the weak bonding between particles. The room temperature compression strength was comparable to the alloys produced using IM route [10, 11] and PM [12]. The compressive strength in general was found to increase with decreasing grain size of the alloy. In the present case, the strength was lower than that reported by Oehring et al. [9].

Overall the compressive strength at room temperature was found to be dependent on the grain size. The lower the grain size, the higher the strength is.

4.6.2.2 Elevated temperature properties

With elevated temperature tensile testing at 900^{o}C, a low yield strength in the range of 70-90 MPa was observed, with an elongations in the range 80-165%. The variation in the tensile elongation observed is likely to be due to highly inhomogeneous microstructure and low level of interparticle bonding in the as-forged material. The cavitation observed in the tested samples after tensile testing was similar to a few studies reported from the literature (13, 14), in which the cavitation was much higher in powder metallurgy (PM) alloys than the ingot metallurgy alloys (IM), which is expected due to the initial amount of porosity in the samples along with thermally induced porosity.

The formation of cavities is mainly due to the residual pores present in the as-forged sample along with possibly thermally induced porosity. Some fractions of the pores were likely to be due to the lack of full scale atomic bonding between particles. Although the weak interparticle bonding was present in the present alloy, the UFG structure of the grains was expected to control the plastic deformation at high temperatures. The high temperature yield strength in tension was comparable to that of UFG Ti-47Al-3Cr alloy produced using PM route [15]. The elevated temperature mechanical behaviour of the alloy was typical to that of UFG γ- TiAl based alloys.

In compression the alloy showed good plasticity without any fracture at true strain of upto 0.69. The yield strength of the alloy was comparable to that of nanostructured TiAl alloys prepared using PM route [9, 11], but was less than the TiAl alloys with coarse grain structures prepared using IM route [16]. The microstructure of the specimens after compression testing resembled that of as-forged material with Ti rich regions being homogeneously distributed, however, a few places in the compression tested samples were found to have pores, indicating that 50% compressive deformation was not sufficient to close all the pores. The presence of Ti rich regions even after the compression test at 900^{o}C indicates that it is difficult to homogenize the microstructure at this temperature.

On the other hand pores and low interparticle bonding in the as-forged condition have a significant effect on the tensile properties than that in compression. The slightly low compressive yield strength, as compared to the tensile yield strength was expected to be due to the orientation of the specimens used for tensile and compression testing, since the testing directions were different with respect to the forging direction (Figure 4.16(b)). The anisotropy of the properties in different directions is expected to be possible reason which may cause the discrepancy between the tensile and compressive yield strengths of the alloy. The effect of sample orientation on mechanical properties is yet to be proved. On the other hand the heating rate was not expected to affect the compressive yield strength, since a faster heating rate was used in compression testing as compared to that of tensile testing. The compressive yield strength of the as-HIPed material shown in Chapter 3, is lower than that of powder compact forged sample. However the higher aspect ratio of the compression testing specimens cut from the forged material as compared to that of as-HIPed material may cause this difference.

While dealing with UFG materials grain growth during elevated temperature deformation can affect the deformation characteristics of the UFG materials. This is due to the large amount of stored grain boundary enthalpy of the UFG materials. The grain size of the material during deformation plays an important role here. In the present case since the temperature for compression testing (900^{o}C), was much less than the temperature used during forging, grain growth was not expected to take place. The deformation induced grain growth cannot be ruled out, but the negligible strain hardening indicated that the grain growth did not occur during deformation at 900^{o}C.

4.6.2.3 Formability

The powder compact forging at 1150^{o}C resulted in a bulk solid material with a high formability despite the fact that titanium aluminides are difficult to form. The consolidated material in the present case was found to be easily deformed at 900^{o}C, both in tensile and compressive directions. From the literature, IM processed materials needed multiple processing steps to produce a material having a good formability. For example a study on Ti-47Al-2Cr-0.2Si alloy by Clemens

et. al [4] used IM and thermomechanical processing to produce the samples, which were highly formable at 800^{o}C as shown by elongations to fracture of ~ 100%. Similar results were reported by Bhowal et. al [5] on Ti-47Al-2Nb-1Mn-0.5(W, Mo, Si) processed using IM route, but the elongation to fracture was far lower. On the other hand the TiAl based alloys processed using PM processing technique [6, 11, 13, 17] have demonstrated a high elongation to fracture at ~ 800^{o}C in the tensile direction indicating good formability.

The initial microstructure and chemical composition in all these cases strongly affected the formability. It is very difficult to obtain a submicron grain size in the cast alloys with initial coarse-grained non-homogeneous structures. However, in the PM TiAl alloy, the UFG structure is easily formed even in large-scale billets [18]. This can be explained by faster relaxation capability in the alloys with UFG structure due to more active grain boundary sliding and dislocation-grain boundary interactions in UFG structure [11, 16, 19]. The formability of the TiAl based alloys in compression were found to follow the same trend to that observed in tension. In the case of IM processed alloys the formability temperature was found to be above 1000^{o}C [2, 16, 20]. The PM processed alloys with an UFG structure, were found to be easily formable at 600^{o}C and above [9, 11]. In general deformations above 50% were obtained and the yield strengths were found to be considerably less than that of IM processed alloys. The deformation mechanisms acting in UFG TiAl based alloys and their coarse grained counter parts are same, except the temperature regime at which these mechanisms become active are lower for UFG TiAl based alloys. This is the main reason for the high formability of UFG TiAl based alloys. The UFG TiAl based alloy produced by powder compact forging was found to be deformable at low temperature as compared to the coarse grained counterparts. From the above, it can be concluded that the UFG TiAl based alloy produced using powder compact forging was found to have good formability at 900^{o}C, both in tensile and compressive deformation, indicating favourable conditions for secondary processing, leaving a large space to improve the quality of the material.

4.7 Summary

The present study has demonstrated that powder compact forging can be used to produce a bulk ultrafine grained Ti-47Al-2Cr (at %) alloy. It was found that canning of the powder compacts had little effect on constricting the flow of the material during forging. Higher density green compacts need to be produced, for canning to be effective in achieving a homogeneous material flow. The microstructural study on the powder forged samples confirmed that inhomogeneous material flow was responsible for the variation in the density and microhardness of the samples at the central region and the periphery region of the sample. The powder forged specimens showed a relatively low room temperature tensile fracture strength of ~125 MPa, partly due to the relatively high level of porosity and partly due to incomplete interparticle bonding. However at elevated temperatures the alloy has demonstrated fairly high elongations to fracture in the range of 80-160%, true strains to fracture of 0.6-0.96, with yield stress in the range of 70-90 MPa. Cavity formation and coalescence in the samples tensile tested at 900^{o}C was observed.

In compression tests, the alloy was found to be brittle without any yielding at room temperature, while at elevated temperatures, the samples were easily compressed to 50% without any fracture, with a yield stress of ~ 65 MPa. In tensile testing, strain softening occurred, and this was likely to be due to the cavitation occurring in the samples, while in compression steady state flow was observed, which is expected due to the GBS occurring in the sample. From the present study it can be said that direct powder forging can be used to produce bulk consolidated material, which is easily formable at elevated temperatures, both in tensile and compressive deformation, indicating favourable conditions for near net shaping using forging, rolling and super plastic forming. A good understanding of the effects of processing parameters can make this process economical and promising for producing bulk UFG TiAl based alloys.

References

1. L. Zhao, J. Beddoes, D. Morphy, W. Wallace, Material science and engineering A, 1995. **192/193**: 957-964.
2. Z. H. Huang, Intermetallics, 2005. **13:** p. 245.
3. V. Nadakuduru, D. Zhang, P. Cao and B. Gabbitas, International. Journal of Modern Physics *B,* 2009. **23**: p. 1739.
4. H. Clemens, W. Glatz and F. Appel, Scripta Materialia, 1996. **35**: p. 429-434.
5. P. R. Bhowal, H. F. Merrick and D. E. Larsen, Material Science and Engineering A, 1995. **192-193**: p. 685-690.
6. R. Gerling, F-P Schimansky and H. Clemens, Gamma Titanium Aluminides, TMS, 2003. 249-255.
7. H. Clemens, D. Lorich, N. Eberhardt, W Glatz, W Knabl and H. Kestler, Z. Metallkd, 1999. **90**: p. 569 – 580.
8. Jiancheng Tang, Baiyun Huang, Wensheng Liu, Yuehui He, Kechao Zhou, Aihua Wu, Kun Peng, Wen Qin and Youwei Du, Materials Research Bulletin, 2003. **38**: p. 2019-2024.
9. M. Oehring, F. Appel, Th. Pfullmann, and R. Bormann, Applied Physics Letters, 1995. **66**: p. 941-943.
10. Yun Qi Yan, Zhen Qi Zhang, Guo Zhen Luo, Ke Guang Wang and Lian Zhou, Material Science and Engineering A, 2000. **280**: p. 187-191.
11. R. Bohn, T. Klassen, R. Bormann, Intermetallics, 2001. **9**: p. 559-569.
12. M. Usta, H. Wolfe, D. J. Duquette, N. S. Stoloff and R. N. Wright, Materials science and Engineering A, 2003. **359**: p. 168-177.
13. T. G. Nieh, L. M. Hsiung and J. Wadsworth, Intermetallics 1999. **7**: p. 163-170.
14. G. Wegmann, R. Gerling, F. P. Schimansky, H. Clemens and A. Bartels, Intermetallics, 2002. **10**: p. 511
15. M. R. Shagiev, O. N. Senkov, G. A. Salishchev and F. H. Froes, Journal of Alloys and Compounds, 2000. **313**: p. 201-208.
16. H. Y. Kim, W. H. Sohn and S. H. Hong, Material Science and Engineering A, 1998. **251**: p. 216-225.
17. L. M Hsiung, and T.G. Nieh, Materials Science and Engineering A, 2004. **364**: p. 1-10.
18. R. M Imayev, G. A. Salishchev, V.M. Imayev, M. R. Shagiev, A.V. Kuznetsov, F. Appel, M. Oehring, O. N. Senkov and F. H. Froes, Gamma Titanium Aluminides 99, TMS, Waarendale, PA, 1999. p. 565-572.
19. R. M. Imayev, N. K. Gabdullin, G. A. Salishchev, O. N. Senkov, V. M. Imayev and F. H. Froes. Acta Materialia, 1999. **47**: p. 1809–1821.
20. J. Beddoes, L. Zhao, W. Wallace, Materials Science and Engineering A, 1994. **184**: p. L11-L15.

Chapter 5

Brittle to Ductile Transition of UFG Ti-47Al-2Cr (at %) alloy Produced Using Mechanical Milling and Hot Isostatic Pressing

5.1 Introduction

Gamma TiAl based alloys are important materials with a great potential in aerospace and automotive applications, due to their low density and high specific strength. However the major road block to the applications of these materials are due to their low room temperature ductility and limited workability. Although numerous investigations have been done by many researchers during past two decades, the increase in room temperature ductility reported so far was not sufficient for many applications. Hot working processes at temperatures above the brittle to ductile transition temperature of these alloys are used to shape TiAl based alloys.

So the lower is the brittle to ductile transition temperature (BDTT), the lower the hot forming temperature of these alloys, resulting in lower tooling and production costs. In this sense, BDTT is an important parameter for TiAl based alloys. In the present study an attempt has been made to determine BDTT for the Ti-47Al-2Cr (at%) alloy produced using hot isostatic pressing of mechanically milled powders, by conducting tensile testing at different temperatures.

5.2 Experimental Details

Elemental powders of Ti, Al, Cr were mixed to make up a composition of Ti-47Al-2Cr (at %) composition. The powders mixture was initially mixed for 6 hrs without any interval under high purity argon in a Retsch planetary mill with spherical stainless steel balls of diameter 12.5 mm, and a rotation speed of the vial of 100 rpm. The mixed powders were subsequently milled for a net time of 12 hrs using the same vial, balls and the mill, but with a rotation speed of 400 rpm. The

milled powders were cold pressed and cold isostatically pressed (CIPed) to produce green powder compacts of 40 mm in height, 34 mm in diameter. The CIPed compacts were canned using 316 stainless steel tubes, and the cans were degassed at 300^{o}C for a duration of 1 hour. Hot isostatic pressing of the canned powder compacts was carried out at 1000^{o}C for duration of 3 hrs. Tensile testing samples with a gauge length of 8.5 mm were cut from the bulk material using a EDM wire cutting machine. The tensile testing was carried out at room temperature, and three different elevated temperatures 700 ^{o}C, 750 ^{o}C and 800 ^{o}C. A strain rate of 1 x 10^{-4}/sec was used for tensile testing at room temperature and a strain rate of 1.88 x 10^{-4}/sec was used at elevated temperatures.

5.3 Results

5.3.1 Powder Characteristics

The mean particle size of the 12 hrs milled powder was 33 μm as determined using laser particle size analysis (Figure 5.1(a)). The morphology and microstructure of the powder particles used for HIP is shown are the Figure 5.1 (b)-(e).

Mechanical milling of the mixture of TiAl and Cr resulted in three types of powder particles: (i) Ti/Al/Cr layered composite structured particles; (ii) composite powder particles, consisting of a mixture of Ti and Al, in which layered structure was not observed and (iii) Ti rich powder particles. This showed that the composition of the powder particles produced after 12 hrs milling, was not homogeneous. This was mainly due to the sticking of the powder onto the wall of the vial. The density of the green powder compacts after cold isostatic pressing was ~ 70%. Study of the thermal behaviour and phase structure of the 12 hrs milled powder used for the consolidation experiments in this study confirmed that mechanical alloying between Ti, Al and Cr did not occured during milling.

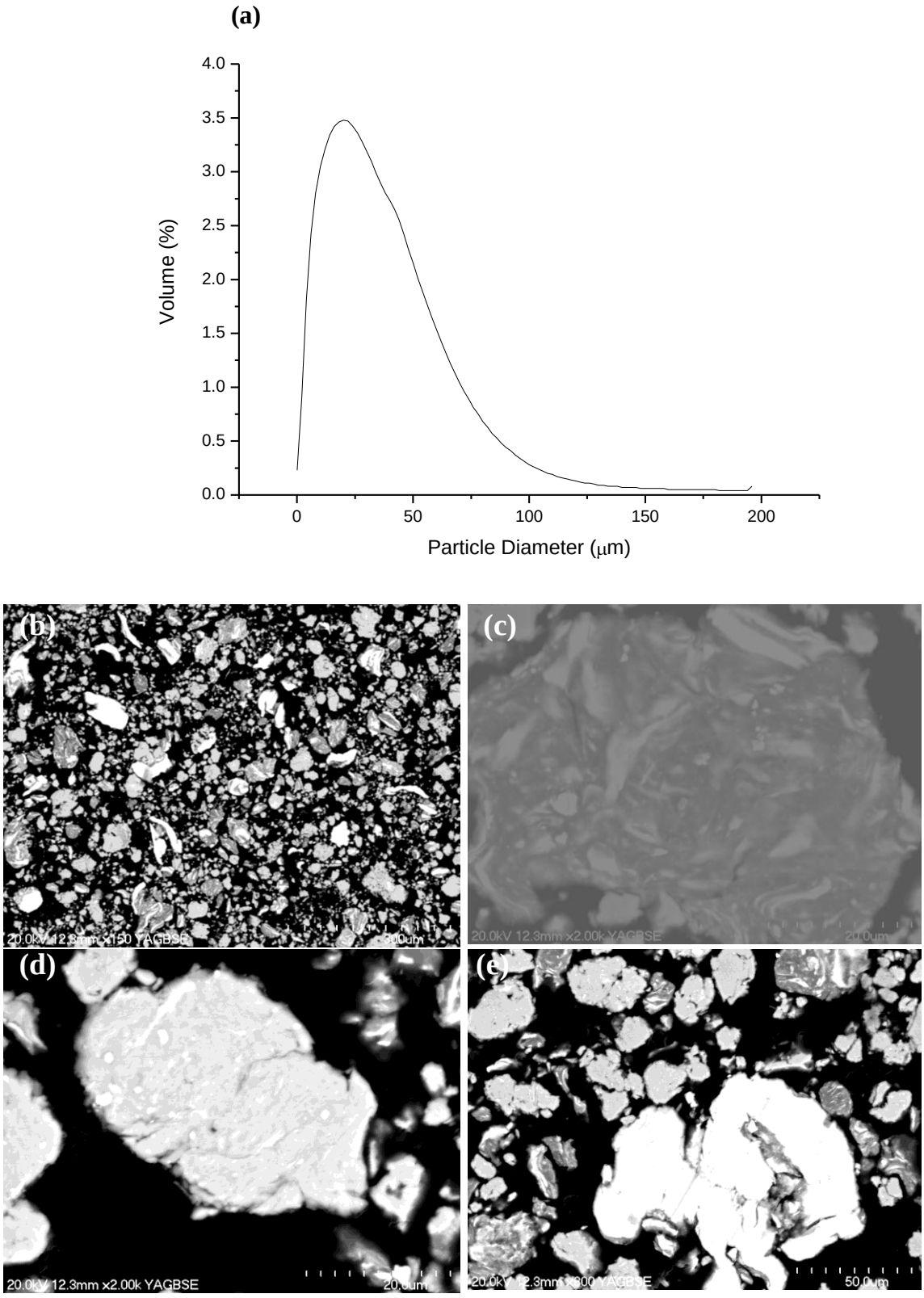

Figure 5.1: (a) particle size distribution curve and; SEM back scattered images of the 12hrs milled powders used for HIP (b) morphology of the powder particles; (c) Ti/Al/Cr layered composite particle; (d) composite powder particles in which no layered structure was observed, consisting of Ti and Al; and (e) Ti rich powder particle.

5.3.2 Microstructure of the HIPed samples

The samples before and after hot isostatic pressing are shown in Figure 5.2. A volume contraction of about 25% was observed after HIP, indicating that the HIP of powder cans was successful. In the present case, the can material could not be chipped off easily from material, as a little bit of material was found to be bonded to the can material (Figure 5.2(e)). After HIP the bulk material had a density of ~ 98%. The XRD pattern of the as-HIPed sample showed TiAl, $Ti_{3.3}Al$ and Ti peaks (Figure 5.3). The Ti phase in the consolidated sample was due to the inhomogenity in the powder particles composition, caused by sticking of the powder to the vial wall observed during milling. The HIPed sample prepared in this study had a higher density than that of the HIPed sample prepared in the study presented in Chapter 3. This is due to the longer HIP time in this study (3 hrs in comparison with 2 hrs).

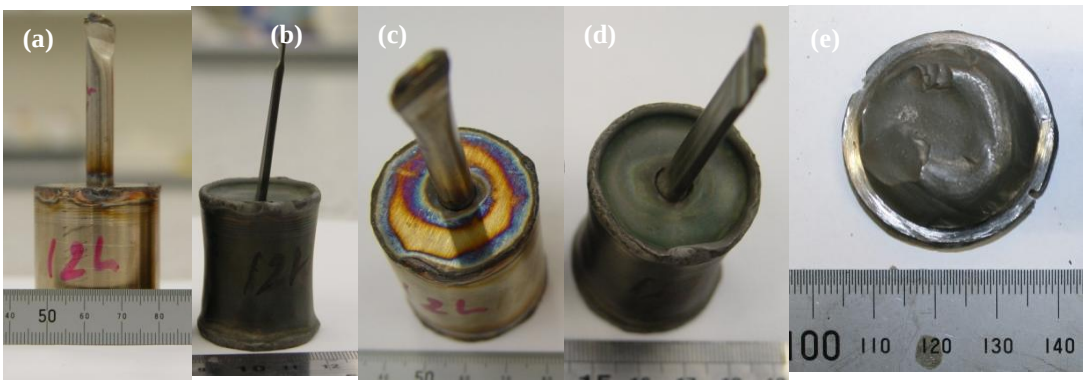

Figure 5.2: (a) & (c) can before and (b) & (d) after HIP and (e) can material showing consolidated material bonded to stainless steel.

The optical microscopy image of the etched sample (Figure 5.4) showed white, grey and dark regions, indicating multiphase structure. The oxygen content of sample was determined to be 1.15%. The SEM back scattered images (Figure 5.5 (a) and (b)) showed that the level of porosity in the sample was considerably low, although a few pores were observed in some regions (Figure 5.5(c)). The macrohardness of the consolidated sample was measured to be ~ 53 Rc. TEM examination (Figure 5.6) showed the microstructure of the HIPed sample consisted of equiaxed grains with sizes predominantly ranged between 200 – 500nm.

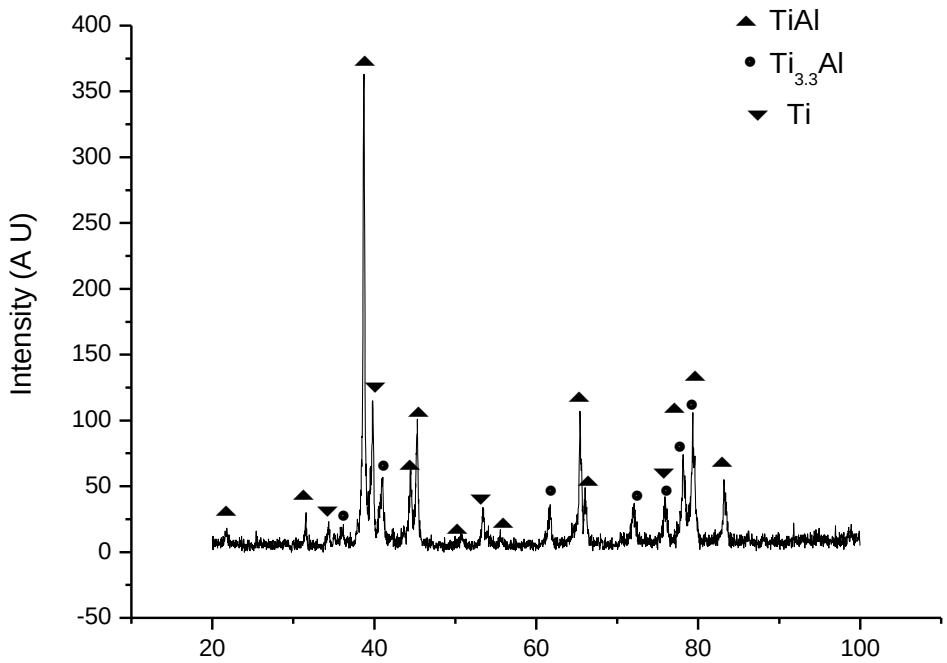

Figure 5.3: XRD of the as-HIPed alloy.

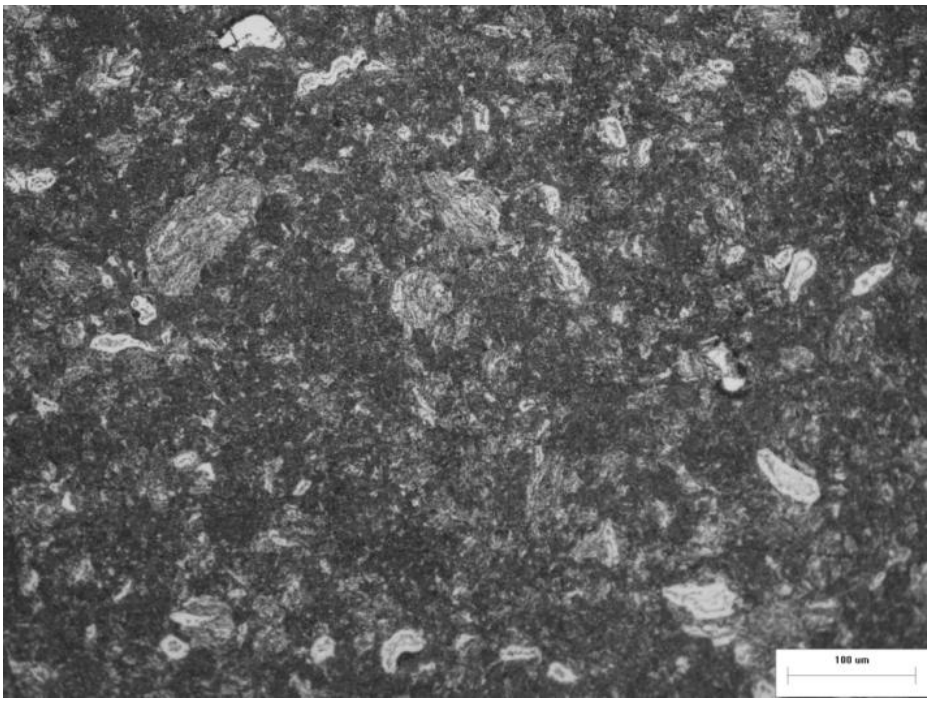

Figure 5.4: Optical microscope image of the etched surface of as-HIPed sample.

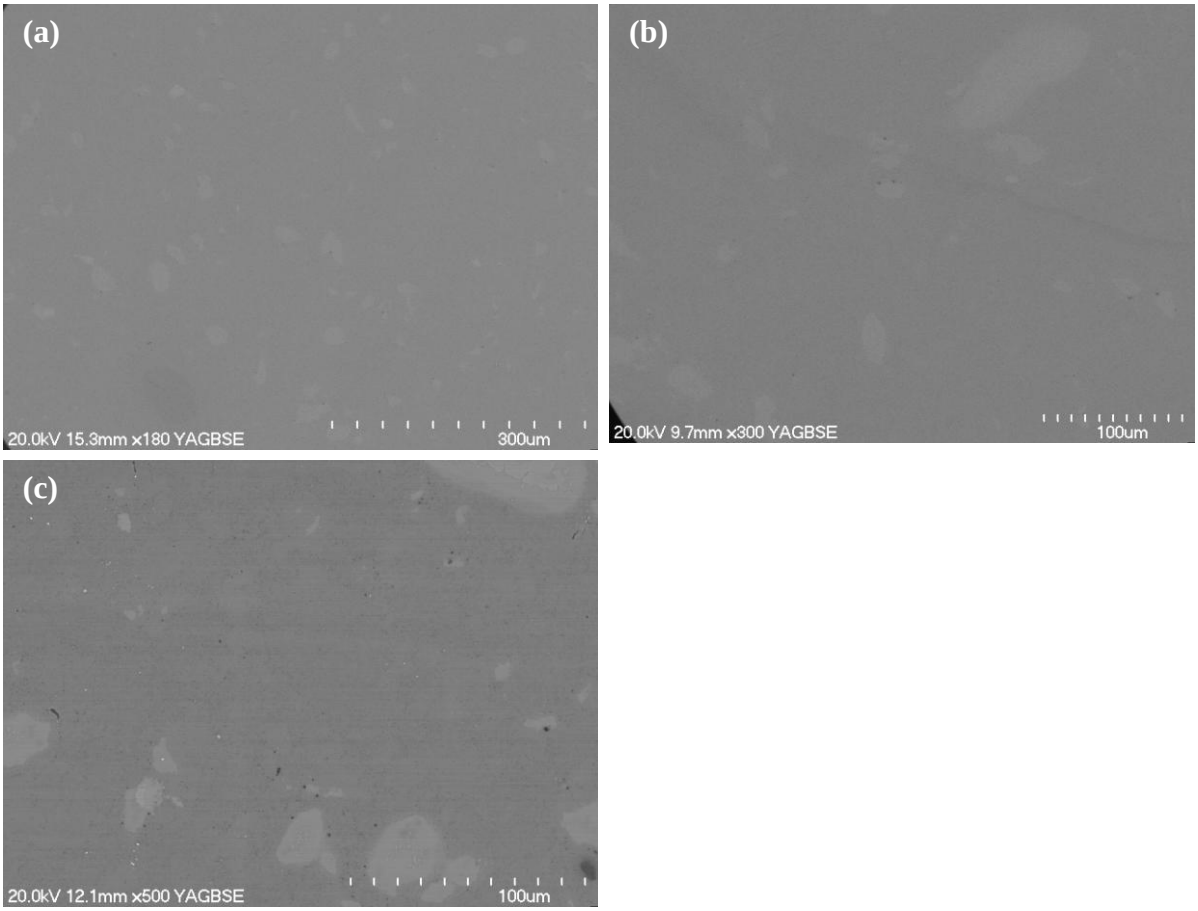

Figure 5.5: (a), (b) & (c) SEM back scattered electron images of the as-HIPed material

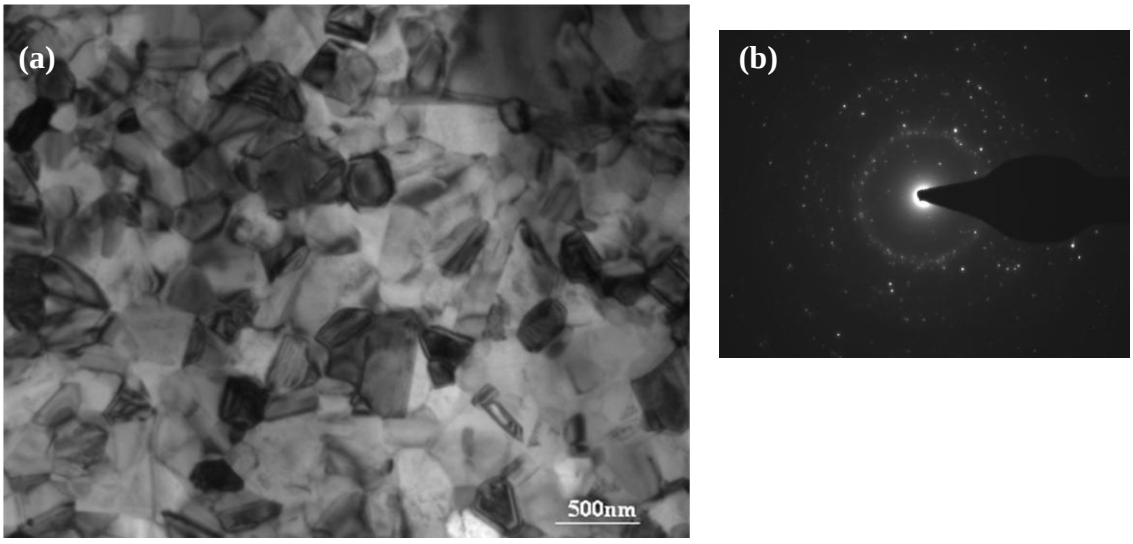

Figure 5.6: TEM bright field image of the as-HIPed material and; (b) selected area diffraction pattern (SADP)

5.3.3 Mechanical Properties of HIPed samples

The tensile true stress - true strain curves of the specimens tested at room temperature and 700°C are shown in Figures 5.7 (a) and (b). The samples tested at room temperature and 700°C showed brittle failure without any elongation. Most of the samples tested at these temperatures fractured at both locations of section change. The fractured samples after room temperature and 700°C tensile testing are shown in Figure 5.8. The average fracture strength of the specimens was 228 MPa and 220 MPa at room temperature and 700 °C, respectively.

When the testing temperature increased to 750°C, the sample became ductile, and was extended by a large amount before fracture (Figure. 5.9(a) and Figure 5.10). A serrated stress strain curve has been obtained at this temperature. The elongation to fracture of the specimens was between 95 -117%, equivalent to a true strain to fracture of 0.69 to 0.78. When the specimens were tested at 800°C, they showed a yield strength of 170 – 190 MPa and an elongation to fracture of 71-100%, equivalent to a true strain of 0.55-0.69 (Figure 5.9(b)). The samples after tensile testing at 750°C and 800°C are shown in Figure 5.10.

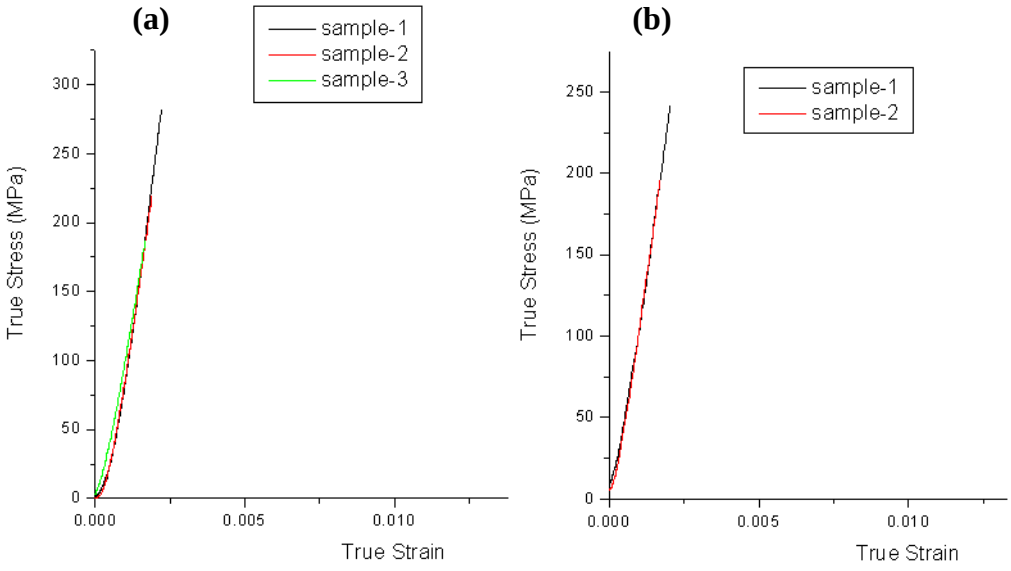

Figure 5.7: tensile true stress true strain curves of as-HIPed alloy tested at; (a) room temperature; and (b) 700°C

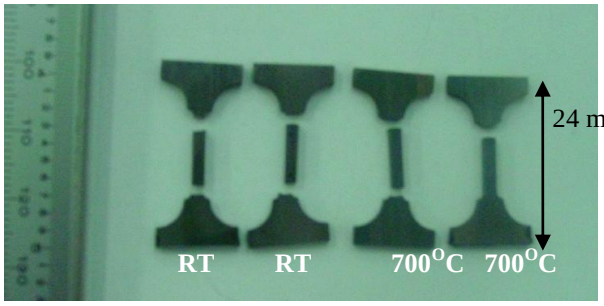

Figure 5.8: Specimens tested at room temperature (RT) and 700°C respectively.

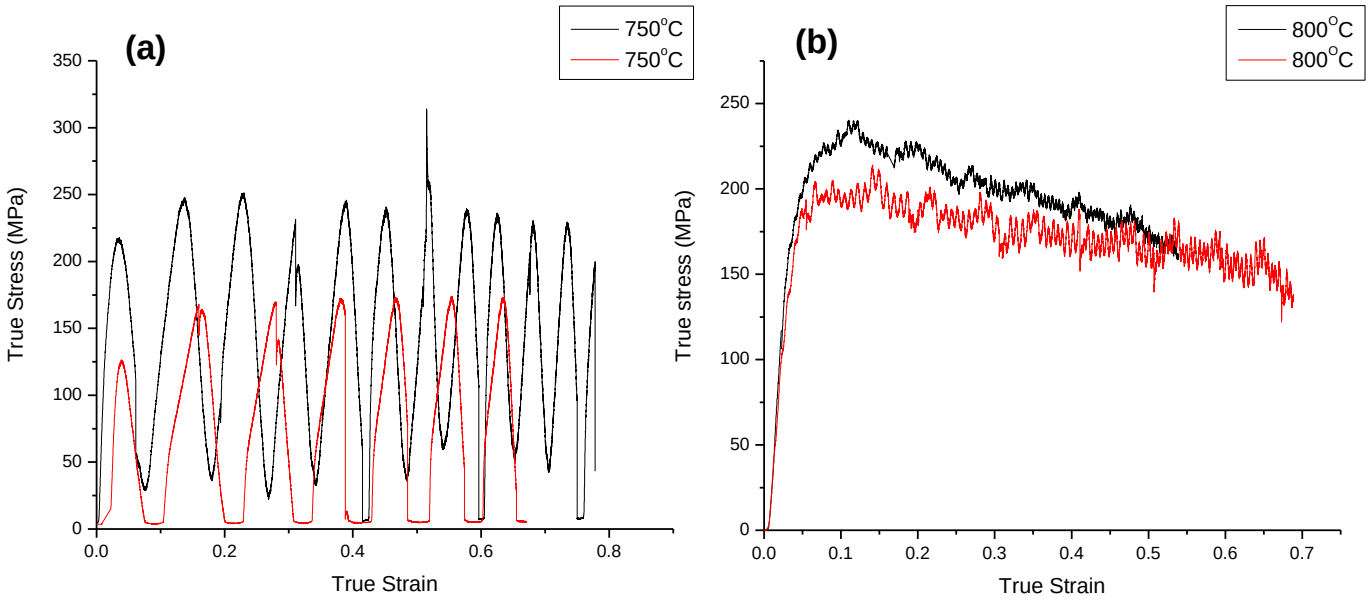

Figure 5.9: True stress true strain curves of the samples tested at (a) 750°C; and (b) 800°C.

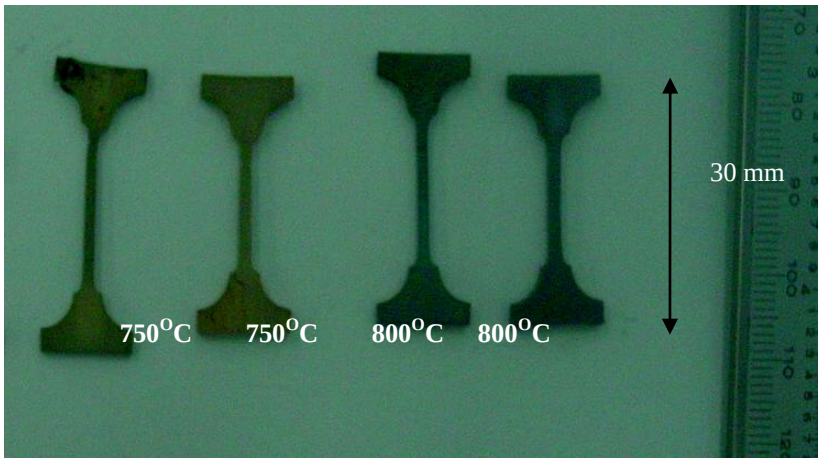

Figure 5.10: Specimens tested at 750°C and 800°C, respectively.

5.3.3.1 Microstructure in the head sections after elevated temperature tensile testing

TEM examination of the samples tensile tested at 700^{o}C, 750^{o}C and 800^{o}C was done to observe the microstructure in the head sections just after the tensile testing. The TEM micrograghs along with corresponding selected area diffraction patterns are shown in (Figures 5.11 (a)-(f)).

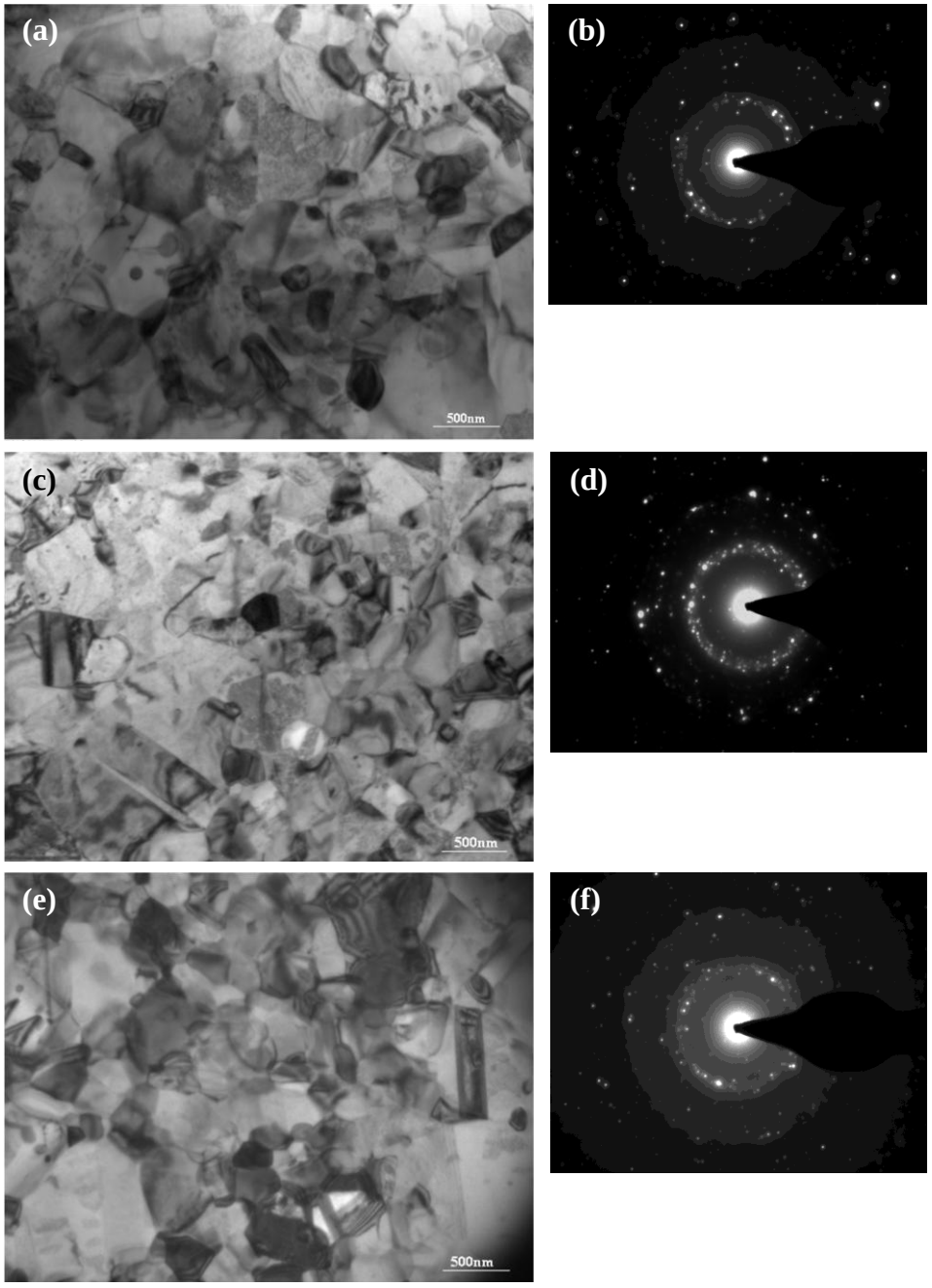

Figure 5.11: TEM bright field images of the head sections of the tensile tested samples at (a) 700^{o}C; (c) 750^{o}C; (e) 800^{o}C; and (b), (d) and (f) SADP at corresponding temperatures

The microstructure of the head sections of the samples tested at different temperatures was found to be similar to that of as-HIPed microstructure. The grains remained equiaxed in shape. This shows that the microstructure did not change significantly during exposure to heat treatments during the tensile tests at temperatures in the range of 700 – 800^{o}C. However a few large grains were observed in the microstructures which are expected to be from the original material and not due to the heat treatment.

5.3.3.2 Microstructure after plastic deformation at elevated temperature tensile testing

The microstructural evolution in the gauge sections also followed the same trend (Figure 5.12 (a)-(f)) along with corresponding SADP. From the microstructure of the samples, tested at 750 and 800^{o}C, the grains were not elongated, indicating that dynamic recrystalisation (DRX) occurred during deformation. It appeared that the DRX and the limited grain growth led to a microstructure which characterized by equiaxed and ultrafine grains during the whole process of tensile deformation at 750 and 800^{o}C respectively.

According to Clemens et. al [1], DRX leads to a grain size stabilisation, in which if the initial grain size is smaller than the corresponding grain size in the steady state one dynamic coarsening will occur, and grain refinement will occur if the initial grain size is larger than that in the steady state. There is a balance between grain growth and refinement. In the present study the microstructure in the gauge sections of the samples tested at 750^{o}C and 800^{o}C, indicated that a considerable grain growth has not occured.

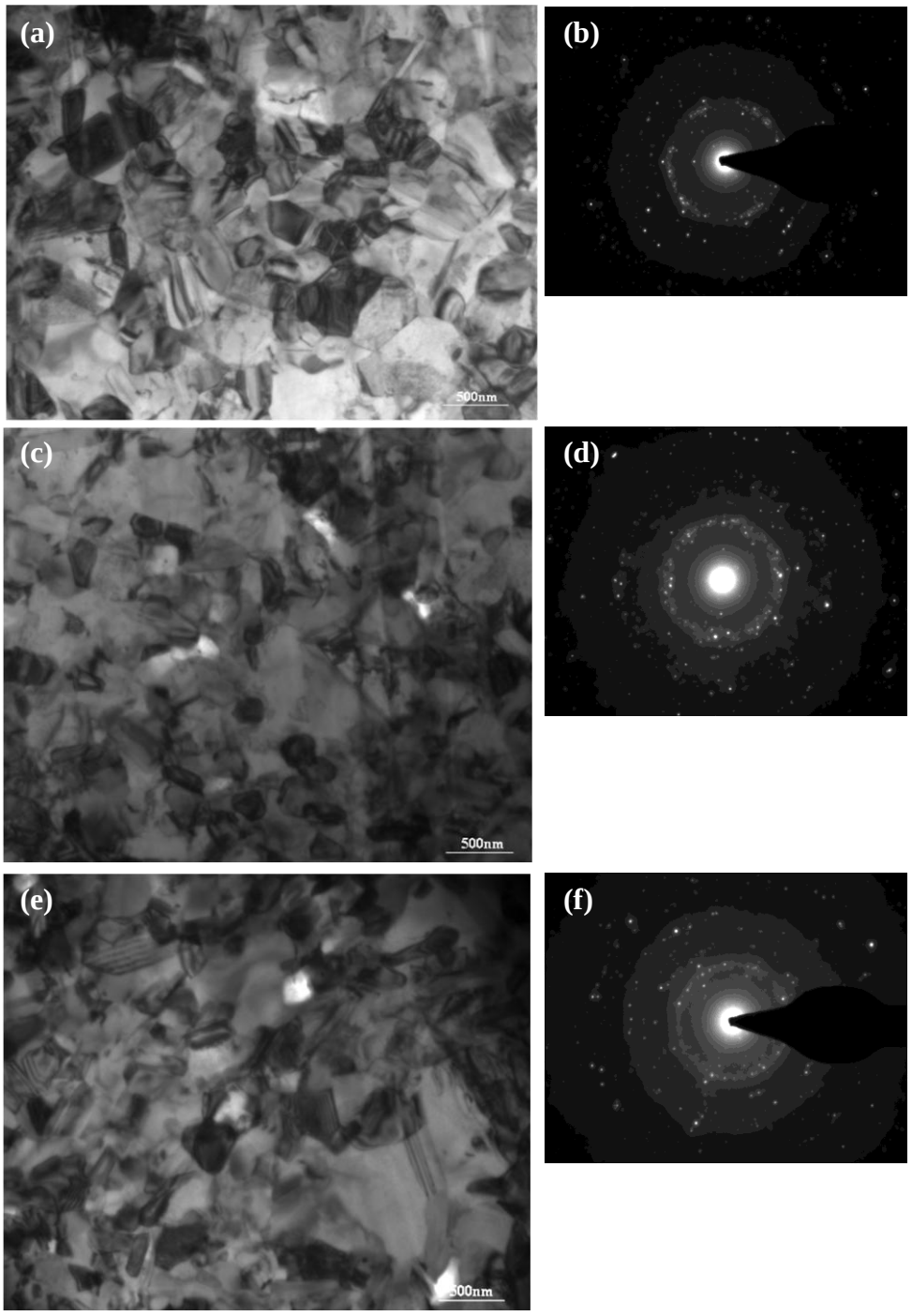

Figure 5.12: TEM bright field images of the guage sections of the tensile tested samples at (a) 700^{o}C; (c) 750^{o}C; (e) 800^{o}C and (b), (d) and (f) SADP at corresponding temperatures

5.3.4 Fracture Behaviour of HIPed samples

The fracture at room temperature is a brittle type of fracture, as shown by river patterns on the fractured surfaces (Figures 5.13 (a) & (b)). The fracture behaviour was found to be the same for the samples tested at 700^{o}C (Figures 5.13 (c) & (d)). As the testing temperature increased to 750^{o}C, a fibrous type of fracture was observed (Figure 5.13 (e) & (f)), and also voids were found on the fracture surface. The same type of behaviour was observed for the samples tested at 800^{o}C (Figures 5.13 (g) & (h)). The fracture morphology in the samples tested at 750^{o}C and 800^{o}C mainly consisted of tearing and micro void related dimpling. The change of fracture behaviour from quasi cleavage type to fibrous type between 700^{o}C and 750^{o}C temperatures indicating the presence of brittle to ductile transition in this temperature range.

On the other hand the longitudinal sections of the specimens with in the gauge length, tensile tested at room temperature are similar to the as-HIPed material, showing no porosity, the same trend was observed in the samples tested at 700^{o}C (Figures 5.14 ((a)-(d)). While the evolution of pores in the gauge sections was observed after tensile testing at 750^{o}C and 800^{o}C, which can be seen from the Figures 5.14 (e)-(h). The pores in the present case were expected mainly due to two reasons: (a) accommodation of shear strain; and (b) thermally induced porosity. Since high plastic elongations were observed in the present case, it is expected that pores formed at certain locations where shear strain was not properly accommodated. The other possibility (thermally induced porosity) was ruled out, since the pores were only observed at 750^{o}C and 800^{o}C and not at 700^{o}C.

For the samples tested at room temperature and 700^{o}C, the microstructure, in the gauge sections resembled the as-HIPed microstructure indicating no preferred orientation (Figures 5.15(a) and (d)). On the other hand the second phase particles, in the gauge sections of the samples tested at 750 ^{o}C and 800^{o}C have shown a tendency to align 45° to the tensile direction. Evolution of most of the pores was observed at the interface of the white phase (Figures 5.15 (c) and (d)), which are expected to be in rich in Ti phase. Since Ti is having high affinity to oxygen, it is

expected to act as an oxygen sink and become brittle. So the formation of pores was mainly observed at the boundaries of brittle Ti rich phase.

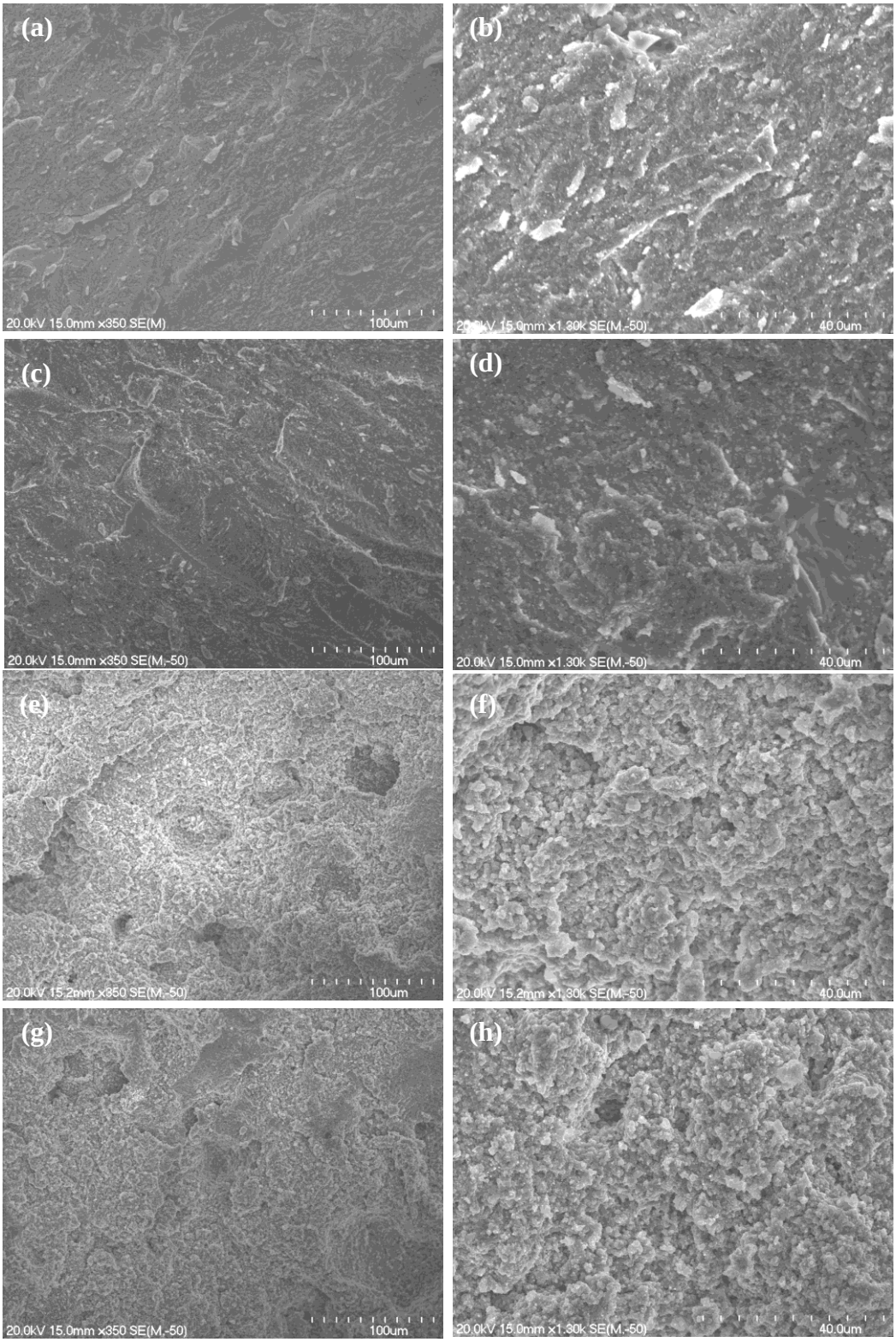

Figure 5.13: Fracture surfaces of tensile test specimens tested at different temperatures: (a) & (b) room temperature; (c) & (d) 700^{o}C; (e) & (f) 750^{o}C; and (g) & (h) 800^{o}C.

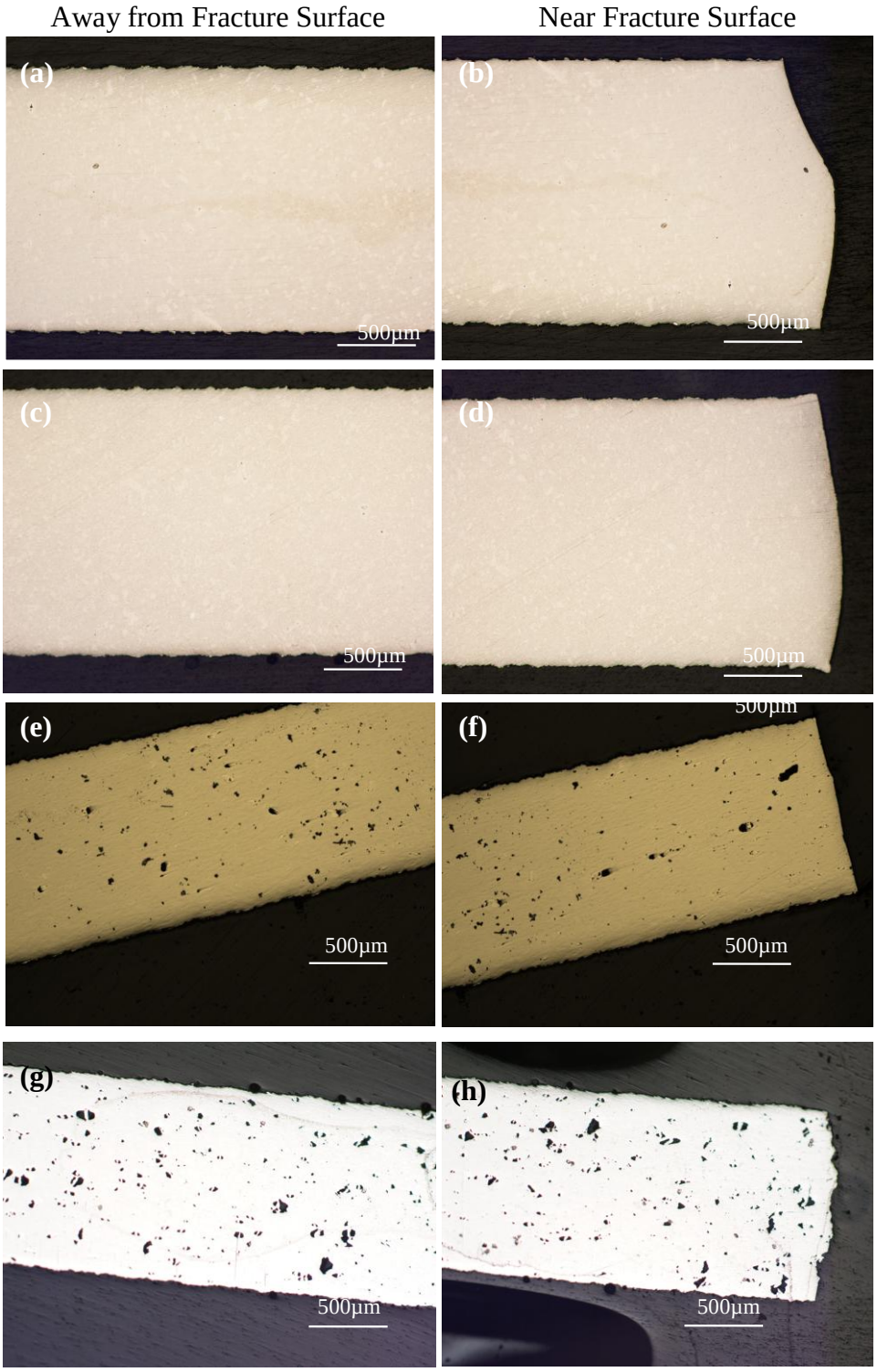

Figure 5.14: Optical micrographs of longitudinal sections of specimens with in the gauge length tested at different temperatures: (a) & (b) room temperature; (c) & (d) 700^{o}C; (e) & (f) 750^{o}C; (g) & (h) 800^{o}C.

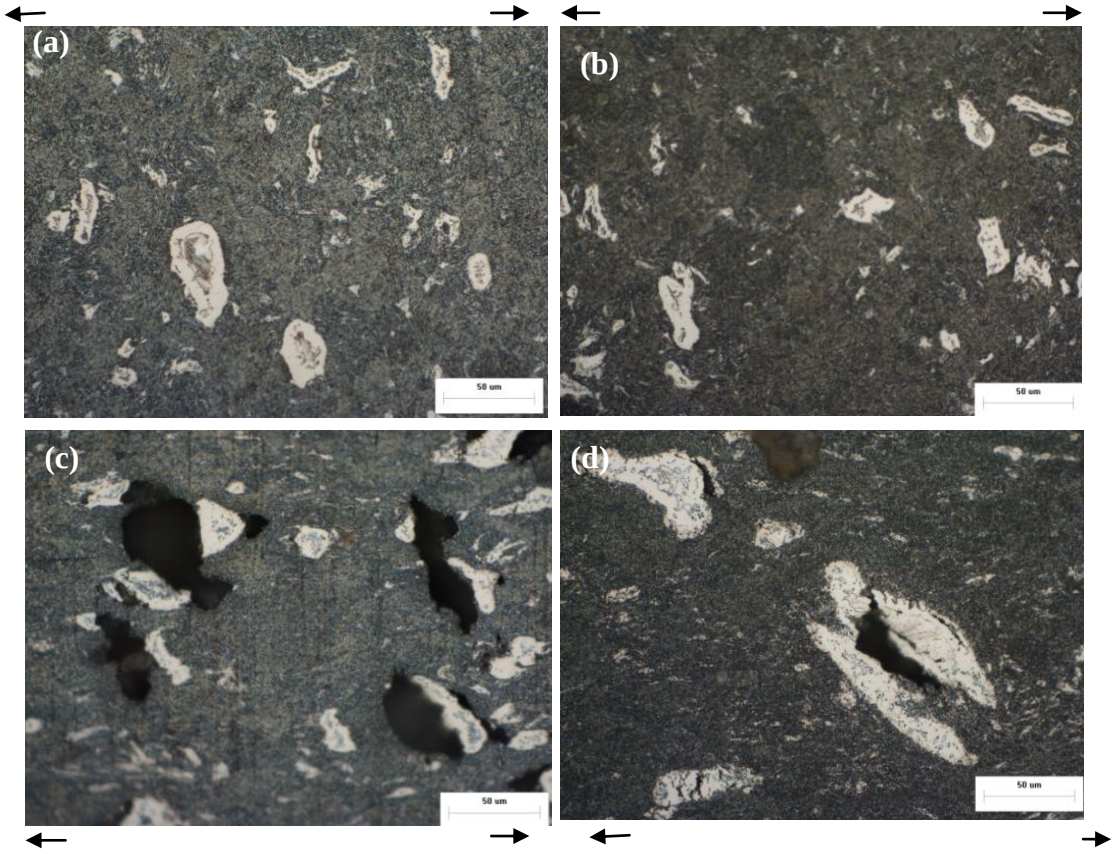

Figure 5.15: Optical micrographs of etched longitudinal sections of tensile test specimens within the gauge length tested at different temperatures: (a) room temperature; (b) 700^{o}C; (c) 750^{o}C; (d) 800^{o}C; (Arrows indicate the direction of tensile force)

5.4 Discussion

The brittle to ductile transition in TiAl based alloys consists of a general yielding of the material above a critical temperature, which is generally determined by the competition between cleavage fracture mechanisms and dislocation activity. The cooperative mechanism of activated dislocations results in a massive dislocation activity of the type associated with the BDTT in these alloys. The temperature and form of such transitions are determined by the effects of strain rate and temperature on dislocation mobility, the relative orientation of cleavage and dislocation glide planes and the distribution of dislocation sources. The strain rate dependence of the BDTT arises from the motion of pre-existing dislocations and

dislocations which are thermally nucleated below the BDTT by the cooperative process [2].

In the present case, since the tensile testing was conducted in a temperature interval of 50^{o}C, a sharp transition was not observed. The drastic change in the ductility of the alloy between 700^{o}C and 750^{o}C indicated that the brittle to ductile transition of this alloy occured in this temperature range. However according to Imayev et al. [3], the brittle to ductile transition is a thermally activated two stage process, in which the noticeable increase in ductility after the first stage is due to grain boundary mechanisms of relaxation, in which the brittle fracture is retained. After the second stage the development of relaxation processes covering the grain interior along with the grain boundary relaxation leading to a transition from brittle to ductile one. So in the present case where a direct fracture transition from brittle to ductile has been observed, the first stage was not observed. This indicated that the brittle to ductile transition is occurring somewhere between 700 and 750^{o}C. According to Booth et al. [2], the transition happens over a very narrow temperature range (typically < 10^{o}C).

The BDTT of the UFG Ti-47Al-2Cr alloy observed in the present case was slightly higher to PM processed Ti-47.5Al-3Cr alloy with fine grained microstructure, in which a BDTT was reported to be ~ 700^{o}C [4]. It is comparable to that of fine grained PM processed Ti-46.5Al-4(Cr,Nb,Ta,B) alloy reported by Clemens et al. [1]. In their study, a BDTT of ~ 750^{o}C was observed. The study by Lee et al. [5] on PM processed Ti-46.8Al-1.6Mn alloy demonstrated a much lower BDTT of ~ 500^{o}C. The much lower BDTT reported by Lee et al. [5] was found to be due to the high amount of equiaxed grains and a better balance between the grain size and the brittleness of the α_2 phase in the TiAl based alloy.

In general TiAl based alloys with ternary additions such as Cr and Mn, BDTT is observed. This is due to the enhanced dislocation mobility as compared to alloys without these additions. Since alloying elements such as Cr are not effective in substitutional solid strengthening, resuting in the enhancement of dislocation movement. On the other hand the BDTT of the alloy in the present study is lower than coarse grained TiAl based alloys (BDTT of ~ 800^{o}C) reported by Liu et al.

[6]. According to their study the TiAl alloys with refined lamellar structures exhibit a general trend of increasing ductility with increasing temperatures. However a few alloys studied by them, showed no clear indication of BDTT. From the above it can be said that the existence of BDTT for the TiAl alloys depends on alloy composition, grain size and microstructure. Similar observations have been reported by Kim et al [7] on TiAl based alloys. The BDTT in the present case is comparable to TiAl based alloys reported by other studies. Also the high temperature elongations are comparable to that of UFG grained TiAl based alloys [8, 9, 10, 11]. On the other hand tensile strength of the Ti-47Al-2Cr(at%) alloy at room temperature was found to be lower than UFG TiAl based alloys reported from various studies [11, 12], while at elevated temperatures the tensile strength was found to be comparable to that of UFG TiAl based alloys [10,11].

Although high elongations were observed at 750 and 800^{o}C, configuration of the tensile flow curves were found to be quite different at 750 and 800^{o}C. The curve corresponding to 750^{o}C shows the formation of oscillations in stress during the deformation, the flow curve oscillates almost at a constant level as seen from Figure 5.9 (a). It should be noted that the high temperature ductility of TiAl is strongly dependent on the deformation processes occurring during the deformation. Dynamic strain aging (DSA) is a time dependent strengthening or hardening phenomenon which manifests itself in the form of serrated stress–strain curves, yield stress plateaus, reduced tensile elongation, and so on. Therefore, the possibility of the flow oscillations caused by DSA can be excluded due to the higher elongations observed in the present case. Since DRX is expected to occur both at 750 and 800^{o}C, the observation of the flow oscillations at 750^{o}C, is mainly expected due to the cyclic occurance of the DRX. The behavior of cyclic DRX was observed in the Ni-base super alloy 718 alloy [13], in which flow oscillations were observed, but the stress strain curve in that study, has shown an elastic region. However the elastic region in the stress strain curve was not observed in the present case. In order to confirm this behaviour, more samples have to be tested at 750^{o}C.

5.5 Summary

Hot isostatic pressing of mechanically milled powders has resulted in Ti-47Al-2Cr (at %) alloy with ~ 98% density, the low amount of porosity has resulted in a TiAl alloy with slightly high fracture strength at room temperature, as compared to that reported from previous chapters. The alloy was found to be brittle, with no ductility upto 700^{o}C. The ductility of the alloy increased drastically at 750^{o}C, indicating that the BDTT occurr between 700 and 750^{o}C. The flow oscillations observed at 750^{o}C, might be due to cyclic DRX. However more samples needed to be tested at 750^{o}C to confirm the oscillation behaviour. The cavitation observed after elevated temperature deformation is likely due to the improper accommodation of the shear strain.

References

1. H. Clemens, A. Lorich, N. Eberhardt, W. Glatz, W. Knabl, and H. Kestler, Z. Metallkd, 1999. **90**: p. 8.
2. A. S. Booth and S. G. Roberts, Acta Materialia, 1997. **45**: p. 1045-1053.
3. V.M. Imayev, R.M. Imayev, G.A. Salishchev, Intermetallics, 2000. **8**: p. 1-6.
4. J. Beddoes, L.Z., P.Au, W. Wallace, Material Science and Engineering A, 1995. **192/193**: p. 324-332.
5. I. S. Lee, S.K.H., W.K. Prak, J.H. Lee, D. H. Park, H. M. Kim and Y. T. Lee, Sripta Metallurgical et Materialia, 1994. **31**: p. 57.
6. C. T. Liu, J.H.S., P. J. Maziasz, J. L. Wright & D. S Easton, Intermetallics, 1996. **4**: p. 429-440.
7. Y. W. Kim, Material Science and Engineering A, 1995.**192/193**: p. 519-533.
8. R. Bohn, T.K., R. Bormann, Intermetallics, 2001. **9**: p. 559-569.
9. D. M. Dimiduck, Material Science and Engineering A, 1999. **263**: p. 281-288.
10. G. Wegmann, R. Gerling, F-P Schimansky, Intermetallics, 2002. **10**: p. 511-517.
11. R. Gerling, F-P Schimansky and H. Clemens, Gamma Titanium Aluminides, TMS, 2003. p. 249-255.
12. G. X. Wang and M. Dahms, Journal of Material Performance, 1993. **45**: p. 52-56.
13. Y.Wang, W.Z. Shao, L. Zhen, C. Yang, X.M. Zhang, Journal of Alloys and Compounds 2009. **471**: p. 331–335

Chapter 6

Conclusions and Recommendations

6.1 Conclusions

- Mechanical milling of a mixture of elemental Ti, Al, Cr powders resulted in a powder consisting mainly three types of powder particles; (a) Ti/Al/Cr layered composite structured particles; (b) particles, consisting of a mixture of Ti and Al in which layered structure is not observed and (c) Ti rich powder particles. The inhomogenity in the powder particle composition after 12 hrs of milling along with high oxygen content of the powders indicated that the quality of the powders produced in the present study is not very good.

- The bulk alloy samples produced by HIP for 2 hrs (HIP1) at 1000^{o}C had porosity of approximately ~ 5%, indicating that the HIP time was not sufficient to close the pores. The microstructure mainly consisted of TiAl as the major phase and Ti(Al) and Ti_3Al as minors, the unreacted Ti(Al) phase in the microstructure was mainly due to the initial powder condition, in which a small fraction of powder particles were rich in Ti.

- At room temperature, the HIPed alloy was fairly brittle, and had fracture strength of ~ 100 MPa. At elevated temperatures they became ductile, as reflected by considerable amounts of tensile elongations at 800^{o}C and above. The maximum amount of elongation was found to be between 70 – 80% at 900^{o}C. The tensile yield strength at 800^{o}C was in the range of 84 - 90 MPa and decreased to 55-58 MPa with the testing temperature of the samples to 900^{o}C. In compression the alloy showed plastic yielding and a yield strength of ~ 1.4 GPa at room temperature. Compression testing at 900^{o}C revealed that compressive deformation equivalent to a height reduction of 50% could be easily achievable without cracking.

- Direct powder compact forging using canned powder compacts of the Ti/Al/Cr composite powder was successfully used to produce bulk consolidated Ti-47Al-2Cr alloy samples. It has been observed that the density of the bulk consolidated alloy sample after forging varied from the centre to the periphery.

- Mechanical testing of the powder forged samples showed that the samples exhibited brittle type of fracture both in tension and compression at room temperature and the fracture strengths of the samples were in the range of 115 – 130 MPa in tension and 1.38-1.4 GPa in compression without any yielding. When being tested at 900^{o}C, the samples became very ductile showing yield strength in the range of 70-90 MPa and elongation to fracture between 80-165% in tension, and yield strength of ~ 65 MPa and 50% deformation in compression was easily achievable.

- Porosity and weak interparticle bonding in the UFG Ti-47Al-2Cr alloy affected the room temperature mechanical properties adversely.

- HIP of the mechanically milled powders for duration 3 hrs resulted in a bulk Ti-47Al-2Cr material (HIP2) with approximately 98% density. TEM observations confirmed that the grains are at ultrafine level (200-500 nm) with equiaxed shape. Tensile testing of the alloy samples at different temperatures revealed that the brittle to ductile transition temperature of the alloy was in the range of 700 and 750^{o}C.

- Irrespective of the processing technique used to produce the bulk UFG Ti-47Al-2Cr alloy, the microstructure of the bulk consolidated material, consisted of Ti rich regions, which was mainly due to the inhomogenity in the powder particle composition used for consolidation.

- The as-milled powder was found to be the main source of oxygen in the bulk consolidated material. The large surface area of the milled powder particles, result in a high amount of oxygen absorption. The degassing temperature of 300^{o}C used is not sufficient to remove all volatile materials

absorbed on to the powder particles, and also the entrapped oxygen during cold pressing.

- Porosity in the samples observed after tensile testing at elevated temperatures was mainly due to coalescence of residual pores and nucleation and growth of cavities to accommodate the plastic deformation.

- The UFG Ti-47Al-2Cr alloy produced using HIP and powder compact forging has demonstrated good formability at elevated temperatures, and can be used as a suitable precursor for near-net shaping using thermomechanical processes such as forging and superplastic forming, leaving a large space to improve the quality of the material.

6.2 Recommendations for Future work

- It is essential to improve the powder production technique by: (a) controlling the sticking of the powders to the vial material by reducing the milling speed; (b) to transfer the milled powders directly into the powder compacting and canning steps without exposing them to air; and (c) Increasing the degassing temperature to reduce the amount of oxygen and volatile content in the powder compact.

- Powder compact forging of the Ti-47Al-2Cr alloy and other TiAl based alloy powders in a protective atmosphere without canning the powder compacts, can be fruitful in producing high quality bulk TiAl based alloy materials.

- Secondary processing of the Ti-47Al-2Cr alloy using forging and rolling is done to improve the quality of the material.

- Tensile testing of the samples between 700^{o}C - 750^{o}C to exactly determine the BDTT.

- TEM studies of the UFG Ti-47Al-2Cr alloy, to get an indepth understanding of microstructure/processing/property relationship.